UiT
THE ARCTIC UNIVERSITY OF NORWAY

Faculty of Science and Technology

Department of Geology

Petrographic investigation of methane-derived authigenic carbonate crusts from Barents Sea and Norwegian Sea

Silje Røde

GEO-3900 Master's thesis in Geology
June 2016

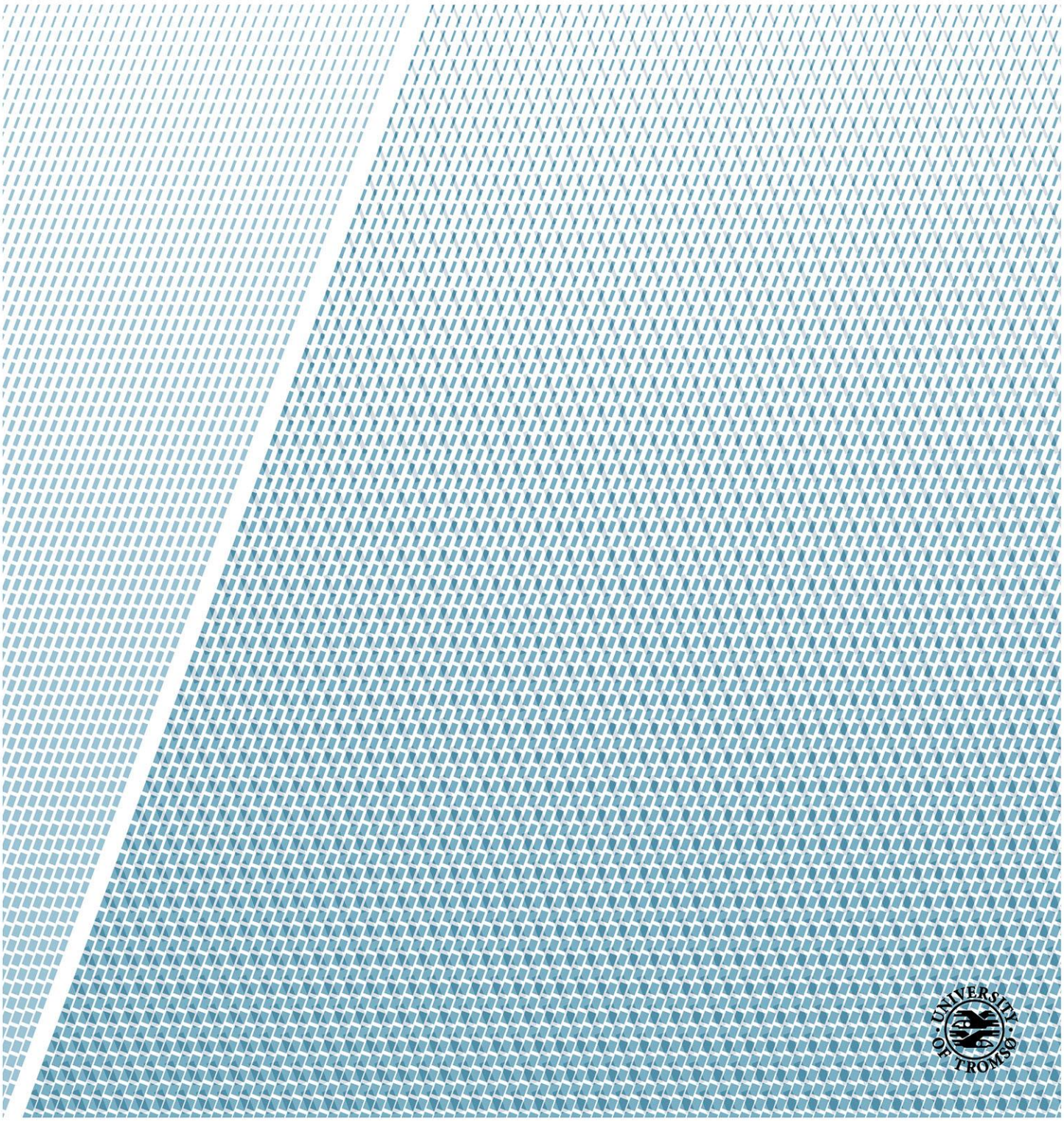

ACKNOWLEDGEMENTS

First of all I have to thank my supervisors: Giuliana Panieri, thank you for giving me the opportunity to write this thesis, for sharing some of your knowledge and for all your help! Aivo Lepland, thank you for helping me when I was lost, for all your advices, and for all your help.

This work was supported by the Research Council of Norway through CAGE, Center of Excellence for Arctic Gas Hydrate Environment and Climate project number 223259.

I would also like to thank the wonderful people in the lab, Trine for all your help with the SEM, Karina, for providing me with the radio and keeping my motivation up.

To the amazing people I have met during these five years; my fellow students; it has truly been the time of my life! It feels like we have travelled the world together, from Skibotn, Crimea to Hawaii. But mostly we went to Skibotn, which was OK because it was always fun being on field trips with you! My sweethearts, Karianne and Maren, through ups and downs, we share the most fantastic memories and I am grateful that you have been such a huge part of my life these five years! Frank, the one and only, thank you for all your advices – which I never followed. And Ida, for popping by the office and getting my mood back up again.

Aleksander, for feeding me when my blood sugar was critical, and for all your patience.

Finally, to my family, for your endless support and belief in me. Mum, dad, Christin, I am forever grateful, you have been there for me all the way!

Silje Røde

Tromsø, 15.juni.2016

ABSTRACT

In recent years, the scientific attention regarding methane has increased due to its effect on the global climate. Understanding modern methane seep environments gives a better understanding of fossil seep environments, related chemical processes and associated fauna. Different proxies are being used to investigate methane seepage sites, and in this thesis I focus on two different proxies: methane-derived authigenic carbonate (MDAC) crusts, and the tests of foraminifera occurring in the crusts.

MDAC crusts from four seepage sites at the Loppa High in the southwestern Barents Sea, and one seepage site at Hola, off Vesterålen in the Norwegian Sea, have been investigated, with the main focus of understanding if and how the tests of benthic and planktonic foraminifera occurring in the crusts could serve as nucleation centers for the precipitated carbonates.

Polished thin sections (dimensions 50mm*75mm) obtained from the crusts were provided by NGU, and in this thesis they were analyzed mainly using Scanning Electron Microscope (SEM), equipped with and energy-dispersive X-ray (EDS) detector - BSE-images obtained with the SEM together with EDS-analysis were investigated for petrographic and elemental characterization of biogenic components, detrital sediments and associated authigenic MDAC.

The results of my investigation indicate that there were no differences in alteration of the tests between benthic or planktonic foraminifera -tests, or between species. The main carbonate phase occurring in the crusts was aragonite, but minor Mg-calcite was also present. It is proposed that precipitation of Mg-calcite could use the foraminifera tests as nucleation centers, but for aragonite which has a different crystal structure than the calcite tests, they will not serve as templates for precipitation.

Table of Contents

1 Introduction 2
1.1 Objectives 2
1.2 Gas hydrates 2
1.3 Methane 4
1.3.1 Microbial methane 4
1.3.2 Thermogenic methane 4
1.3.3 Cold seeps 5
1.3.4 SMTZ – sulfate-methane transition zone 5
1.3.5 Methane-derived authigenic carbonates 5
1.3.6 MDAC and carbonate mineralogy 7
1.4 Foraminifera 8
1.4.1 Benthic foraminifera 9
1.4.2 Planktonic foraminifera 9
1.4.3 State of alteration 10
1.5 Foraminifera and methane 10
1.5.1 Recent studies 11
2 Study areas 14
2.1 Barents Sea 14
2.1.1 Gas in the Barents Sea 16
2.1.2 Loppa High 17
2.1.3 Gas in Loppa High 18
2.2 The Lofoten-Vesterålen Margin 18
2.2.1 Hola 20
2.2.2 Gas in the Hola area 20
2.2.3 Geological history 21
2.2.4 Present day topography and sediment distribution 21

2.2.5 Currents 22
3 Previous work on MDAC crusts in this thesis 24
4 Material and Methods 26
4.1 Thin sections 26
4.2 Methods 26
4.2.1 Scanning electron Microscope, “TM3030”. 27
4.2.2 Element mapping 28
4.2.3 Procedure 28
5 Results 30
5.1 Interpretation of the electron backscatter-images (BSE), elemental maps and the EDS point-analyses 31
5.2 Loppa High 38
5.2.1 PR1 38
5.2.2 PR3 44
5.2.3 PR4 47
5.2.4 PR5 49
5.2.5 Short summary of the Loppa High sections 50
5.3 Hola 51
5.4 Summary and comparison 54
6 Discussion 56
6.1 Sediments within the MDACs 57
6.2 Authigenic pyrite 59
6.3 Biogenic components 60
6.3.1 Siliceous spicules 60
6.3.2 Bivalve shells 61
6.4 Foraminifera 62
6.4.1 Planktonic foraminifera 62

6.4.2 Benthic foraminifera 63
6.4.3 Cibicides sp. 64
6.4.4 Cassidulina sp. 65
6.4.5 Buliminella sp. 66
6.4.6 Agglutinated foraminifera 67
6.5 Cement mineralogy 68
6.6 Carbonate mineralogy of precipitated authigenic carbonates and foraminiferal tests 69
6.7 Nucleation centers or not 71
6.8 For further studies using tests of foraminifera related to methane seeps and MDAC 72
7 Summary and conclusions 74
8 References 76
9 Appendix 82

1 Introduction

1.1 Objectives

The aim of this study is to investigate the methane-derived carbonate crusts and describe diagenetic carbonate phases that associate with foraminifera within MDAC crusts and to assess if foraminifera serve as nucleation templates during AOM (anaerobic oxidation of methane) in the SMTZ (sulfate methane transition zone).

1.2 Gas hydrates

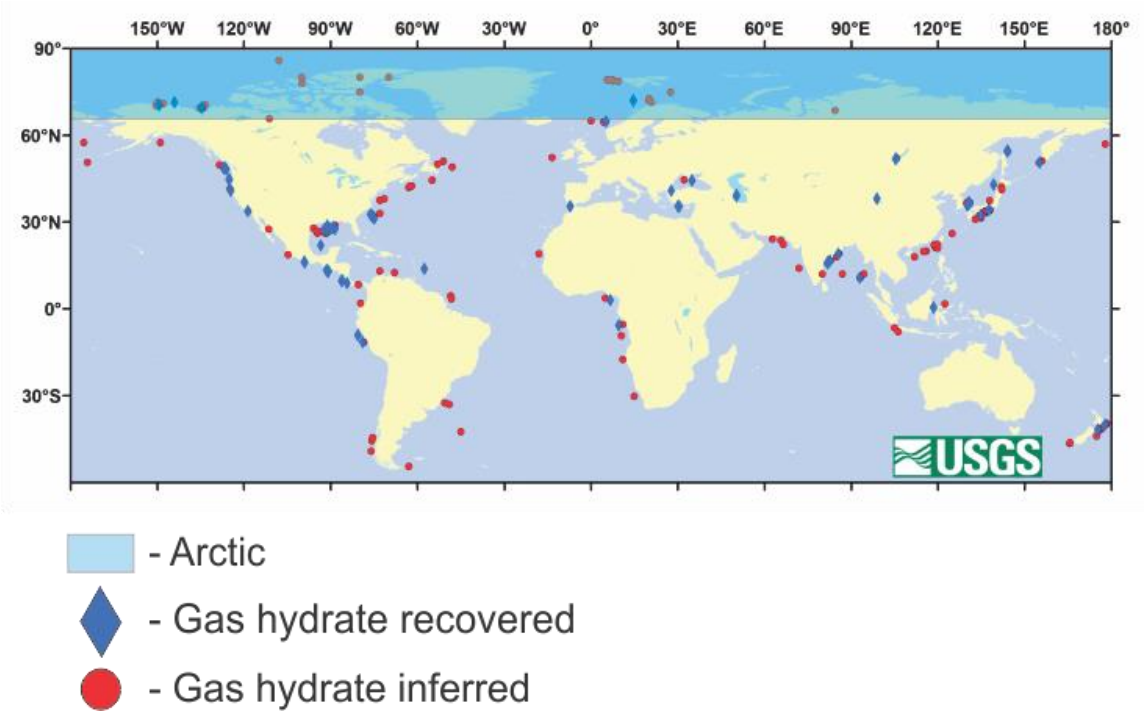

Fig 1.1: Worldwide distribution of gas hydrates, the Arctic region is located within the light blue area at 66°N. The blue diamonds are locations where gas hydrate has been recovered. The red circles are inferences of gas, most often based on discovery of a seismic interface (BSR, Bottom Simulating Reflector). Map edited from "USGS Gas Hydrates Project".

Gas hydrates or gas clathrates are naturally occurring ice-like substrates consisting of light hydrocarbons and water; most commonly methane, but also ethane, propane, normal butane, nitrogen, dioxide and hydrogen sulfide, which are entrapped by a rigid cage of water molecules (Sloan, 1998). Gas hydrates are distributed along many continental margin settings and in onshore permafrost or offshore relict permafrost (Fig 1.1). Gas hydrates can be found in environments with high pressure and low temperature, they are typically stored in the pore space of the uppermost zone within sediments at high latitude and on continental margins (Hustoft *et al.*, 2009; Kvenvolden, 1993).

The hydrates formed in nature can be found in different shapes, from small nodules (<12 cm), small lenses or they can form layers that are several meters thick (Makogon, 2010).

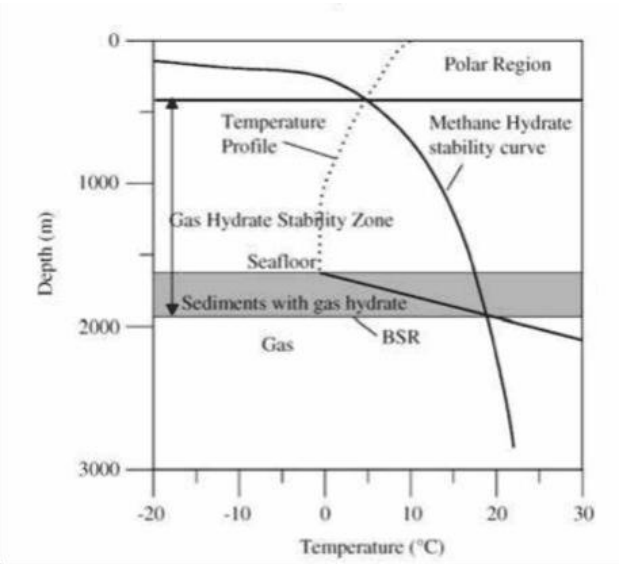

Fig 1.2: Schematic diagram showing the gas hydrate stability field in Polar Regions, this example is from offshore Norway (Chand & Minshull, 2003). Figure from (Chand & Minshull, 2003)

Formation of gas hydrates requires adequate natural gas and water existing at very specific pressure and temperature (Kvenvolden, 1988). The zone where the gas hydrates are stable is situated between the sediment water interface, and the sub-bottom depth where the geothermal transects the methane-hydrate-water equilibrium curve, (Fig 1.2) (Kvenvolden, 1988). Due to these restricted conditions the gas hydrates are confined to the upper few hundred meters of sediments, called the gas hydrate stability zone (GHSZ) (Hustoft *et al.*, 2009). Settings determining the GHSZ thickness are the temperature of the ocean bottom waters, geothermal gradient, salinity of the formation water, gas composition and varying sea level (Bunz & Mienert, 2004; Sloan, 1990).

In Arctic regions gas hydrates occur in deep-sea sediments or shallow seafloor, they are an enormous potential seepage source (Milkov *et al.*, 2004). Methane originates from free gas below the BSR (bottom-simulating reflectors) or by being released from gas hydrate dissociation (due to e.g. climatic warming, sea level fall) (Paull *et al.*, 1991).

On seismic profiles the presence of gas hydrates creates an anomalous seismic reflector, referred to as bottom-simulating reflectors (BSR), where the base mimics the seafloor but with a polarity reversal (Hustoft *et al.*, 2009; Kvenvolden, 1988). The BSR generally corresponds to the base of the GHZS and is the result of an acoustic impedance contrast between hydrate bearing sediments and free gas trapped in the sediments underneath gas hydrates (Hustoft *et al.*, 2009; Kvenvolden, 1988). As a result of its pressure-temperature dependence the BSR often mimics the seafloor thereby crosscutting stratigraphic horizons (Chand & Minshull, 2003).

1.3 Methane

The chemical compound methane, CH_4, is the simplest hydrocarbon consisting of one carbon atom covalently bound with four hydrogen atoms in a tetrahedron (Wheeler & Stadnitskaia, 2011). Methane is a strong greenhouse gas, causing 25 times more effect than CO_2 but it is also important player in the global carbon circle, it is common and widespread beneath the seafloor. Due to the large amount of methane stored in the gas hydrates, it is an important reservoir for organic carbon (Kvenvolden, 1998).

Methane is mainly a product of the alteration of organic matter in different temperature regimes, termed as biogenic methane (Schoell, 1988). Organic matter, made up by hydrogen and carbon molecules is a product formed during photosynthesis, and later enters the marine food chain. When the organism dies the organic matter is decomposed by microbial decay, to simpler hydrocarbon compounds near the seabed and this process produces microbial methane (Judd *et al.*, 2002). Generation of hydrocarbons and formation of thermogenic methane is a result of thermal break-down of buried organic matter, depending on the depth of burial. The microbial and thermogenic methane have a specific stable carbon isotopic composition, which is used when distinguishing the source of the methane (Schoell, 1988).

1.3.1 Microbial methane

Microbial methane is a product of the process where methanogenic archaea decompose the organic matter involving a consortium of diverse microorganisms. It occurs mainly at relatively shallow depths within sediments where sulfate levels have been depleted by the activities of sulfate-reducing bacteria (Judd *et al.*, 2002). Biogenic methane is highly fractionated and has $\delta^{13}C$ ranging from= -50‰ to -110‰ (Whiticar, 1999).

1.3.2 Thermogenic methane

The thermogenic methane is generated when organic matter is buried deep enough and experience temperatures from 80-150°C. The organic matter is altered by high pressure and high temperature and is transformed into methane (Kvenvolden, 1988). Thermogenic methane is isotopically less fractionated than biogenic methane, and has $\delta^{13}C$ ranging from= -20‰ to -50‰ (Whiticar, 1999)

After the formation, the methane starts migrating towards the sediment surface because of buoyancy. The gas could be present in solution in the pore water, or as free gas phase (bubbles), both phases are lighter than normal pore water and therefore they will start ascending to the surface (Park *et al.*, 1990).

1.3.3 Cold seeps

It has become clear that the migration of fluids (most significantly methane) is a very important and ongoing geological process (Judd *et al.*, 2002). Features such as shallow gas accumulations, pockmarks, seeps, mud volcanoes and gas hydrates, often associated with cold seep communities and methane-derived authigenic carbonate (MDAC), are present in a world wide variety of environments; nearshore, continental shelf to the deep ocean (Judd *et al.*, 2002).

Hydrocarbon-rich fluids are referred to as cold seeps to separate them from hot and CO_2-rich hydrothermal vents found at mid-ocean ridges and at sites of submarine volcanic activity. Cold methane-rich seeps occur at passive continental margins and slopes, up to water depths of 3.000 m (Judd & Hovland, 2007). Chemosynthesis-based benthic communities are found in the cold seep environments, as the fluids are the principal source of energy for the species (Sibuet & Olu, 1998)

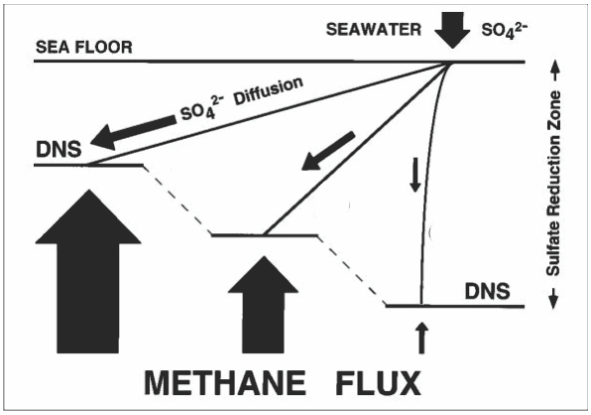

Fig 1.3: Schematic diagram showing how the depth of the SMTZ varies with the intensity of the methane flux. Figure modified from (Borowski et al., 1996).

1.3.4 SMTZ – sulfate-methane transition zone

The sulfate-methane transition zone (SMTZ) is a horizon within the sediments, where sulfate-reducing bacteria (SRBs) and the methanotrophic archaea in consortium utilize the upward diffusing methane from deeper sources (Borowski *et al.*, 1996; Peckmann & Thiel, 2004). The depth of the SMTZ and sulfate-profile are regulated by the intensity of the upward methane flux, if the sediment characteristics and sulfate diffusion from seawater into the sediment are considered constant, see Fig 1.3 (Consolaro *et al.*, 2015). This microbial consortium causes methane oxidation generation of carbonate alkalinity that in turn results in precipitation of authigenic carbonates in situ, referred to as methane-derived authigenic carbonates (MDAC) (Peckmann *et al.*, 1999; Ritger *et al.*, 1987).

1.3.5 Methane-derived authigenic carbonates

Within the SMTZ there is a phenomenon resulting in the precipitation of methane-derived authigenic carbonates (MDAC) (Reeburgh, 1980); the combined effect of anaerobic oxidation

of methane (AOM) and sulfate reduction in these anoxic sediments facilitates the precipitation of carbonates. The process is not fully understood but it is accepted that the coupling of microbial activity where methane oxidizing archea and sulfate-reducing bacteria utilize the upward flux of methane (CH_4) and sulfate (SO_4) from downward diffusing seawater, which increases the alkalinity and results in carbonate precipitation (Niewöhner *et al.*, 1998; Peckmann & Thiel, 2004). The following net reaction given by (Devol & Ahmed, 1981; Devol *et al.*, 1984; Reeburgh, 1980) showing this coupled sulfate-methane reaction and the increase of carbonate alkalinity by the production of bicarbonate (HCO_3^-).

$CH_4+SO_4^{2-}\rightarrow HCO_3^-+HS^-+H_2O$ (Equation 1)

Which favors the precipitation of authigenic carbonates:

$2HCO_3^-+Ca^{2+} \leftrightarrow CaCO_3+CO_2+H_2O$ (Equation 2) (Feng & Roberts, 2011).

MDAC are common features of methane seeps at any water depth (Judd & Hovland, 2007) where there is, a relatively slow but pervasive upwards flow of methane-charged fluids (Luff, Roger *et al.*, 2004). The microbes in the SMTZ can consume up to 90% of the methane in the sediments (Niewöhner *et al.*, 1998). The MDAC occur as slabs, crusts and lumps in cold seep environments, both within the seafloor sediments or at the seafloor surface (due to erosion of the surrounding sediments). The MDAC comprise normal seafloor sediments cemented by the precipitated carbonate minerals (mainly calcite and aragonite, but dolomite is also found), and can also contain diagenetic pyrite (Judd & Hovland, 2007). MDAC are typically characterized by negative $\delta^{13}C$ values indicating that a significant source of carbon is the methane-derived dissolved inorganic carbon (DIC), from the AOM (Aloisi *et al.*, 2002; Ritger *et al.*, 1987). The carbon in MDAC can also include other sources than methane, resulting from mixing with seawater or with DIC from other sources during the migration of the fluids to the seep site (Ritger *et al.*, 1987). The magnitude of the $^{13}\delta C$-depletion reflects the source of methane, either microbial (-110 to -50 ‰) or thermogenic methane (-50 to -20 ‰) (Schoell, 1988; Whiticar, 1999).

The cementation, or growth of inorganic calcite crystals can occur in different crystal sizes, from micron-scale rhombs (overgrowths) filling the sediment pore space to a much larger scale (infilling cavities) (Sexton, P. F. *et al.*, 2006). Judd and Hovland (2007) also observed that the occurrences of MDAC were closely associated with the evidence of seafloor fluid flows, such as pockmarks. The MDAC mainly occur as centimeter-to-decimeter thick crusts, formed at very shallow depth in the sediments, but exposed to the seabed due to erosion or

gravitational processes (Luff, Roger *et al.*, 2004). The formation of the crusts are dependent on several parameters; sufficient amount of dissolved methane in the fluids and its flux rate, low bioturbation, and low sedimentation rates (Luff, Roger *et al.*, 2004). A several cm thick crusts can be formed within a few hundred years (100-500), due to clogging of the sediment and suppression of AOM the crust will prevent its own growth (Luff, Roger *et al.*, 2004).

1.3.6 MDAC and carbonate mineralogy

Carbonates are made up by the carbonate ion CO_3^{2-} and one or more cations (Fig 1.4). The majority of the carbonate minerals form either rhombohedral or orthorhombic crystal structures; where smaller cations such as Mg, Fe, Mn, Zn and Cu are favored in the rhombohedral structures, and the larger cations such as Sr, Pb, and Ba are favored in the larger orthorhombic structure. Calcium can form carbonates of both of the structures; calcite (rhombohedral) and aragonite (orthorhombic) (Milliman *et al.*, 2012). Sodium, magnesium, calcium, potassium, strontium, chlorine, sulfur (predominantly as sulfate), bromine and carbon (primarily as bicarbonate and carbonate) are major elements found in seawater, which contributes with more than 99,9% of the total dissolved salts in the ocean (Milliman *et al.*, 2012).

.

Element	(Common ionic state)	Atomic weight	Ionic radius (Å)
B		10.82	0.23
Fl	(−1)	19.00	1.36
Na	(+1)	22.99	0.95
Mg	(+2)	24.32	0.66
S	(+6)	32.07	0.30
Cl	(−1)	35.46	1.81
K	(+1)	39.10	1.33
Ca	(+2)	40.08	0.99
Mn	(+2)	54.94	0.80
Fe	(+2)	55.85	0.74
Ni	(+2)	58.71	0.69
Co	(+2)	58.94	0.72
Cu	(+2)	63.54	0.72
Zn	(+2)	65.38	0.74
Sr	(+2)	87.63	1.12
Ba	(+2)	137.36	1.34
Pb	(+2)	207.21	1.20

	Calcite $CaCO_3$	Aragonite $CaCO_3$
crystal system	rhombohedral uniaxial negative	orthorhombic biaxial negative
other cations	Mg, Fe, Mn, Zn, Cu	Sr, Ba, Pb, K

Fig 1.4: The most usual cations making up carbonate minerals, with their atomic weight and ionic radius. Modified figure from (Milliman et al., 2012).

The mineralogy of the carbonate crusts is generally dependent on the chemistry of the expelled fluids (sulfate concentration, alkalinity, Ca^{2+}/Mg^{2+} ratios and carbonate saturation state) (Aloisi *et al.*, 2004; Burton, 1993) so it varies widely (Ritger *et al.*, 1987). The MDACs are composed of the host sediments lithified by carbonate cement (Judd & Hovland, 2007).. Authigenic pyrite is also a common feature in the crusts, dissolved iron from detrital minerals reacts with hydrogen sulfide (a product from the bacterial sulfate reduction) and precipitates pyrite during the AOM in an anoxic environment (Cremiere *et al.*, 2016b; Luff, Roger *et al.*, 2004; Ritger *et al.*, 1987). The most common composition of modern carbonate sediments are calcite (commonly separated into low-Mg calcite and high-Mg calcite) or aragonite (Aloisi *et al.*, 2000; Burton, 1993), but dolomite occurs as well (Peckmann & Thiel, 2004).

The different carbonate phases reflect changes in the seep environment. Conditions favoring precipitation of aragonite over Mg-calcite are when the levels of sulfate concentrations are relatively high, in combination with high methane flux in shallow subsurface sediments. Mg-calcite forms deeper within the sediments where the levels of sulfate are lower and the AOM with the following carbonate precipitation are slower (Aloisi *et al.*, 2000; Crémière *et al.*, 2016). It is also accepted that hydrated Mg^{2+} ions have an inhibiting effect on the calcite structure, which also facilitates precipitation of aragonite (Aloisi *et al.*, 2002; Ritger *et al.*, 1987). Presence of aragonite will give a peak in strontium concentrations compared to Mg-calcite (Ritger *et al.*, 1987).

1.4 Foraminifera

Foraminifera are single celled organisms that belong to the order protozoa; they live either in the water column, (planktonic species) or, at the seafloor (benthic species). Foraminifera can be found in nearly every marine environment; from fresh water to the deep sea, and from tropical to Arctic areas. They have adapted to tolerate different salinities and temperatures, they can be found in saltmarshes, shallow brackish water in estuaries, in the deep ocean or on the seafloor on the continental shelf (Armstrong & Brasier, 2005). They constitute the most diverse group of shelled microorganism and have a spectacular fossil record (Sen Gupta, 2003). Today most of the foraminifera are benthic species, only 40-50 of the species are planktonic (Sen Gupta, 2003). The majority of the species build the tests with calcium carbonate, $CaCO_3$, but there are three different basic wall compositions, organic, agglutinated and secreted calcium carbonate (or more rarely silica) (Armstrong & Brasier, 2005). When

foraminifera calcify their test, they incorporate chemical and isotopic signals from ambient seawater which makes them very useful tools for paleoceanographic studies (Armstrong & Brasier, 2005).

1.4.1 Benthic foraminifera

Benthic foraminifera are amongst the most abundant and diverse group of shelled microorganisms in the marine environment (Sen Gupta, 2003). Benthic foraminifera live at the seafloor, either on sand, rocks, mud and plants (epifauna), or in the pore space of the (from 1 to 20 cm bsf, below seafloor) sediment (infauna). In marine environment the distribution of benthic foraminifera is mainly affected by food availability, substrate type, water salinity and temperature and the amount of dissolved oxygen (Murray, 2006).

Benthic foraminifera can have different kind of tests. Agglutinated foraminifera form the test of either random or specific grains (in terms of mineralogy, grain size), or the shells of other microorganisms bound together by an organic, calcareous or ferric oxide cement (Armstrong & Brasier, 2005).

Organic-walled forms have tests of protinaceous mucopolysaccharide i.e. the allogromina and do not preserve well in the fossil record (Sen Gupta, 2003) and will not be further discussed in this thesis.

The majority of the foraminifera secrete their tests of calcite, and they are subdivided into three main types; microgranular, porcelanous and hyaline (Armstrong & Brasier, 2005). Microgranular forms comprises microgranular calcite with mural pores, which gives them a fibrous appearance (Armstrong & Brasier, 2005). Porcelanous tests do not contain pores, and are distinctively milky white while inspected in reflected light. They comprises small needles of high-Mg calcite (Armstrong & Brasier, 2005). Hyaline forms have a characteristic “glassy” and perforated look when studied with reflected light, but the clarity could be obscured by ornamentation and diagenesis. The tests could either be of low/to high-Mg calcite or aragonite (Armstrong & Brasier, 2005).

1.4.2 Planktonic foraminifera

Planktonic foraminifera live in the surface layer of the open ocean (0-200 m), the majority are found in the photic zone (Sen Gupta, 2003). The mixed layer and the upper thermocline are the most densely populated, while virtually no living individuals are found at depths below 1,000 m (Vincent & Berger, 1981).

1.4.3 State of alteration

The alteration of the tests varies on the different compositions. Agglutinated tests with organic cement or loosely attached grains will disintegrate during diagenesis or in many sedimentary environments (Sen Gupta, 2003). Both planktonic and benthic types of pristine tests are smooth even to a submicrometer scale, cross sections of the test walls have a pervasive microgranular structure (Sexton, P. F. *et al.*, 2006). During diagenetic alteration or burial within the SMTZ and affected by AOM and carbonate precipitation, the tests could experience alterations to the pristine characteristics due to "neomorphism", a process where a particular mineral (in this case biogenic calcite) is replaced by the same mineral but with different crystal form (inorganic calcite) (Sexton, P. F. *et al.*, 2006) which will be referred to as recrystallized. Another diagenetic process is the addition of new inorganic calcite, or cementation. During cementation, growth of inorganic calcite crystals can appear on the foraminifer test or as infilling of the chambers (Sexton, P. F. *et al.*, 2006). Both recrystallization and overgrowth will overprint the primary stable isotopic values within the test. Upon formation of micron-scale overgrowths the pristine "glassy" appearance of the tests will be altered to a "frosty" look (Drury *et al.*, 2014; Sexton, P. F. *et al.*, 2006) when viewed under the microscope. The term "glassy" is based on the appearance of the test seen in the living as well as in the unaltered tests of the majority of the foraminifera. The "glassy" test is translucent (under a reflected light microscope) and retain the smooth test walls as well as the primary microstructure. Whereas the "frosty" test appears opaque (when viewed in a reflected light microscope) due to inorganic calcite crystals overgrowth on the inner and outer test walls (Drury *et al.*, 2014; Sexton, P. F. *et al.*, 2006).

1.5 Foraminifera and methane

Several species have adapted to live in extreme natural environments, such as habitats near bacterial mats at hydrocarbon vents, not as exotic species but they are recruited from the "normal" surrounding areas (Sen Gupta, 2003). Bacterial mats within the seep area provide an important food source for the foraminifera (Torres *et al.*, 2003). Benthic foraminifera are common in methane seep environments, and it is observed low $\delta^{13}C$ values in their tests, due to ingested microbes which utilize the dissolved inorganic carbon (DIC) from AOM in the surrounding sediments and further incorporated in the secreted tests (Barbieri & Panieri, 2004; Panieri *et al.*, 2009). In methane seep environments, the carbon isotopic signature of DIC in sediment pore waters and sometimes overlying seawater is dramatically ^{13}C-depleted

($\delta^{13}C_{DIC}$ can be lower than -40‰) (Torres *et al.*, 2003) relative to the normal marine environment (-1‰ to 1‰) (Ravelo & Hillaire-Marcel, 2007).

Because the planktonic foraminifera live in the surface layers in the ocean, they are normally unaffected by the methane seepages. If the flux of methane is high enough to escape the seafloor; it will be consumed by methanotrophic aerobic microbes near the seafloor or in the adjacent water column (Niemann *et al.*, 2006). For that reason, planktonic foraminifera do not usually show negative, methane-related $\delta^{13}C$ value. But both planktonic and benthic tests can be altered when the tests are deposited and buried through the SMTZ, and the AOM process leads to precipitation of diagenetic carbonates, which induces MDAC and can cause carbonate overgrowth on the tests of the foraminifera (Fig 1.5) (Consolaro *et al.*, 2015; Panieri *et al.*, 2009).

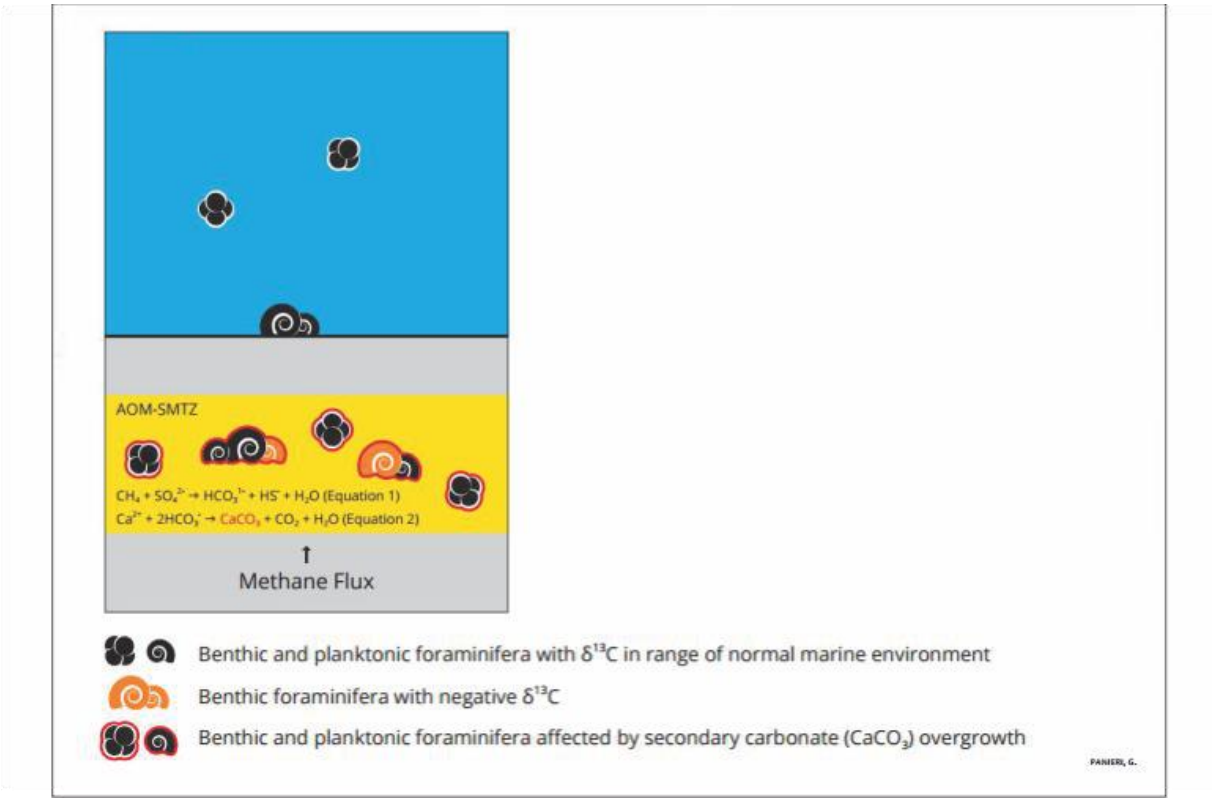

Fig 1.5: Schematic diagram showing a scenario where both planktonic and benthic show low $\delta^{13}C$ values. When the methane flux is low and the downward flux of sulfate encounters the upward flux of methane within the SMTZ, the AOM generated bicarbonate will induce precipitation of MDACs and carbonate overgrowth on the tests of the foraminifera (Consolaro et al., 2015). Edited figure from (Consolaro et al., 2015)

1.5.1 Recent studies

In the recent years, the scientific attention regarding methane has increased due to its effect on the global climate. The total emissions of methane add up to ~600Tg Ch_4/year globally where

5-10% of the current atmospheric input origins from geologic reservoirs on the seafloor (Milkov, 2004; Torres *et al.*, 2010). Studies of ancient seep environments and fossils have shown that these chemosynthesis-based paleoenvironments have been diverse and variable, in terms of both geologic settings and taxonomic compositions through more than 3 billion years (Campbell, 2006). Understanding modern seep environments gives a better understanding of fossil seep environments and its fauna (Campbell, 2006; Panieri *et al.*, 2012). Proxies using foraminifera as methane release indicators have been developed and calibrated; including the "biotic" record based on incorporation of methane-derived DIC by foraminifera; and the "abiotic" record found in methane-derived authigenic carbonates (Torres *et al.*, 2010). Precipitated carbonates from AOM in seep environments exhibit negative $\delta^{13}C$ signatures ($\delta^{13}C_{DIC}$ can be lower than -40‰) (Campbell, 2006; Peckmann & Thiel, 2004).

Benthic foraminifera are useful proxies of local methane emissions (Barbieri & Panieri, 2004; Panieri *et al.*, 2012; Panieri *et al.*, 2009). Whereas living planktonic foraminifera rarely experience the direct effects from methane seeps, because the methane is predominantly utilized by microbes before it reaches the water column (Niemann *et al.*, 2006). Post depositional alteration by formation of high-Mg calcite overgrowth on both planktonic and benthic tests also reflects the influences of methane seepages (Consolaro *et al.*, 2015; Torres *et al.*, 2010). Several studies aim to reconstruct past marine methane emissions and modern methane seepages by examining the carbon isotope composition ($\delta^{13}C$) of the foraminifera (Barbieri & Panieri, 2004; Consolaro *et al.*, 2015; Panieri & Sen Gupta, 2008).

Another proxy for methane emissions are the methane-derived authigenic carbonates (Torres *et al.*, 2010). They comprise the seafloor sediments and the biogenic debris lithified with carbonate cement (Judd & Hovland, 2007). Because the carbon in the MDAC is derived from the metabolic activities of microbes utilizing the methane, the MDAC have negative $\delta^{13}C$ values (Reeburgh, 1980). The different carbonate phases in MDAC could reflect different methane flux rates, with higher flux favoring aragonite as the precipitation occurs close to the sediment-water interface under relatively more open, seawater influenced conditions, whereas Mg-calcite reflects precipitation at greater depths at reduced methane flux (Cremiere *et al.*, 2016b). MDAC in the stratigraphic records can be used as an evidence of methane seepage; but since they from in the diagenetic environment post-dating the sedimentation, the assignment of the MDAC to specific, temporarily constrained seepage episodes may be difficult (Torres *et al.*, 2010).

2 Study areas

In this thesis, there are two different study areas, which will be described in the following chapters.

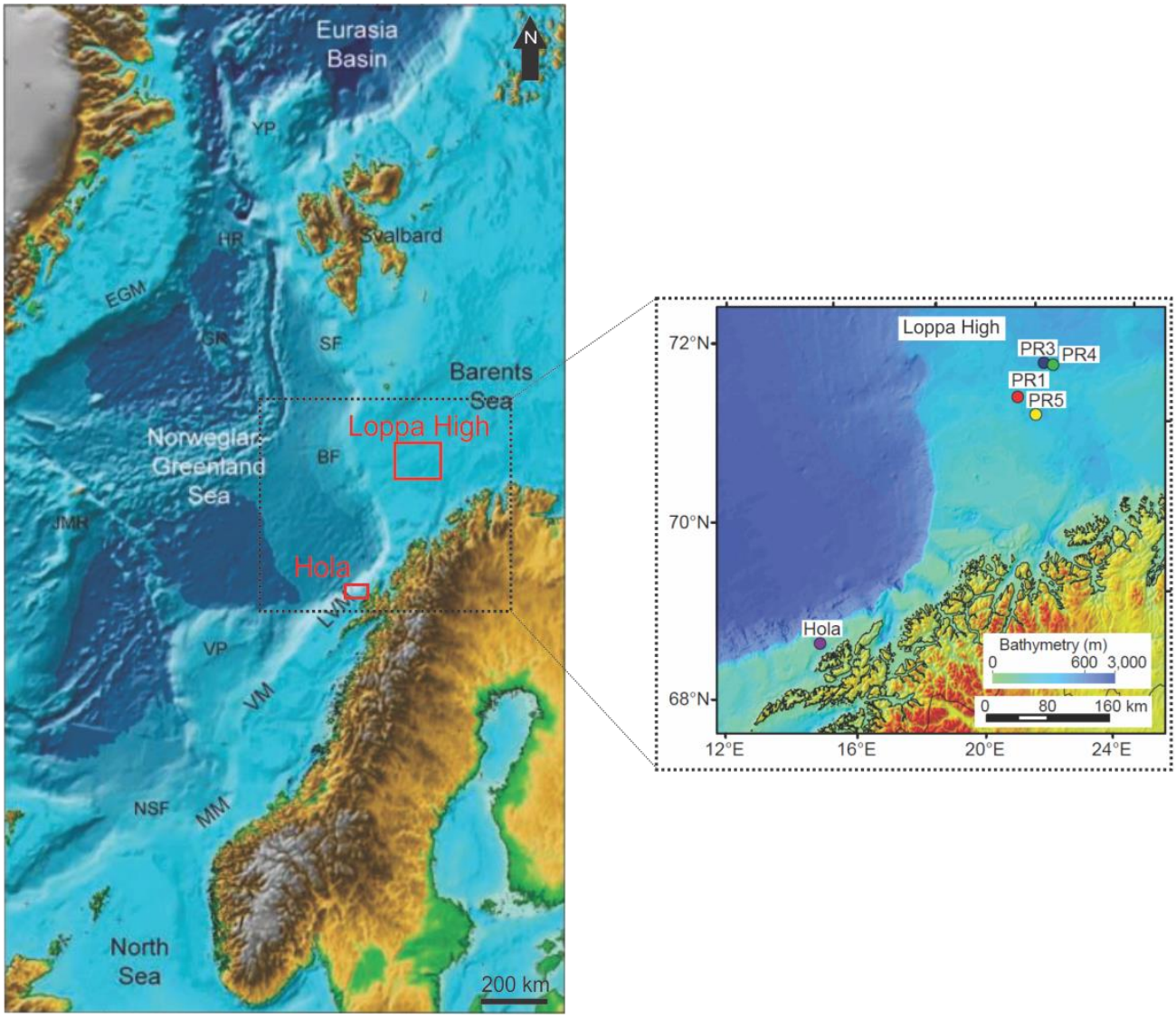

Fig 2.1: Overview of the study areas Loppa High and Hola marked in each respective red square, edited figure from (Faleide et al., 2008). Black dashed line show a close-up of the sample sites at the study areas, edited figure from (Cremiere et al., 2016a).

2.1 Barents Sea

The Barents Sea is a relatively shallow epicontinental sea with water depths ranging from 200-500 m, and the average depth is approximately 230 m. It covers an area of $1.3 * 10^6$ km^2 so it represents the largest continental shelf on the globe (Dore, 1995). It is bounded to the west and the north by continental slopes, to the east by Novaja Zemlya and to the south by the Norwegian mainland and the Kola Peninsula, Fig 2.1.

Barents Sea is characterized by relatively shallow banks separated by deep troughs, making the bottom topography highly irregular. The present day topography is influenced partly by the underlying bedrock, provided by the Caledonian Orogeny, but it is highly affected by a complex combination of large-scale plate movements, varying climatic and depositional processes and further moulded by late Cenozoic glacial erosion (Faleide *et al.*, 1996).

The Norwegian mainland located to the south of the Barents Sea is a part of the Fennoscandian Shield that consists of Archean and Paleoproterozoic rocks, and also Neoproterozoic-Early Paleozoic rocks of the Caledonides, that extend several tens of km offshore on the continental shelf (Siedlecka & Roberts, 1996; Sigmond *et al.*, 2002). Seaward-dipping sedimentary sections of Late Paleozoic and younger age appear further offshore (Bugge *et al.*, 1995). The Barents Sea comprises an almost complete sequence of sedimentary strata ranging from Late Paleozoic to Quaternary, locally exceeding 15 km in thickness (Gudlaugsson *et al.*, 1998).

One important geological factor is the uplift and erosion during the Cenozoic (Reemst *et al.*, 1994), the most recent occurred during the glacial period in Pliocene-Pleistocene. The glaciation with the following erosion affected the sedimentation and erosion over the entire area of the SW Barents Sea (Laberg *et al.*, 2012; Sættem *et al.*, 1991). The grade of uplift varied in the different areas of the Barents Sea; the lowest values (<500m) in southwest, (500-1000 m) on Loppa High, and increasing uplift and erosion towards the north and northwest (>2000 m) on the Stappen High (Larsen *et al.*, 2003). The uplift resulted in the removal of 1-2 km of sedimentary overburden, which led to cooling of source rocks below the shelf as well as changes of the flow regime (Henriksen *et al.*, 2011). The uplift also facilitated fluid migration from the seafloor subsurface and escaping of fluids into the water column (Nøttvedt *et al.*, 1988).

A glacial erosion surface (Upper Regional Unconformity, URU) separates the sub-horizontal Quaternary succession from sedimentary bedrock (Laberg *et al.*, 2012). Glacially derived diamictic sediments mainly make up this succession with varying thickness (>10-<200 m) (Sættem *et al.*, 1991). The western part of the shelf was ice covered 2-3 times during the Late Pleistocene glaciations (Vorren *et al.*, 1988; Winsborrow *et al.*, 2010), and large geomorphological features on the seabed were made by the Late Weichselian Ice Sheet (Andreassen *et al.*, 2008; Ottesen *et al.*, 2008).

2.1.1 Gas in the Barents Sea

Geological and geophysical studies of the Barents Sea started in the 1970s, in 1980 hydrocarbon exploration drilling started, and the first gas discoveries were made in 1981 (Dore, 1995). In 1984 the Snøhvit field was discovered, and it is still the largest gas and oil discovery in the Norwegian Barents Sea, it contains mainly gas in reservoir rocks of Middle Jurassic age (Dore, 1995).

During the last glacial maximum (LGM) 18.000-20.000 ^{14}C ago, modelling shows that the ice cap covering the Barents Sea was at least 1200 m thick (Siegert *et al.*, 2001). Under these conditions of glacial loading, the methane hydrate stability zone (MHSZ) would have been present over the entire SW Barents Sea to at least 600 m below the present seafloor (Chand *et al.*, 2012). It is therefore assumed that the retreat of the glaciers made the gas hydrates that formed during the last glaciations unstable and dissociated methane gas lead to fluid seepage and expulsion into the water column, which lasted until recently (Chand *et al.*, 2012).

According to Rise *et al.* (2014) the shallow gas in the Barents Sea could be of mixed origin; both sourced from shallow microbial alternation of organic matter and thermogenic deep strata.

The study area Loppa High is located in the southwestern part of the Barents Sea; which is divided into four main basins; Bjørnøya, Tromsø, Hammerfest and Nordkapp, with intervening structural highs; Senja Ridge, Loppa High and Veslemøy High (Fig 2.2).

2.1.2 Loppa High

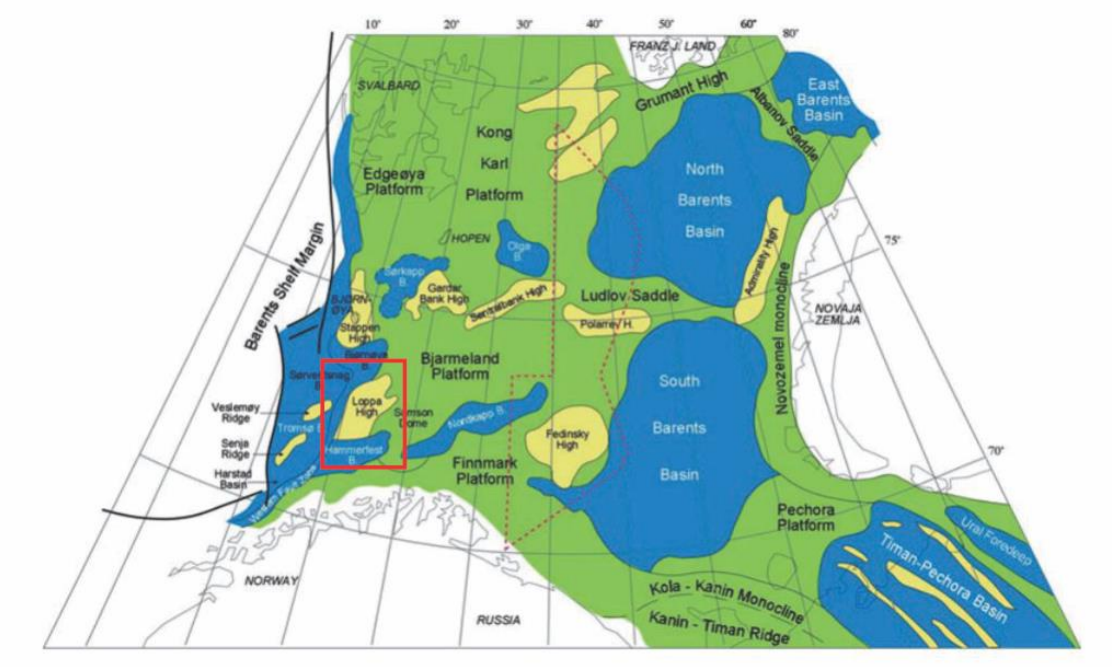

Fig 2.2: The main elements of the southern Barents Sea, Loppa High is located within the red rectangle. Modified figure from (Worsley, 2008).

Loppa High is an isolated N-S trending structural high, located on the shelf in the southern part of the Barents Sea. It is one of the main structural elements in the area; others are The Hammerfest and Nordkapp Basins, the Finnmark and Bjarmeland Platforms, including several other smaller structural elements. Dividing and bordering these elements are a series of complex fault zones; Troms-Finnmark, Ringvassøy-Loppa, Bjørnøyrenna, Måsøy, Nysleppen and Asterias Fault Complexes (Fig 2.2).

Loppa High is situated between fault complexes and basins; in the south it is bounded by the Hammerfest Basin and the Asterias Fault complex, and by the Tromsø and Bjørnøya basins to the west (Gabrielsen *et al.*, 1990). The northeastern limit is defined by the Svalis Dome (a major salt structure) and its rim syncline; the Maud Basin (Gabrielsen *et al.*, 1990).

Loppa High's geological history is complex; indicated by strong erosional events at several stratigraphic levels (Sund, 1984), starting back to the Carboniferous. There have also been several phases of uplift/subsidence and subsequent tilting. The Loppa High is a result of late Jurassic to early Cretaceous and late Cretaceous-Tertiary tectonism (Gabrielsen *et al.*, 1990). Early Carboniferous terrigenous clastics were onlapped by Upper Carboniferous and Permian Carbonates which were eroded during Early Triassic (Wood *et al.*, 1989), due to the uplift and tilting of Loppa High, and were onlapped by sequences of Lower to Middle Triassic. During Late Jurassic to Early Cretaceous the Loppa High experiences another uplift which lead to

erosion of Jurassic sediments (Wood *et al.*, 1989). Loppa High became an island, which led to erosion of exposed Jurassic and Triassic sediments. It gradually subsided and the crest was onlapped during the Early Paleocene when the Loppa High was submarine again. In Tertiary Loppa High again experienced uplift and erosion as a result of a combination of thermal uplift due to the evolution of the ocean basin and a general fall in sea level (Haq *et al.*, 1987). The erosion formed an unconformity with Tertiary and older sediments below, with overlying Quaternary glacio-marine sediments; this was the last stage of the formation of the present day structure of Loppa High (Wood *et al.*, 1989).

2.1.3 Gas in Loppa High

The Loppa High has a fair potential for oil and gas exploration, in the late 1980s there were uncertainties about reservoir rocks and the hydrocarbon migration, but in 2013 there were a new discovery of oil and gas in Late Permian carbonate rocks; the Gotha discovery (published by Lundin in 2013).

At the NW flank of the Loppa High pockmarks occur where the water depth exceeds 400 m (Chand *et al.*, 2012)

2.2 The Lofoten-Vesterålen Margin

Three main segments, each approximately 400-500 m long, comprises the Mid-Norwegian margin; Møre, Vøring and Lofoten-Vesterålen (LVM). The Hola trough is situated in the Lofoten-Vesterålen margin, see Fig 2.1. Compared to the adjacent areas the LVM is barely investigated, because it is not yet opened to petroleum exploration (Færseth, 2012).

The continental margin off Lofoten, Vesterålen and Troms is an approximately 400 km long segment, which possess a great variation of marine landscapes which were largely influenced by previous glaciations and oceanographic processes by different water masses (Harris & Baker, 2012). It is characterized by a narrow shelf and a steep slope (Faleide *et al.*, 2008)

On the LVT there are several troughs formed during LGM, separating banks and plains. They are generally over-deepened, and when the width are a few km the trough is able to disturb the dynamic balances that forces water flow to follow bathymetry contours (Harris & Baker, 2012). Due to the flow strength in the troughs the most common sediments in the troughs are sand and gravelly sand, but some areas in the troughs could be covered by gravelly sand mud, or sandy mud as a result of a lower energy environment. On the outer part of the troughs there are commonly till/moraine material (Harris & Baker, 2012).

According to Rise *et al.* (2005) the present-day morphology of the mid-Norwegian continental shelf is mainly the result of a fast progradation of the shelf during the last 3 million years. Compared to wider adjacent shelves off mid-Norway and in the Barents Sea the LV continental shelf is narrow (Rise *et al.*, 2013). The shelf width in the south is 90 km and becomes progressively narrower towards the north (30 km). The water depths varies, on the Lofoten shelf it reaches 100-200 m with locally deeper troughs, but off Vesterålen the banks are shallower (50-100 m) intersected by well-defined troughs (Rise *et al.*, 2013), the deepest is Hola where the maximum depth reaches 270 m (Boe *et al.*, 2009).

The Norwegian shelf comprises sediment strata from Triassic to Pliocene (Rokoengen *et al.*, 1988; Sigmond, 1992).

The last major shaping of the shelf topography took place during the Late Weichselian glaciation, the evidence is geomorphological structures as several types of morainic ridges and glacial lineations (Ottesen *et al.*, 2005). The ice retreated towards the coastal areas 13.000 years ago and the topography has remained nearly unchanged, except from places where major slides occurred (Aarseth, 1997).

2.2.1 Hola

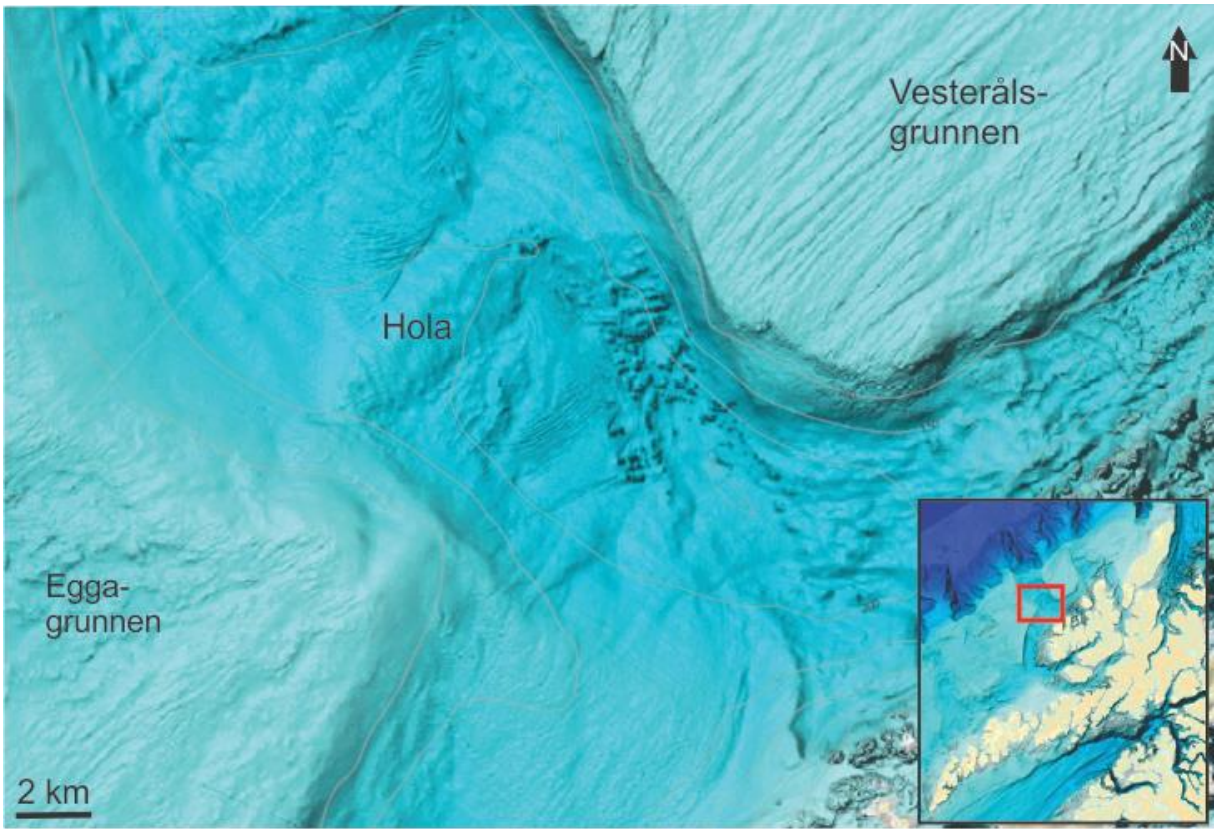

Fig 2.3: Map of the Hola trough located between Vesterålsgrunnen and Eggagrunnen, the location is shown on the overview map within the red square. Location and bathymetry of the Hola trough. Situated offshore of the Coast of Vesterålen, North Norway. Edited map from Mareano/Kartverket.

The study area is located on the continental shelf about 20 km from Vesterålen, and 25 km from the shelf break (Fig 2.3). Compared to the Barents Sea that has been an interest for the petroleum industry for many years, this area is barely investigated. The Hola trough is confined by the shallower banks; Vesterålsgrunnen to the NE and Eggagrunnen to the SW, see Fig 2.3. The trough was formed during the last ice age. The water depth varies from 75 m to 270 m, and the seafloor is relatively flat (Boe *et al.*, 2009). Other interesting geomorphological features located in the trough are two moraine ridges, four major sand wave fields, and the presence of more than 300 coral reefs making a positive relief to the rather flat seafloor (Boe *et al.*, 2009). Mareano has also located several gas seeps with relating carbonate crusts and bacterial mats. Troughs in general have strong currents and areas with sand in motion, this results in scarce fauna (Harris & Baker, 2012).

2.2.2 Gas in the Hola area

During Mareanos autumn cruise onboard G.O. Sars, 2007, echosounder data were collected from Hola. In an area with corals there were also gas bubbles ascending in the water column. The origin of gas leaking from the seafloor here is not known, but results from shallow drilled

wells has shown potential Jurassic reservoir and source rocks. Some of the rocks contains high organic content which may produce gas and oil (Hovland, 2008). According to (Boe *et al.*, 2009) there have been mapped large faults in the subsurface, where the gas could possibly migrate along this faults where open cracks may occur.

2.2.3 Geological history

Interpretation of commercial seismic data by (Boe *et al.*, 2009), has shown that the sedimentary rock succession offshore Vesterålen comprises (from base upwards);

- a) Precambrian basement
- b) 100 m of Lower-Middle Jurassic sandstones with coal layers,
- c) 200 m of Upper Jurassic, sandy and calcareous mudstones
- d) And 2000 m of Lower-Upper Cretaceous claystones, siltstones, mudstones and sandstones with organic rich interval

Several glacial cycles have deposited Quaternary sediments covering the bedrock (Ottesen *et al.*, 2005). The upper glacigenic sequence consists mainly of muddy diamicton or silty sandy clay with scattered gravel. Commonly the diamicton is overconsolidated, and in the bank areas there is a thin cover (<1m) of sand/gravel, in the deepest troughs the cover is finer grained; 1-5 m of m of clay/silt/sand (Hald *et al.*, 1990; Vorren *et al.*, 1989). The formation of this cover occurred mainly during the deglaciation after 15.000 ^{14}C BP, after the ice retreated at c. 10.000 ^{14}C BP only small volumes of sediments have been deposited (Hald *et al.*, 1990).

2.2.4 Present day topography and sediment distribution

The topography in the Hola trough strongly affects the distribution of the sediments covering the seabed; on the ridges and shallow bank areas coarse sediments, and lag deposits occur, in the deeper areas there are finer-grained sediments (Boe *et al.*, 2009). No mud is deposited in the Hola trough at present. According to Boe *et al.* (2009), there are two moraine ridges crossing the Hola trough, where the location is partly controlled by the underlying bedrock.

The seafloor mapping by MAREANOs cruise in 2007 onboard G.O. Sars revealed that the seafloor sediments mainly consisted of sand and gravel. They also reported that the area differs from deep basins and fjords where the currents are not so strong. In the southern part of the Hola trough (location of the sand waves) the direction of the currents are mainly towards the Norwegian mainland, the current direction is opposite in the northern part of the

trough, where the coral reefs have sediment tails pointing in the current direction (Buhl-Mortensen & Buhl-Mortensen, 2007).

2.2.5 Currents

According to Boe *et al.* (2009) the dominating currents in the area are; the Norwegian Coastal Current (NCC) and the Norwegian Atlantic Current (NWAC). The NCC follows the coast from the SW before turning eastwards into the Barents Sea. According to (Ersdal, 2001) the velocity of the NCC is variable and surface current speeds exceeding 1 m/s are frequently observed. The NWAC, which constitutes the main part of the North Atlantic Current (NAC), moves along the continental slope NE to Tromsøflaket, where it splits; one branch running towards N to Spitsbergen the other branch, travels eastwards into the Barents Sea. The large-scale topography of the continental shelf strongly influences the direction of the NWAC, which follows the 500 m contour with a maximum speed of 1.17m/s (Gjevik, 2000). Typical current speeds are 0.2-0.4 m/s (Gjevik, 1996).

3 Previous work on MDAC crusts in this thesis

Previous work on carbonate crusts studied in this thesis has been published in the recent paper; "Timescales of methane seepage on the Norwegian margin following collapse of the Scandinavian Ice Sheet" (Cremiere *et al.*, 2016a).

During the Last Glacial Maximum (LGM) the Norwegian continental shelf and the Barents Sea were covered by the Scandinavian Ice Sheet (SIS) (Landvik *et al.*, 1998; Svendsen *et al.*, 2004). Results of the Glacial loading were several; the GHSZ was extended up to 600 m below the sea floor on both of the study areas, and it reactivated widespread basement-penetrating fault systems which enhanced the migration of gas from Triassic and Jurassic source rocks and hydrocarbon reservoirs (Henriksen *et al.*, 2011). According to (Cremiere *et al.*, 2016a) the conditions during the LGM enabled the formation of wide spread gas hydrate accumulations on the seafloor, when the SIS retreaded it led to gas hydrate dissociation and release of methane, see Fig 3.1.

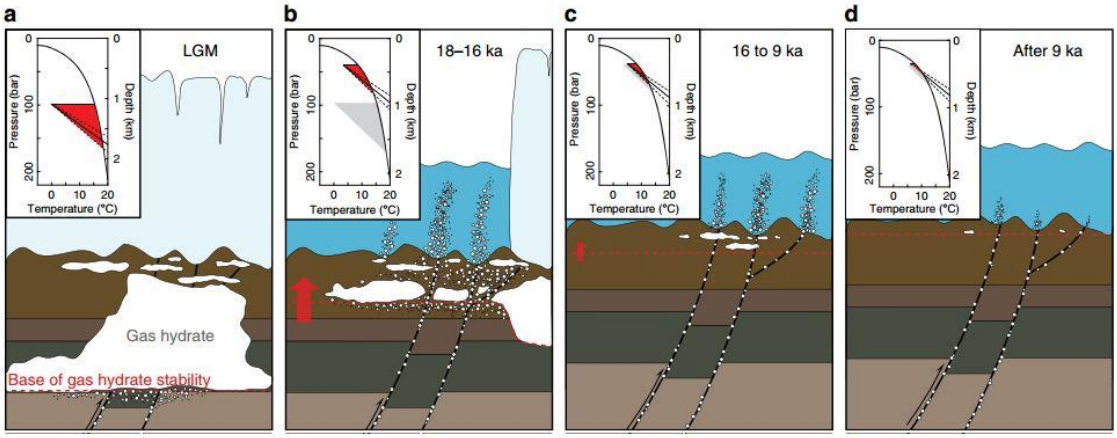

Figure 6 | Schematic sketch illustrating different snapshots of gas hydrate stability at steady state and fluid flow dynamics through time in the southwest Barents Sea shelf. (**a**) During the LGM, gas hydrate stability shown with the red area in the top-left corner was extending up to 600 m below the seabed. (**b**) Methane migrates through fractures and porous media as a result of gas hydrate dissociation triggered by grounded ice sheet retreat 18–16 ka. (**c**) Gas hydrate dissociation continues during the isostatic rebound and bottom water warming from ~16 to ~9 ka. (**d**) After ~9 ka to present, gas plumes occur locally connected to open deep-seated faults. The average geothermal gradient and associated 2σ uncertainties (31 ± 6 °C km^{-1} (ref. 52)) are shown by solid and dashed lines, respectively, at the base of gas hydrate stability fields (red areas). The red arrow depicts relative change of the base of the GHSZ (red dashed line). Temperature and pressure constraints used for assessing change in GHSZ are in Supplementary Table 3.

Fig 3.1: Schematic sketch from (Cremiere et al., 2016a).

Since the precipitation of methane-derived authigenic carbonates are a result of AOM in areas with intense methane fluxes over 100-1000 years (Bayon *et al.*, 2009). Cremiere *et al.* (2016a) dated the crusts with U-Th dating for information of the methane fluxes (Fig 3.2).

The results revealed that the release of methane (17.5 ± 0.7ka) was coincident with the retreat of the SIS (~ 18-16 ka) and deglaciation-induced pressure release and thinning of the GHSZ, and the efflux of methane continued for 7-10 kyr (Cremiere *et al.*, 2016a).

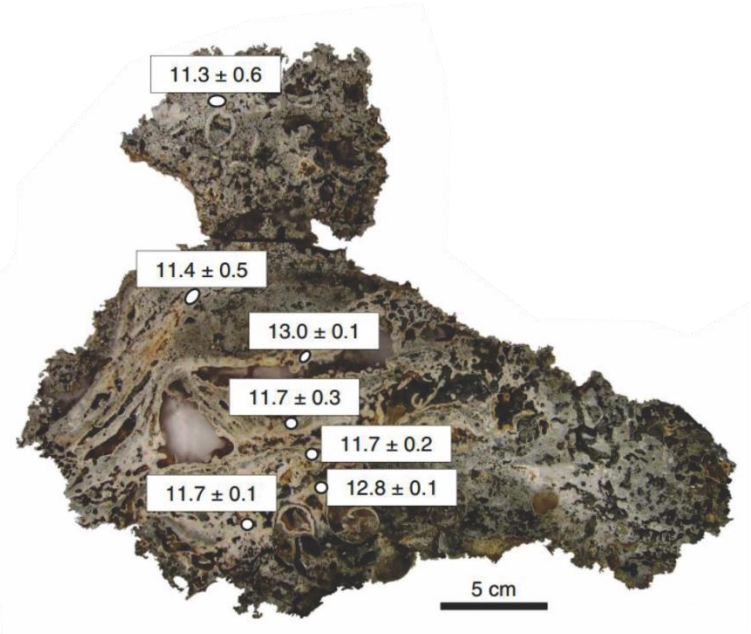

Fig 3.2: A detailed image of U-Th ages(in ka ± 2σ) from the crust P1210002 on representative cross sections, edited figure from (Cremiere *et al.*, 2016a)

Carbon isotope compositions were measured, and the carbonate $\delta^{13}C$ values ranges from -43.1 to – 13.0‰ Vienna Pee Dee Belemnite (VPDB), averaging – 32.3 ± 4.3‰ VPDB, suggesting that the principal source of methane is thermogenic due to the less depleted ^{13}C values than microbial methane (Cremiere *et al.*, 2016a).

4 Material and Methods

4.1 Thin sections

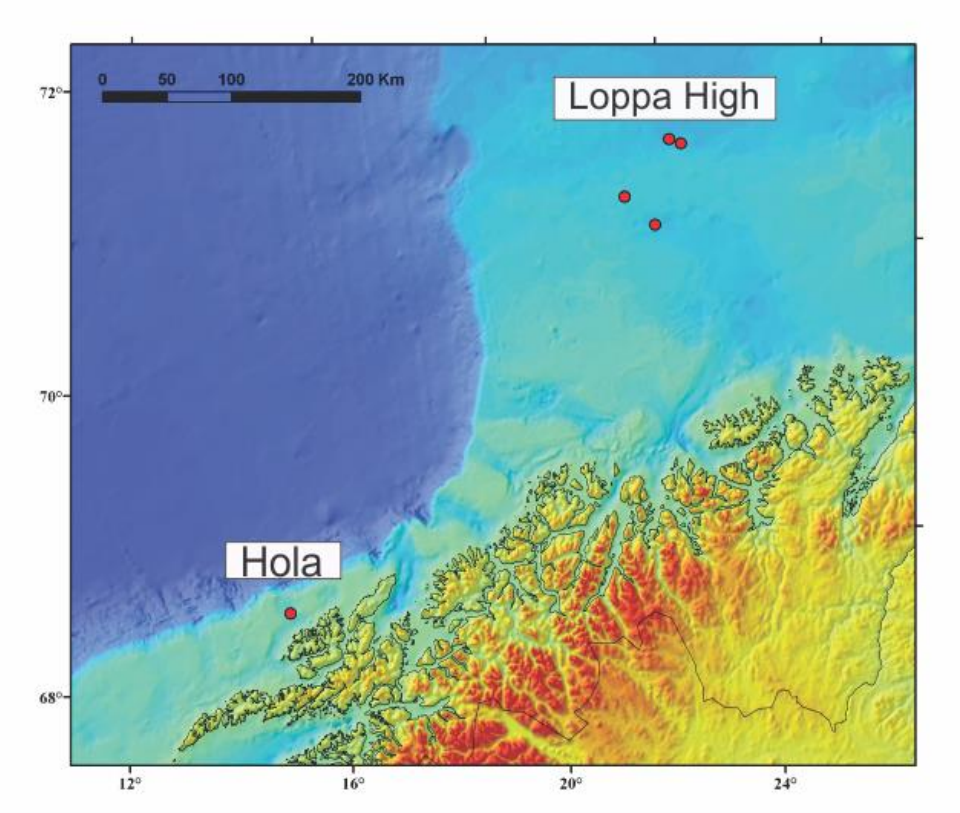

Fig 4.1: Overview of the crust sample locations. Four different locations from the Loppa High area, and one from the Hola area. Figure modified from (Cremiere *et al.*, 2016a).

Thin sections (dimensions 50mm*75mm) of methane-derived authigenic carbonate (MDAC) crusts from four seepage sites at the Loppa High in the southwestern Barents Sea and one seepage site at Hola, off Vesterålen in the Norwegian Sea (Fig 4.1). The crust samples have been collected by remotely operated vehicle (ROV) during cruises in 2011 (Hola) and 2012 (Loppa High). Loppa High sample collection includes 18 specimens of MDAC crust (up to 30 cm thick) whereas the Hola sample set includes two MDAC crusts. Up to seven polished thin sections per crust to cover the entire stratigraphy of the specimen were prepared at the laboratory at NGU. A complete list of the studied MDAC crust specimens and thin sections is provided in the appendix.

4.2 Methods

The thin sections of the carbonate crusts were analyzed using optical microscope, Wilde Heerbrugg M 400, and Scanning Electron Microscope Hitachi Analytical TableTop

Microscope/benchtop SEM TM3030 equipped with an energy-dispersive X-ray (EDS) detector by Bruker Nano GMbH, for petrographic characterization and elemental analyses of the biogenic components (foraminiferal shells, small needle-like structures, and biogenic debris) and associated carbonates that comprise authigenic carbonates and detrital sediments.

4.2.1 Scanning electron Microscope, "TM3030".

The TM3030 is a scann"A tabletop microscope operating under the principle of low-vacuum observation, a narrowly focused electron beam is directed onto the specimen, the resulting backscattered electrons are detected and minute parts of the specimen are enlarged for observation. High-magnification beyond the reach of an optical microscope" (Hitachi, 2013).

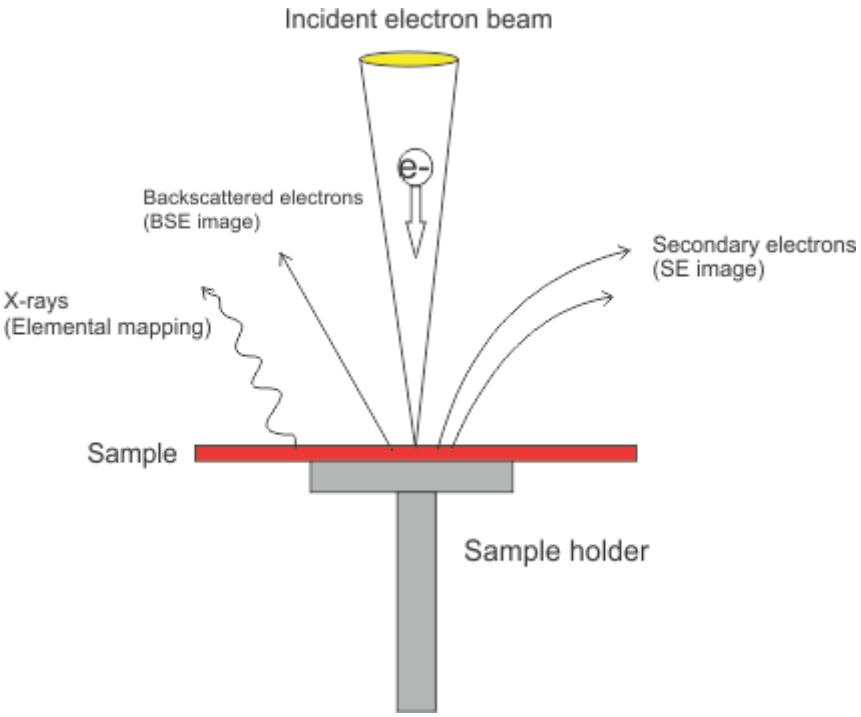

Fig 4.2: A simplified figure of how the different signals are produced when scanning a sample with a finely converged electron beam. This process takes place in a low-vacuum chamber within the SEM. Figure modified from (Hitachi, 2013)

Scanning Electron Microscope or SEM is an instrument, which produces images of a sample by scanning it with a beam of high-energy electrons in a vacuum. The different atoms in the sample interacts with the electrons, generating secondary electrons, backscattered electrons and characteristic X-ray photons (Fig 4.2). This reveals various information about the sample; morphology, chemical composition and crystalline structure.

When the sample is irradiated with the electron beam different signals are produced; secondary electrons (produced near the sample surface) forming an image with fine

topographical structure of the sample and backscattered electrons illustrating the contrasts in composition. The electron backscattering depends on the composition of the sample (average atomic number, crystal orientation etc.). The different elements have their respective atomic number based on the density, so materials with higher atomic number it will result in a higher backscatter response and brighter color on the backscatter image, and opposite applies for materials having a lower atomic number. The signals received from secondary electrons and the backscattered electrons are utilized to form the image present on the monitor screen (Bruker, 2010; Hitachi, 2013).

The SEM used in this thesis was equipped with an EDS (Energy Dispersive X-ray Analyzer), for elemental analysis, revealing the elements present in the sample by utilizing the X-rays generated by the electron beam. Artificial colors are chosen to generate element distribution map.

4.2.2 Element mapping

The element map is an image showing the spatial distribution of elements in a sample. It is produced by progressively rastering the electron beam point by point over an area of interest. The resolution is a result of beam size, and relative response of each element is determined by how long the beam dwells on each point, and the actual concentration (Bruker, 2010).

In comparison to backscatter images, the element maps show the true spatial distribution of each element of interest. They are shown in false colors to help the human eye distinguish subtle variations. The brighter the color on the element map, the higher the abundance of the specific element (Bruker, 2010).

4.2.3 Procedure

The thin sections were cleaned with ethanol and dried with the help of an air compressor prior to the work with the SEM. This was to reduce the risk of contamination by unwanted particles in the chemical analysis. The thin section was placed on a specimen holder where the working distance was set to approximately 8.5 mm. The working distance is the distance from the backscattered electron detector to the specimen, the right distance gives the most correct results when working with EDS and chemical analyses. The (SEM work undertaken in a low-vacuum mode) using un-coated thin sections. The systematic examination of thin sections started in the uppermost left corner, and to cover the whole section the observations were conducted side to side downwards. This procedure was followed for each of the studied thin sections.

Electron backscatter (BSE) images, element maps and EDS points analyses were obtained from areas of interest, primarily from areas containing foraminifera. For a good quality EDS spectrum sufficient acquisition time was needed, minimum five minutes for each target. Element maps and EDS spectra were further analyzed with the help of the software “Bruker”, where the element maps were made.

5 Results

This chapter focuses on the observations of authigenic carbonates associated with foraminifera that are based on several BSE-images, supported by EDS-analysis. The authigenic carbonates in studied MDAC crusts occur as cements filling the pore space of mud to sand size detrital sediments and biogenic debris (including foraminifera) and as cavity fills. The latter occurrence consist typically of rather impurity free clean carbonate. The characteristic examples of foraminifera embedded in authigenic carbonates are illustrated and described with detail in the following chapter whereas the further examples are presented in the appendix.

The MDAC crusts for this thesis were collected from four locations (PR1, PR3, PR4, PR5) at the Loppa High, southwestern Barents Sea and from the Hola site (Hola) - off Vesterålen in the Norwegian Sea. See Fig 4.1 for an overview map of the areas, and Table 1 for coordinates and water depths for each of the crust specimens.

Table 1 Coordinates and water depths for each crust.

Area	Sample	Latitude N (WGS84)	Longitude W (WGS84)	Water Depth (m)
Loppa High:				
PR1				
	P1210001	72° 09’ 28.5"	19° 43’ 38.5"	319
	P1210002	72° 09’ 28.1"	19° 43’ 37.7"	320
PR3				
	P1210010	72° 35’ 20.4"	20° 35’ 10.8"	403
	P1210011	72° 35’ 18.9"	20° 35’ 11.0"	403
PR4				
	P1210017	72° 34’ 03.8"	20° 52’ 21.0"	391
PR5				
	P1210032	71° 59’ 12.4"	20° 28’ 40.5"	393
	P1210036	71° 59’ 12.6"	20° 28’ 41.3"	393
Hola				
	Hola	68° 55’05.8	14° 17’ 02.6"	218

5.1 Interpretation of the electron backscatter-images (BSE), elemental maps and the EDS point-analyses

The BSE images allow to obtain an overview of compositional variability of carbonate phases on the surface of the thin section, which can be further verified using results of elemental mapping and EDS point-analysis. Following is an example of how the backscatter images combined with EDS-analysis were interpreted.

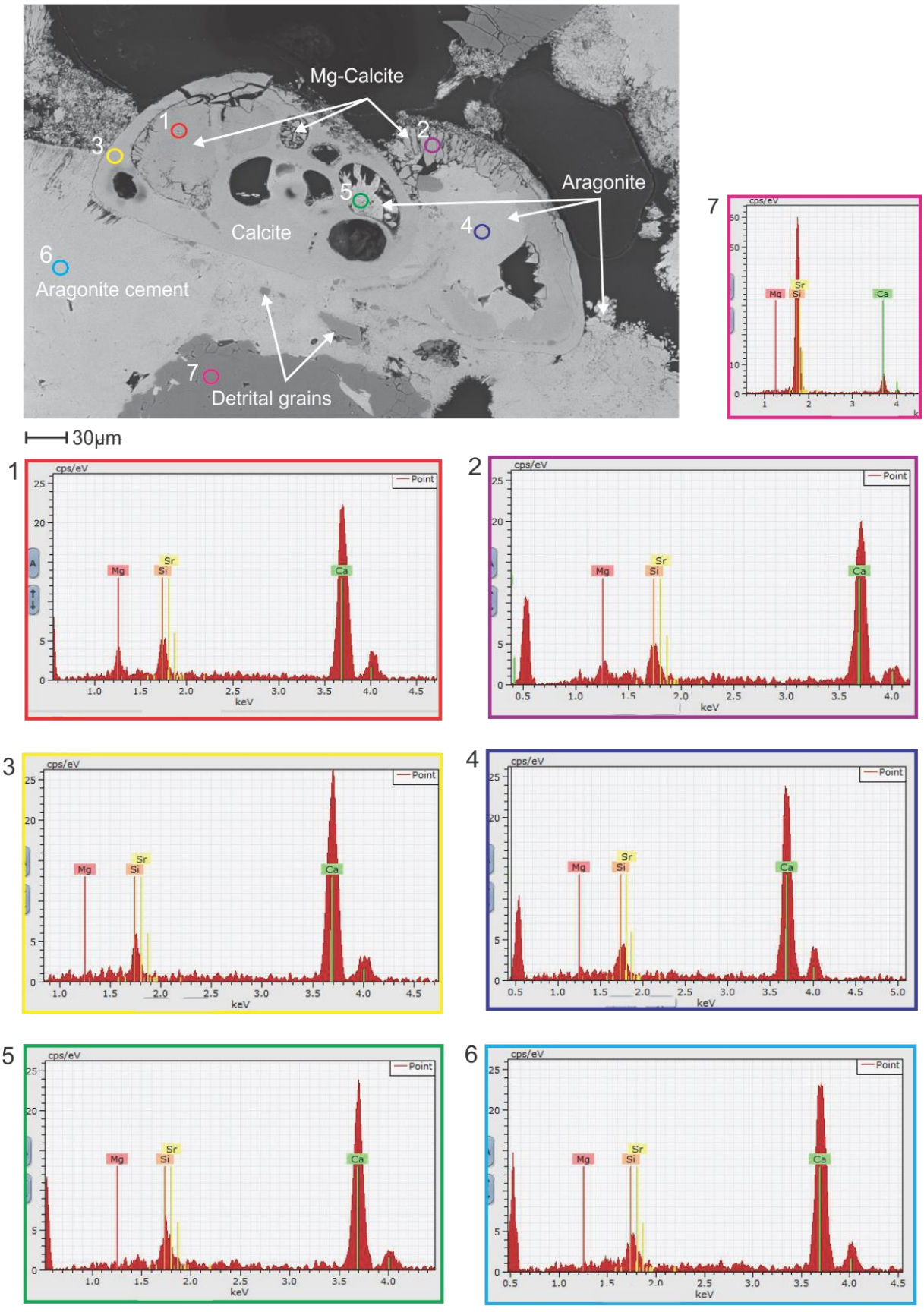

Fig 5.1: A backscatter electron image of a test Cibicides sp. embedded in authigenic carbonates from crust P1210032, and representative EDS spectra with positions shown on the image. The BSE intensity, combined with EDS analyses allows recognizing three carbonate phases. The lowest BSE response (darkest phases on the image) characterizes the Mg-

containing carbonate phase (spectra 1 and 2) occurring as filling and/or overgrowth linings within test chambers. This phase has minor Mg peak in addition to the more intense Ca peak in the EDS spectra and is interpreted to represent Mg-calcite. There is also a Si peak present in all spectra that is derived from surrounding silicates (primarily quartz (spectrum 9)), unrelated to carbonates. Intermediate BSE characterizes the foraminifera test itself consisting of Ca-carbonate (spectrum 3) representing calcite. The highest BSE response (brightest phases on the image) characterizes the most common carbonate phase occurring typically as a cement around the test, but is also present within the chambers of foraminifera. The EDS results (spectra 4-6) show that this phase consists largely of Ca-carbonate, but minor Sr is also evident on some of the spectra suggests that this phase is aragonite. Due to close proximity of Si and Sr peaks in the EDS spectra and generally low Sr abundance in aragonite, the identification of Sr is not always conclusive. In some analytical spots a distinct Sr peak is observed (spectrum 5) whereas in other spots the presence of Sr is interpreted based on an occurrence of a shoulder on the higher energy side of the Si peak (spectra 4, 6). The EDS data are consistent with variable BSE intensity; among the three carbonate phases Mg-calcite has the lowest average atomic number (BSE darker than calcite and aragoinite) and Sr-bearing aragonite has the highest average atomic number (BSE brightest) whereas the average atomic number of calcite is in between Mg-calcite and aragonite.

From Fig 5.1 it is established that there are carbonate phases with three different BSE intensities in studied samples;

- Calcite; rather pure Ca-carbonate which is seen in the foraminifera test. On the EBS-images the calcite appears brighter than Mg-calcite, but darker than aragonite.
- Mg-calcite; Mg-containing calcite, occurs as overgrowths or coatings on the foraminiferal test, or as chamber fills.
- Aragonite; Ca-carbonate with minor content of Sr, occurs as cement between the grains. Aragonite appears brighter than Mg-calcite and due to the SR content also brighter than calcite on EBS images. Aragonite is the most common authigenic carbonate phase in all crusts.

Presented below are the most common examples of microfossils and their respective occurences within the carbonate cement in the MDACs. From tests with pristine characteristics just embedded in the surrounding cement (Fig 5.2), to tests with Mg-calcite overgrowths (Fig 5.3) and to the completely recrystallized tests with overgrowths of bigger Mg-calcite crystals on the inner and outer test walls (Fig 5.4).

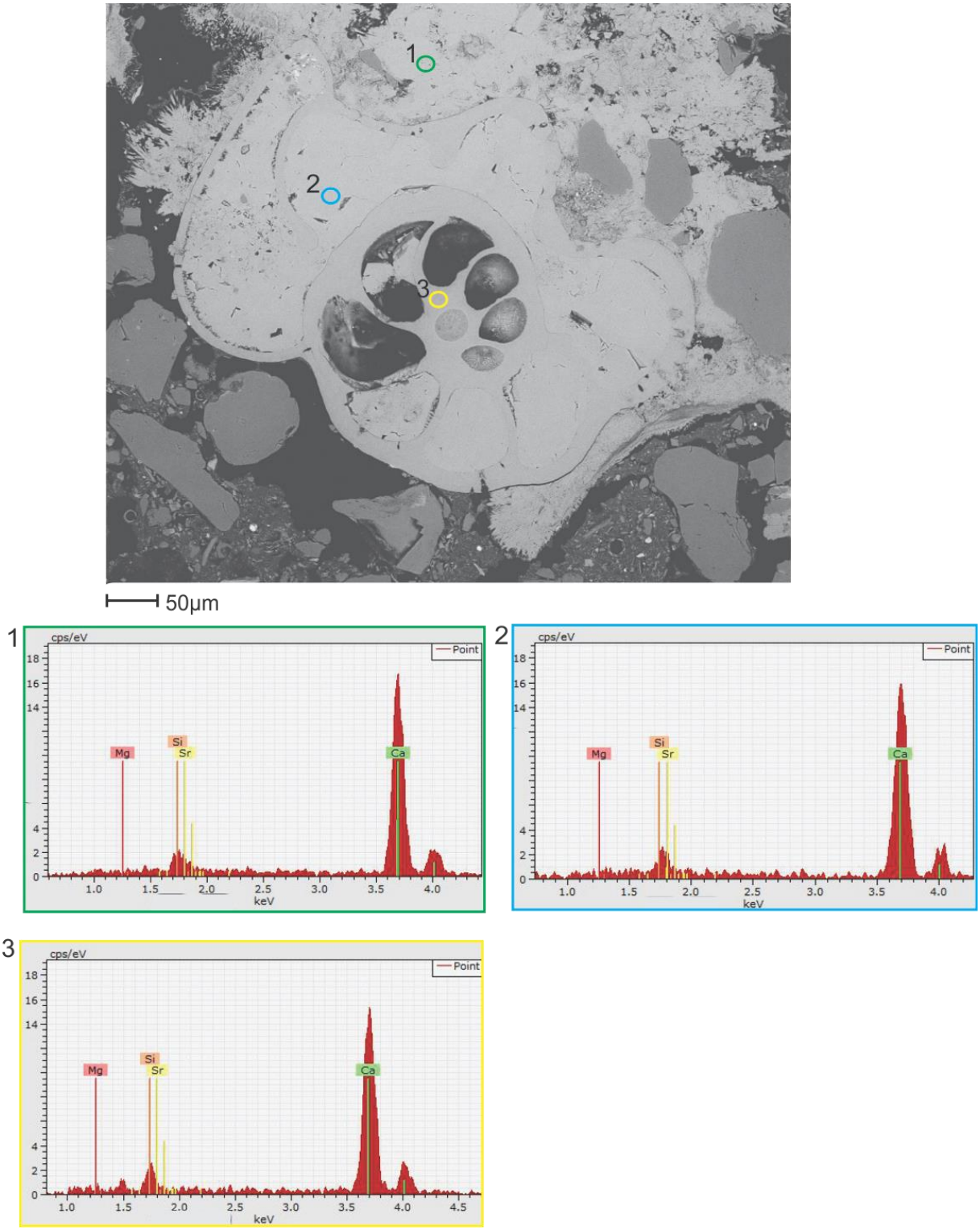

Fig 5.2: BSE-image with supplementary EDS-spectra with positions shown on the image, example from the crust P1210002. The benthic foraminifera Cibicides sp. occurring in the carbonate cement exhibits pristine test, with no signs of Mg-calcite overgrowths, or recrystallization. The test is embedded in aragonite cement, (spectrum 1), this cement fills many of the foraminiferal chambers, cement infill (spectrum 2) shows a similar composition as the surrounding cement. The calcite test (spectrum 3) shows a smooth surface.

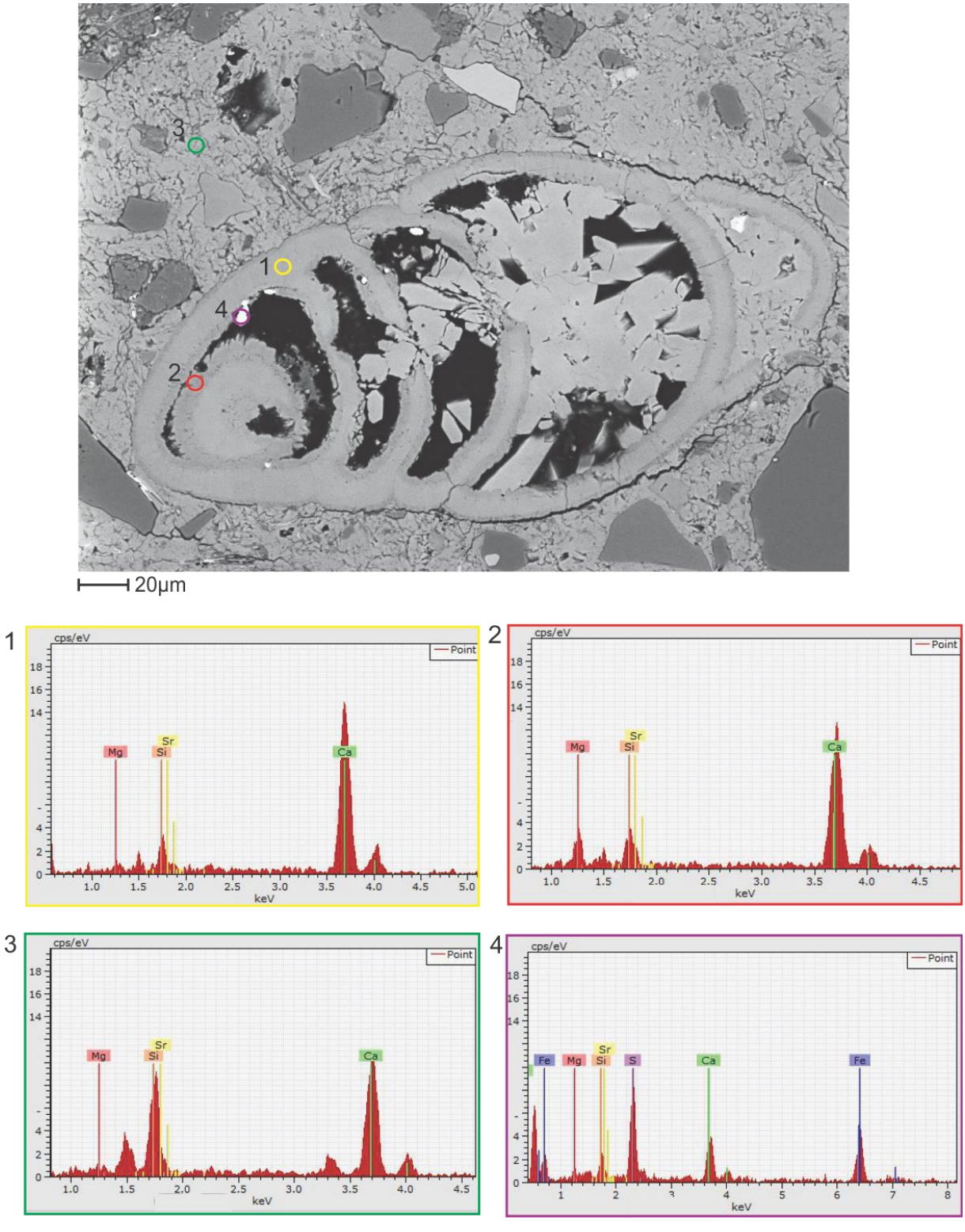

Fig 5.3: BSE-image of benthic foraminifera Bolivina sp., from the Hola crust, with darker Mg-calcite coatings on the inner and outer test walls (spectrum 2). The test of the foraminifera shows a relatively smooth surface (spectrum 1). The surrounding cement is seen as fibrous aragonite crystals, (spectrum 3), larger aragonite crystals occur in the chambers of the test. Pyrite is also present in several parts of the test, seen as the bright white spots, the EDS-spectra in point 4 shows a larger content of S and Fe, which results in the bright color in the BSE-image.

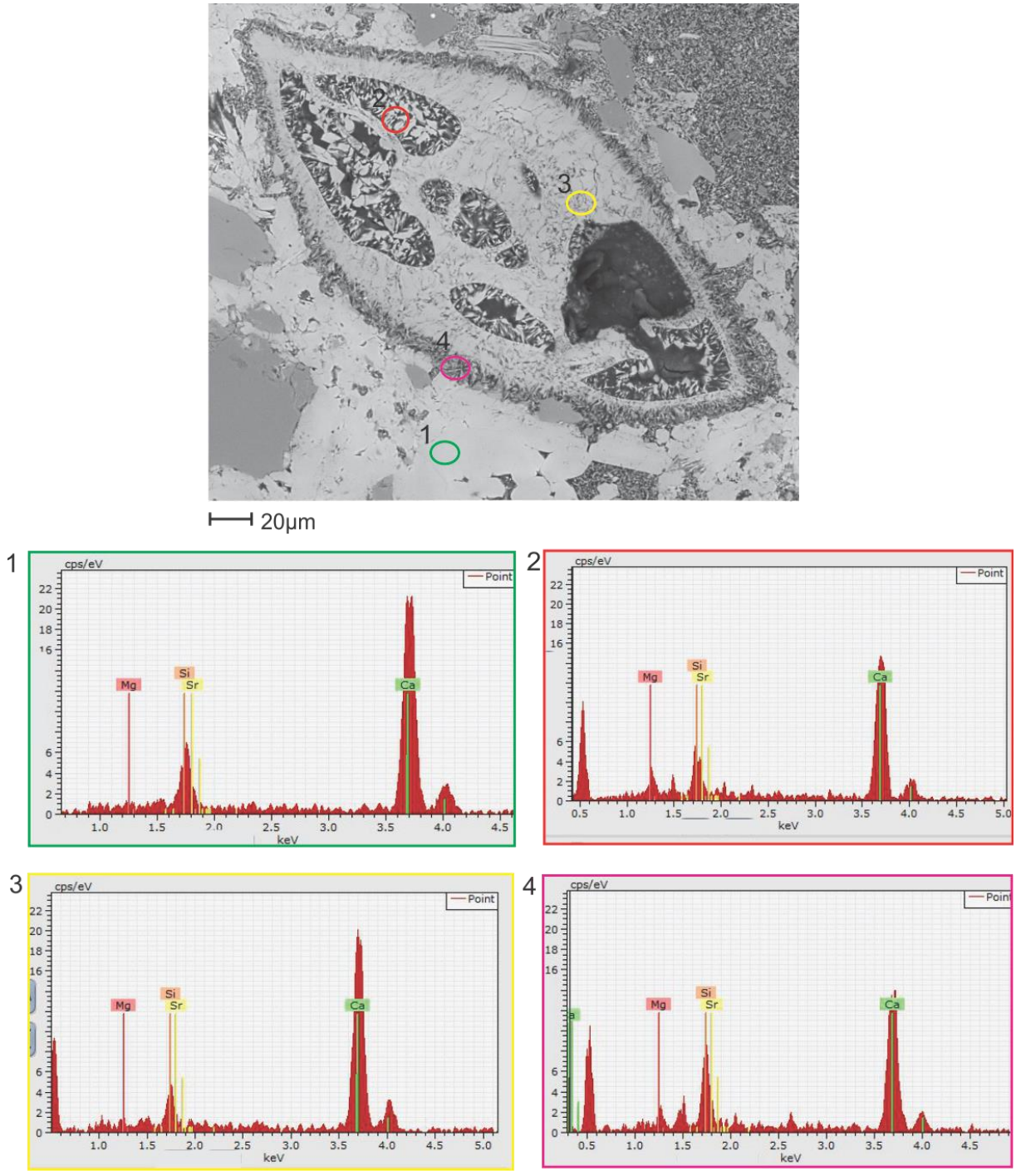

Fig 5.4: This BSE-image is of a Cassidulina sp. from the crust P1210001, which represents one of the most recrystallized tests, found within the crusts. The test shows overgrowth of big crystals on the inner chamber walls and smaller crystals on the outer test wall, both having elevated Mg content and represent Mg-calcite (spectra 2, 4). The carbonate cement (spectrum 1) contains Sr and has a bright color in the BSE-image, representing the aragonite phase. Compared to the previous example in P1210032 (Fig 5.1), this test has no smooth surfaces, but rather a "frosty" appearance. EDS-analysis (spectrum 3) shows that the test is composed of calcite.

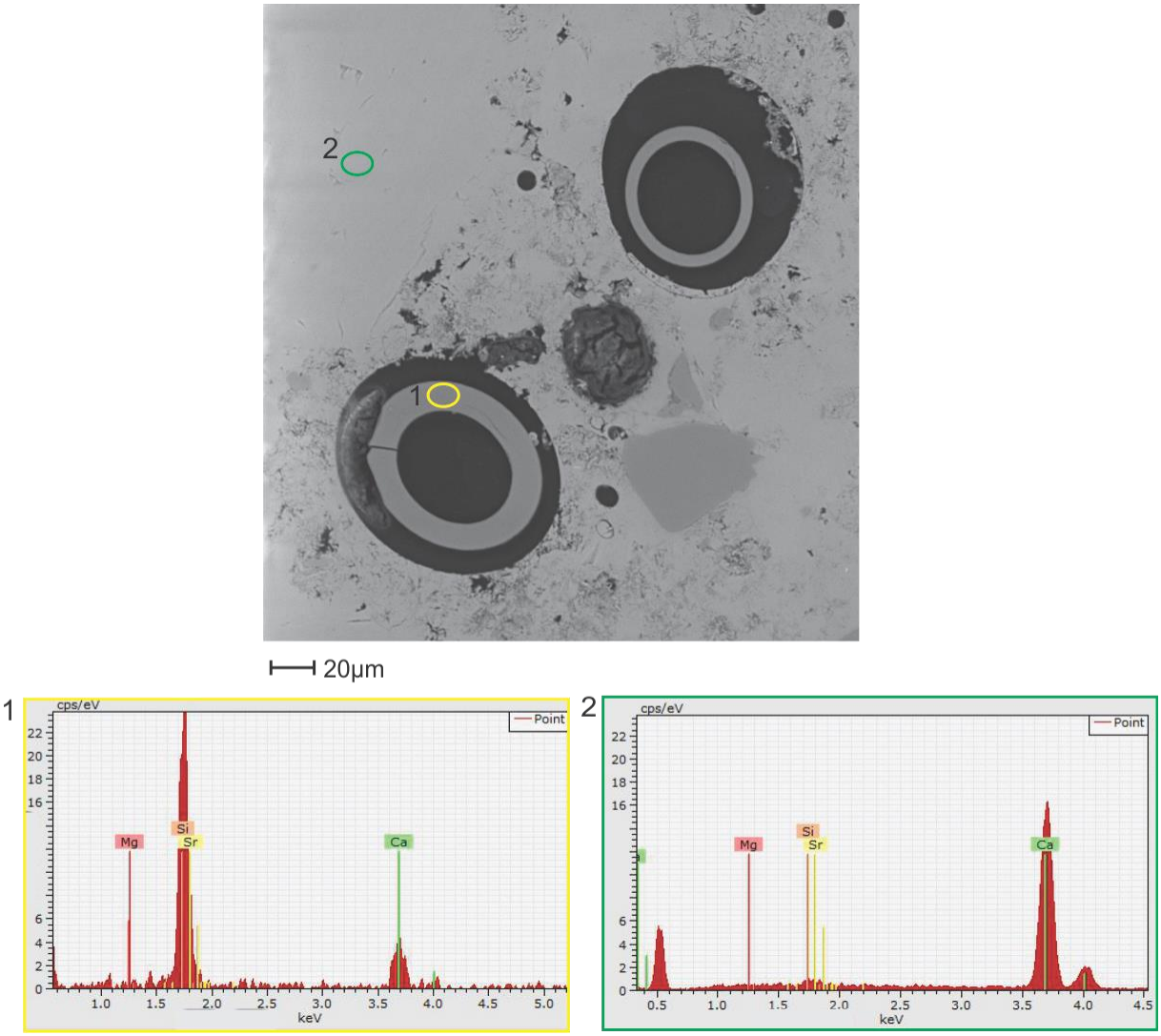

Fig 5.5: BSE-image and EDS spectra of siliceous microfossils (spectrum 1) embedded in aragonite cement (spectrum 2) observed within the crusts, this example is from P1210002.

In all of the crusts from the study area Loppa High, there occur circular, needle-shaped siliceous structures (Fig 5.5). In some parts of the crusts, they are dominant among microfossils present in the carbonate cement, as well as in the sediments found within the cavities.

5.2 Loppa High

Crusts from four different sample sites were collected from study area Loppa High, further information is given in Table 1.

5.2.1 PR1

Following are the crusts studied from the sample site PR1 located on the southwestern part of the Loppa High. The sample site are the shallowest for the Loppa High crusts; water depth 320 m.

P1210001:

*Fig 5.6: Overview image of the crust P1210001, the red rectangles indicates the location of the polished thin sections A-F. The smallest squares in the white grid lines indicates 1 cm * 1 cm.*

As seen in Fig 5.6 the dimensions of the crust is approximately 40 cm *15 cm at the most. Six thin sections were made from P1210001.

P1210001 comprises mainly fine-grained and well-sorted sediments; from mud to sand lithified with carbonate cement. The dominating carbonate phase is aragonite.

The biogenic component found within the carbonate cemented sediments are comprised of different organisms, but mostly bivalves, benthic foraminifera and siliceous microfossils. The P1210001 is variably cemented; in parts of the crust with less cement and in the cavities where the cement is largely absent there is a high content biogenic debris. The composition of biogenic debris in these weakly cemented areas is similar to the cemented areas, but the foraminiferal assemblage is dominated by benthic species.

- Thin sections P1210001A, C and D: most of the foraminifera were observed within weakly cemented sediments.
- Thin section P1210001B: Several foraminifera tests, both planktonic and benthic species have authigenic overgrowths.

- Thin section P1210001E: Dominated by bivalves and fragments of bivalves within the carbonate cement.
- Thin section P1210001F: Fragments of bivalves, areas with high abundance of pyrite. Some benthic species.

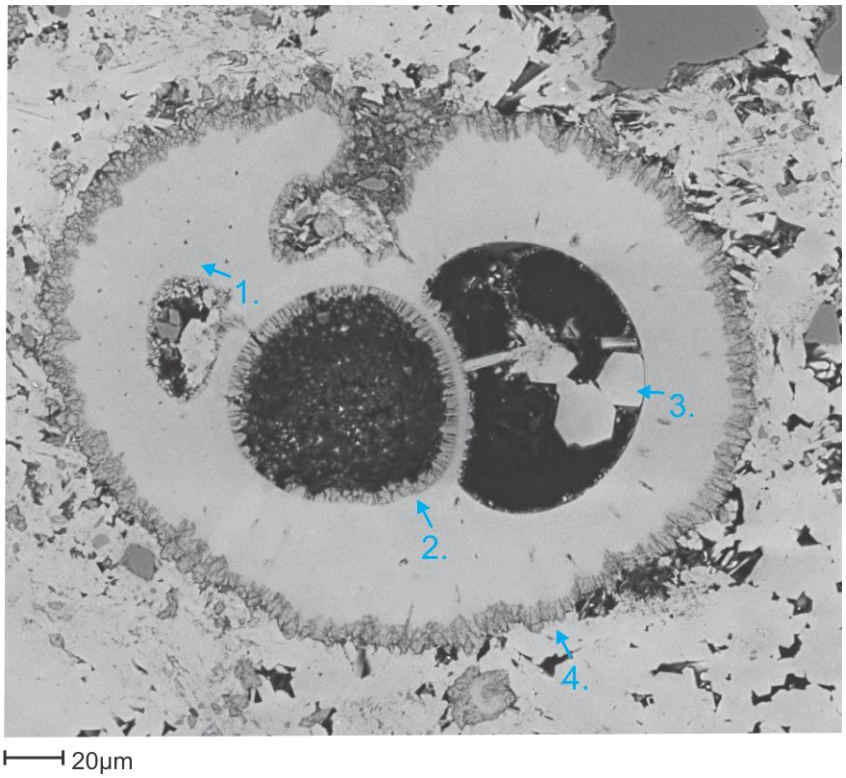

Fig 5.7: One of the planktonic species occurring within the fibrous aragonite cement. One area with primary pores still intact (1). Overgrowth of Mg-calcite crystals on the inner chamber wall (2). Bigger crystals of aragonite within the chamber (3). Overgrowth of Mg-calcite on the outer test wall (4) with a different structure and color than the surrounding cement.

Authigenic carbonate precipitation has variable alteration of test of both planktonic and benthic foraminifera. Some examples of the different alteration and preservation of original features are given in Fig 5.7 and Fig 5.8.

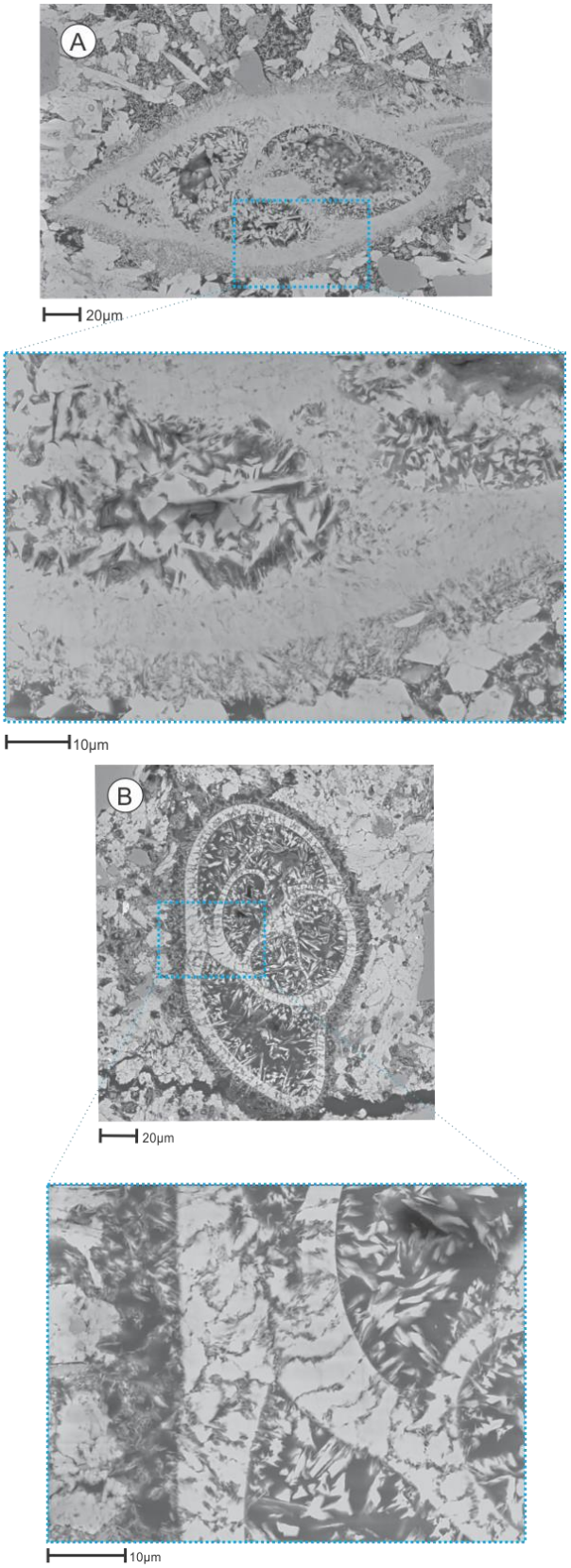

Fig 5.8: Some of the recrystallized benthic species found within the crust. A.) Cassidulina sp. with recrystallized test and overgrowth on inner and outer test walls. The crystals on the inner walls are bigger in size compared to the outer. B.) Unidentified species with recrystallized test and overgrowth

The alteration state of the tests varied within the crust, but some of the most altered examples of foraminifera tests were found within thin section P1210001B. All tests have a “frosty” appearance and there are no smooth surfaces left on the test walls.

Other examples of benthic species with altered tests show that the smooth surfaces have been overprinted by authigenic crystals. The overgrowths of Mg-rich crystals are observed on all the inner chamber walls as well as the outer test wall. The crystals on the inner chambers are similar in size and larger compared to the crystals on the outer wall (Fig 5.8).

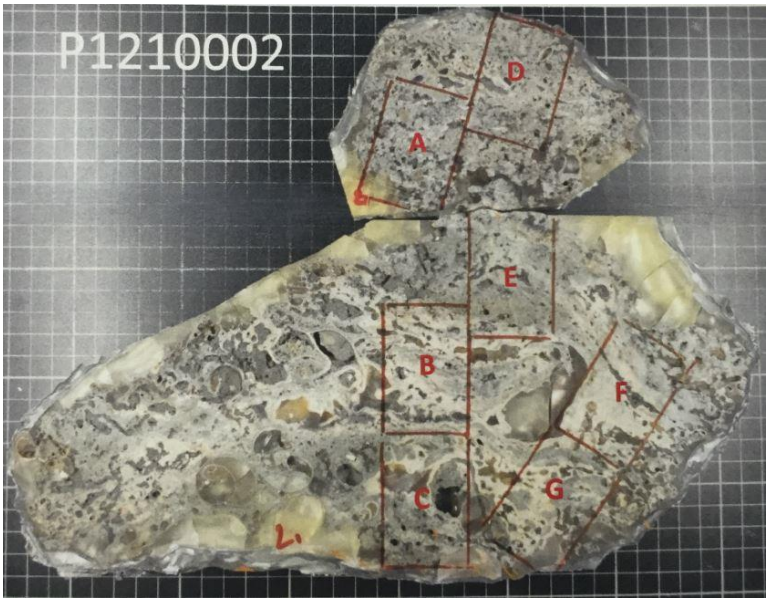

Fig 5.9: An overview of the crust P1210002.

P1210002:

Dimension of the crust is approximately 35 cm * 27 cm (longest and thickest part), and it is the biggest crust studied in the thesis (Fig 5.9). Seven thin sections are made from the crust. The uppermost part of the crust (thin sections P1210002A and P1210002D) contains sediments that are more poorly sorted than the sediments in the lower part of the crust. The size of the sediment grains range from silt to coarse sand and they are a mix of rounded to angular.

The biogenic components consists of several broken parts of bivalves in different size ranges, foraminifera of planktonic and benthic species. Several circular and needle-shaped structures of microfossils were also observed. In some areas, they are the dominating biogenic components of the crust. EDS-analyses showed that these needle- and circular shaped structures were siliceous. The main foraminiferal tests found within the cement were benthic species, but some planktonic species were observed.

The majority of the foraminifera were affected by variable state of alternation and have authigenic Mg-calcite overgrowths, examples are shown in Fig 5.10 where A.) and B.) represent the major alternation state of the tests. Recrystallized tests as seen in C.) did not dominate, but it occurred as well.

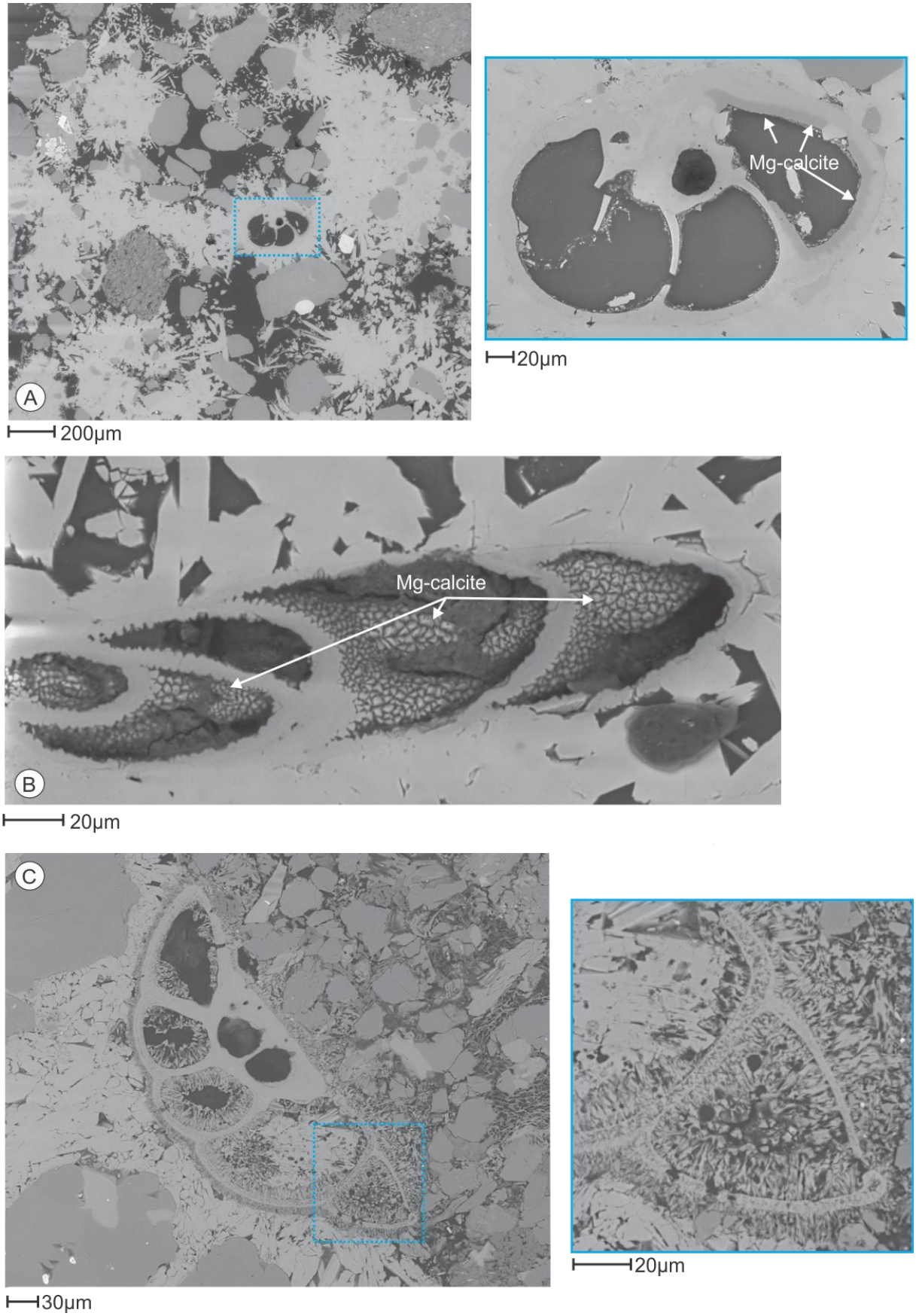

Fig 5.10: A.) Benthic foraminifera within the carbonate cement, the detailed BSE image reveals a darker coating on one of the inner chamber walls, interpreted to be Mg-calcite, confirmed by EDS-analysis. B.) A test of a benthic foraminifer interpret to be a Buliminella sp., no signs of overgrowth on the outer test wall, or recrystallization of the test. Whereas on all

of the inner chamber walls there are overgrowth of well developed rhombohedral Mg-calcite crystals. C.) A Cibicides sp. with overgrowth on the inner and outer walls. The close-up image within the blue square shows a part of the test with recrystallization of the test.

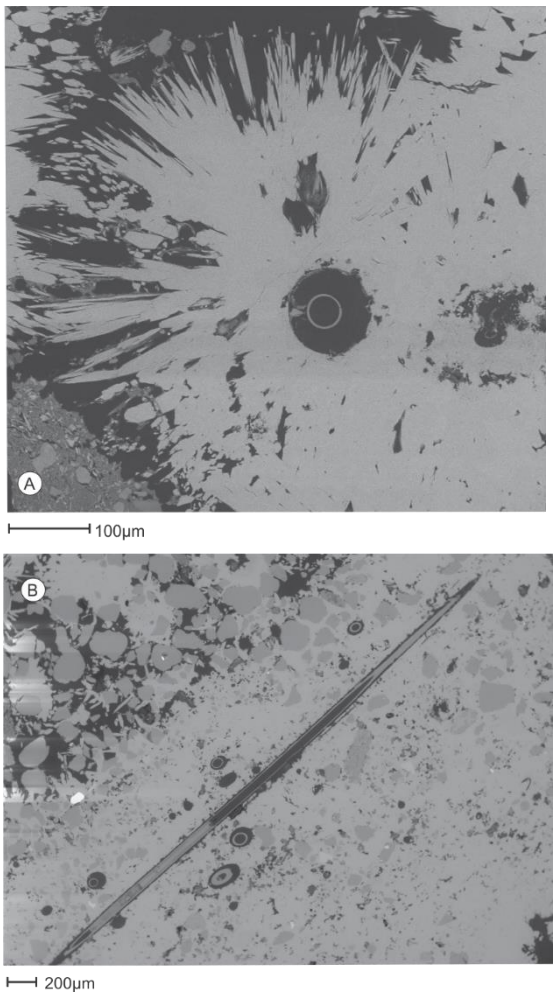

Fig 5.11: Examples of circular and needle shaped siliceous structures of microfossils in the carbonate cement. A.) Aragonite crystals (200µm) radiating out from one of the siliceous structures. B.) Several structures in a variety of sizes.

- P1210002A: Benthic foraminifera with different alternation states, and fragments of bivalves.
- P1210002B: A few benthic species, with Mg-calcite coating on the outer test wall. Predominant biogenic components within the thin section are siliceous microfossils.
- P1210002C, D, E, F, and G: Several benthic species and a few planktonic species within the carbonate cement. With different states of alternation, but mainly with a coating of Mg-calcite either on inner or outer test wall. Other biogenic components comprised siliceous circular structures, and bivalves.

Some examples of the siliceous microfossil are given in Fig 5.11, they had a wide range of different sizes.

5.2.2 PR3

The sampling site PR3 are located at the NE part of the Loppa High, the water depth is 403 m, which is the deepest of all Loppa High sites. Two crusts were examined from this site; P1210010 and P1210011, they comprised finer grained and better sorted detrital sediments compared to the other crusts.

P1210010:

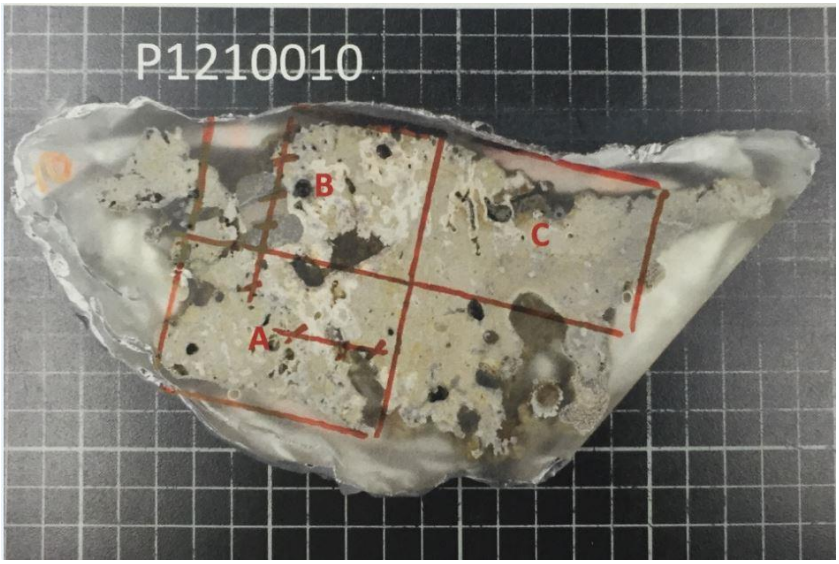

*Fig 5.12: The crust P1210010, the red rectangles indicates where the polished thin sections A-C are from. The white grid lines indicates squares in the dimension 1cm*1cm.*

Dimension of the crust is approximately 22 cm* 10 cm at the longest and thickest part; three thin sections were made from this crust (Fig 5.12). The sediments are well sorted, mainly mud/silt with a small amount of fine-grained sand in some areas.

The biogenic debris that however is not abundtant consists mainly of foraminifera. The majority of the species represent benthic species

- P1210010A: Benthic species with Mg-calcite overgrowth and recrystallized tests.
- P1210010B: A few benthic species present, all with Mg-calcite crystals on outer test walls.
- P1210010C: Planktonic and benthic species with different alternation states.

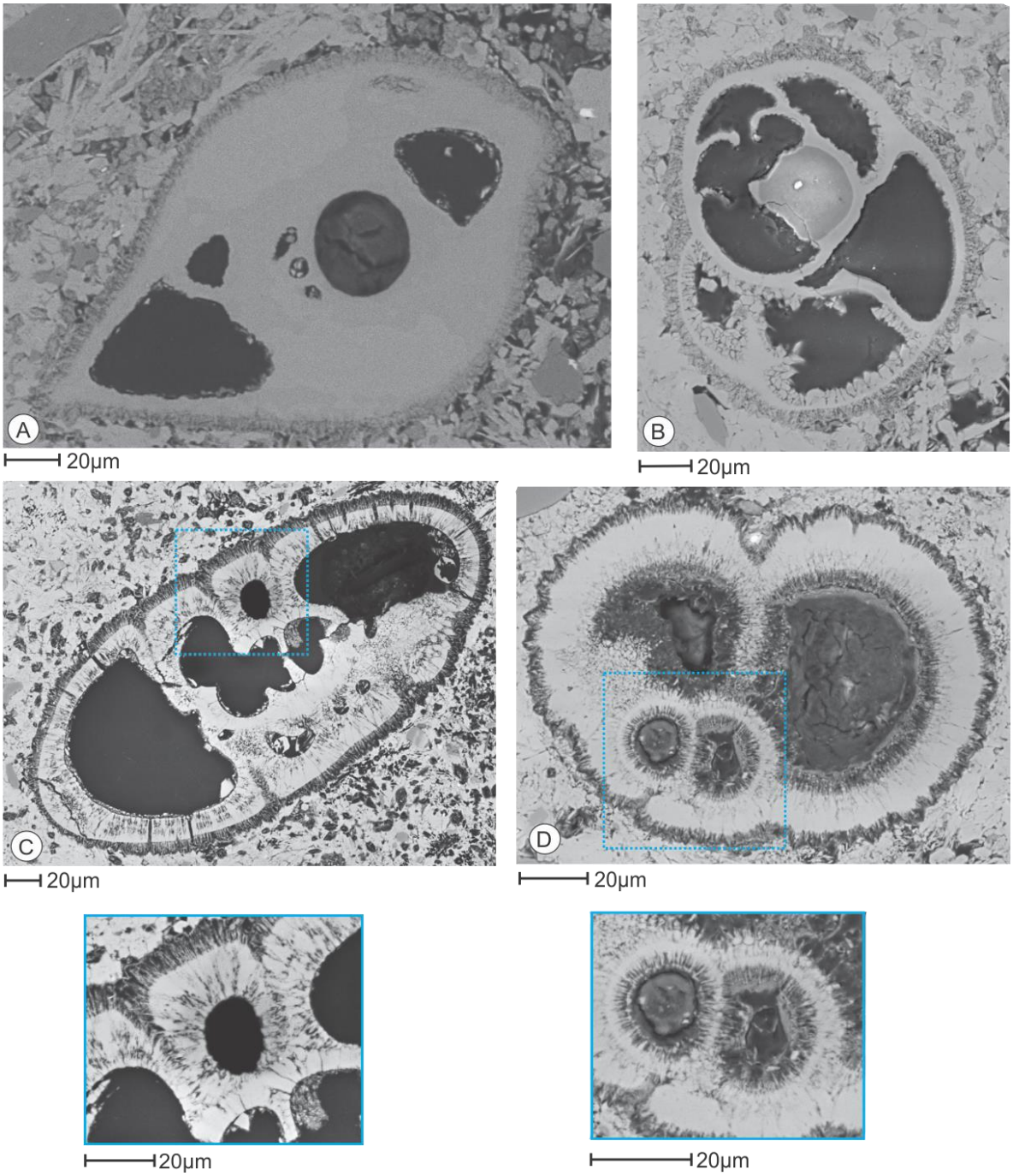

Fig 5.13: Overview of different examples of foraminifera from the crust. A.) A Miliolida sp. with overgrowth on the outer test wall, the crystals are quite uniform in shape and size. The test has a smooth surface. B.) A benthic foraminifera with slightly more overgrowth, the Mg-crystals on the inner chamber walls are uniform in size and shape, but slightly bigger compared to the crystals on the outer test wall. C.) A benthic foraminifera which is completely recrystallized, the overgrowth of Mg-crystals are located on the outer test wall. The secondary crystallization of the test seems to have crystals radiating out from the chambers, seen in the blue square. D.) A recrystallized planktonic foraminifera, where the secondary crystals radiates out from the chambers, seen in the blue square.

Example of an element map as shown in Fig 5.14 shows that the highest amount of Mg-calcite is concentrated along the crystal overgrowth occurring on the outer test, but there is also an enrichment internally in the test.

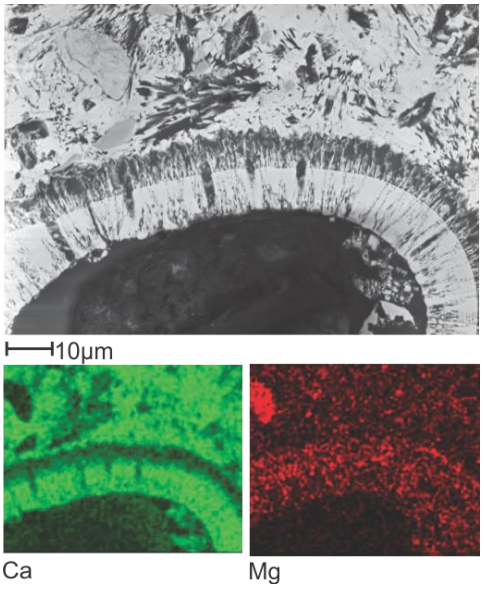

Fig 5.14: From the same foraminifera seen in *Fig 5.13*C), but here with an element map of Ca and Mg. Note that the highest concentrations of Mg follows the rim of overgrowth on the outer test wall.

P1210011:

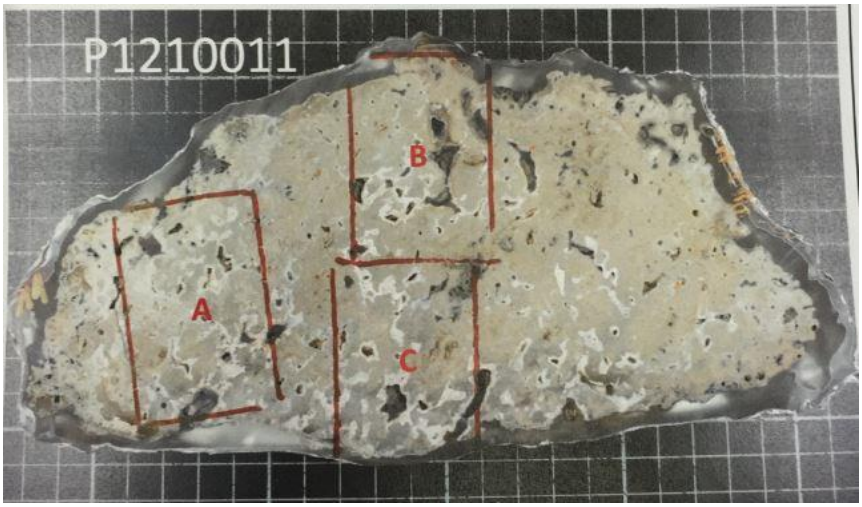

Fig 5.15: The crust P1210011, the polished thin sections A-C are indicated with the red rectangles.

Dimension of the crust is approximately 25 cm * 12 cm at the longest and thickest part; three thin sections are made from the crust (Fig 5.15). The crust consists of well-sorted and very-fined grained sediments, mainly mud/silt. The carbonate cement is not as dominating as in many of the other crusts.

The foraminifera are relatively rare, and the assemblage was almost entirely represented by benthic. The majority of the foraminifera have overgrowth of Mg-calcite crystals on the outer test wall and the chambers are typically free of authigenic precipitates (Fig 5.16 A.). Several of the tests also have larger Mg-calcite overgrowths and large aragonite crystals on the inner walls of the chamber as seen in (Fig 5.16 B.).

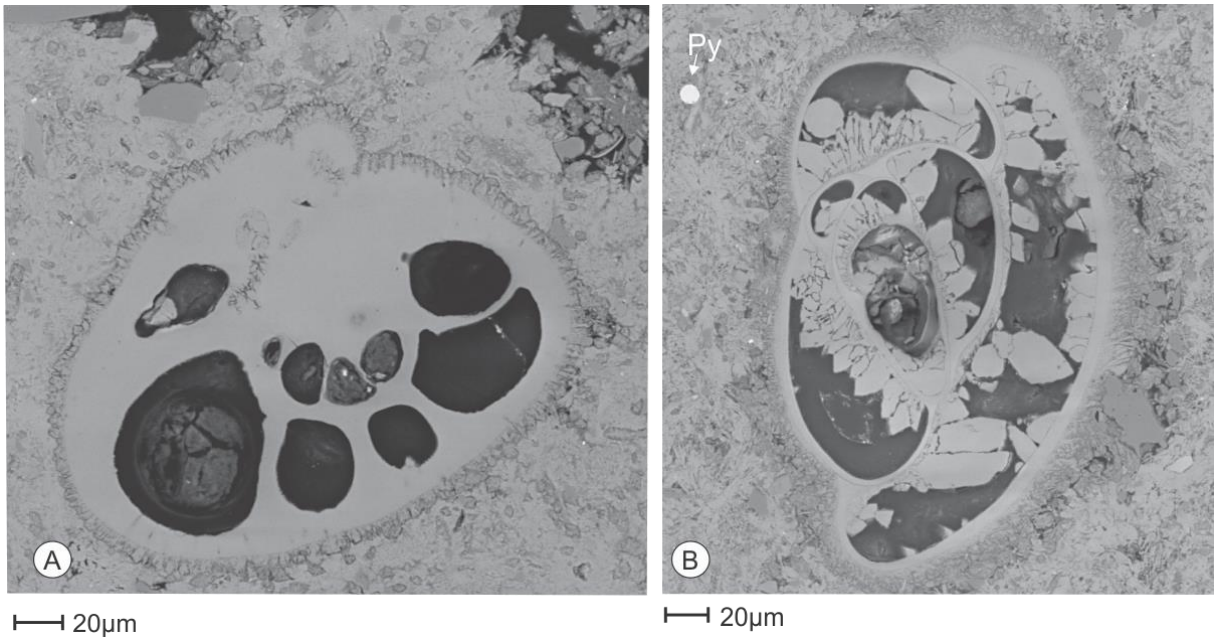

Fig 5.16: Examples of how the majority of the foraminifer tests occur within the crust P1210011. A.) A benthic foraminifera (100 µm), with a smooth test, but overgrowth of Mg-calcite of the same size on the outer test. B.) Overgrowth of Mg-calcite on the outer wall of the test, larger aragonite crystals grows on the inner walls of every chamber of the test, but the test itself seems to be smooth with no signs of recrystallization. Pyrite is indicated in the upper left corner.

5.2.3 PR4

The sample from Loppa High site PR4 is from a water depth at 391 m. Only one crust from this sample site was studied.

P1210017:

Fig 5.17: An overview of the crust P1210017, with the thin sections A-B indicated in the red rectangles.

Dimension of the crust is approximately 17 cm * 8 cm at the longest and thickest part; two thin sections are made from this crust (Fig 5.17). The sorting of the sediments are moderate to well, not much fine grained sediments as they range from very coarse sand to gravel. In the middle part of the crust there is a large cavity filled with 1-2 cm thick layered aragonite.

The content of biogenic debris is relatively low, only a few examples of benthic species were found. As shown in (Fig 5.18) the thin sections are made from the areas with a high level of cavity fill. As observed in other crusts, those cavity fills consisting of impurity-free aragonite

usually do not contain a lot of biogenic material. A few species were observed, but no generalization were made by those observations.

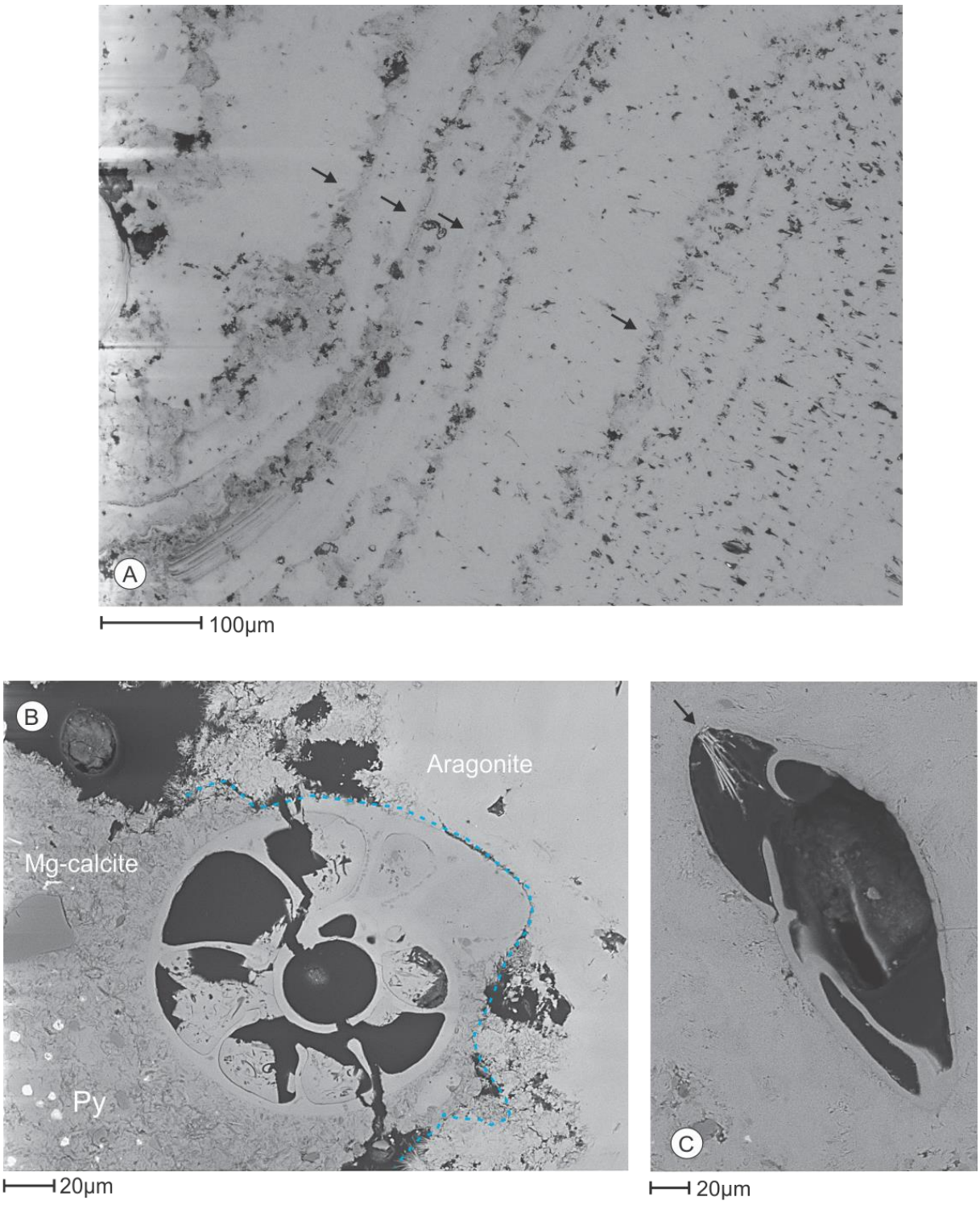

Fig 5.18: A.) Backscatter image of an area with several aragonite layers (indicated by the black arrows) representing different episodes of precipitation. No biogenic components observed in this layered aragonite. B.) A benthic species (60 µm). The surrounding carbonate cement is represented by Mg-calcite with pyrite to a clean aragonite to the right (border marked with dotted blue line). C.) Another benthic species (80 µm), the test is surrounded by aragonite cement and there is no visible overgrowth. It seems that the aperture (indicated by the black arrow) has induced carbonate precipitation to the chamber of the test.

5.2.4 PR5

The samples from Loppa High site PR5 are from a water depth at 393 m. The crusts from this sample site comprised of poorly sorted coarse-grained sediments. They were almost completely barren of foraminifera, the main components of biogenic debris were fragments of shells or bivalves.

P1210032:

Fig 5.19: An overview of P1210032, one thin section made from the crust.

Dimension of the crust is approximately 8 cm * 6 cm, measured at the longest and thickest part of the crust (Fig 5.19). One thin section made from the crust, P1210032A. The sediments ranges in size from very fine sand to pebble and are poorly sorted.

The content of biogenic components is very low, only a few benthic foraminifera were observed. Some siliceous circular remnants of microfossils were also observed.

P1210036:

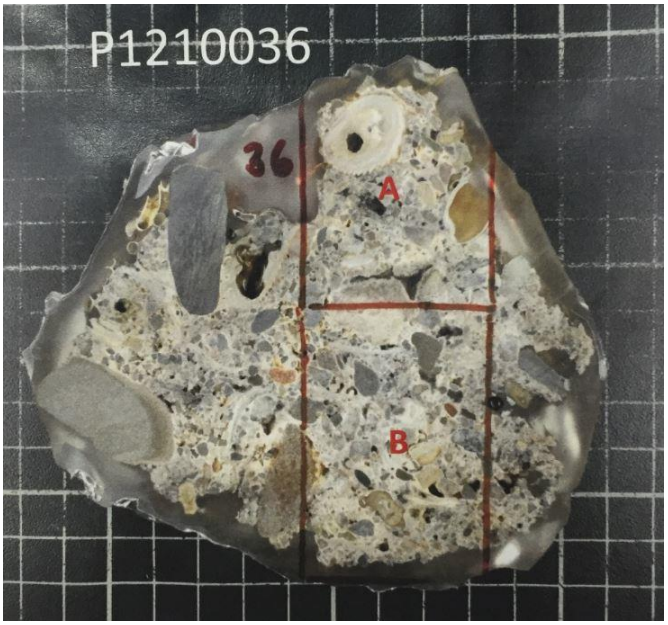

Fig 5.20: Overview of the crust P1210036, with indicated polished thin sections; A-B.

Dimension of the crust is approximately 13 cm * 12 cm, measured at the longest and thickest part of the crust (Fig 5.20). Two thin sections are made from the crust. The sediments are poorly sorted, a mix of grain sizes ranging from coarse sand to gravel and some grains in the pebble size.

The content biogenic components are low, mainly bivalves or broken bivalves (Fig 5.21). Completely barren of foraminifera.

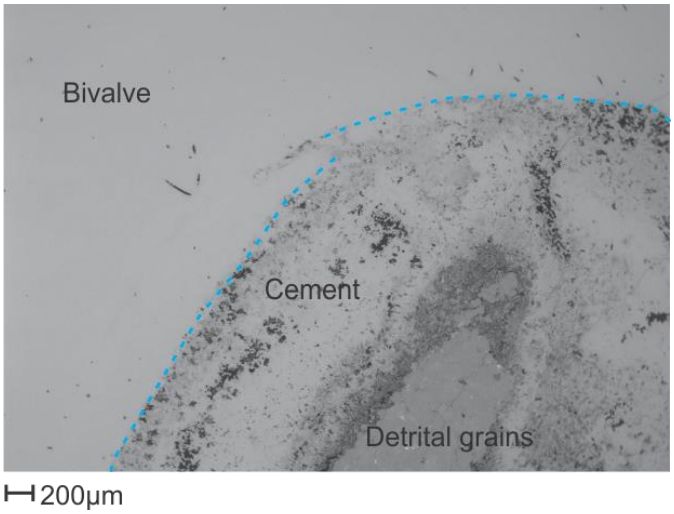

Fig 5.21: BSE-image of a part of a bivalve from thin section P1210036A, where the blue dotted line indicates the border between the shell and the carbonate cement.

5.2.5 Short summary of the Loppa High sections

The observations of the crusts sampled from four Loppa High reveals that there are similarities between the crusts, but mostly it is a big variation both within the crusts and compared to each other. Crusts from PR4 and PR5 consisted of sediments which were less sorted and the sediment grains were bigger compared to the crusts from the other sampling sites, they were also almost completely barren of foraminifera.

The biogenic component were a mix of bivalves, foraminifera and siliceous remnants of microfossils. The amount of occurring foraminifera varied and was mainly dominated by benthic species. Mg-calcite overgrowths only occurred on the tests of foraminifera, both planktonic and benthic.

5.3 Hola

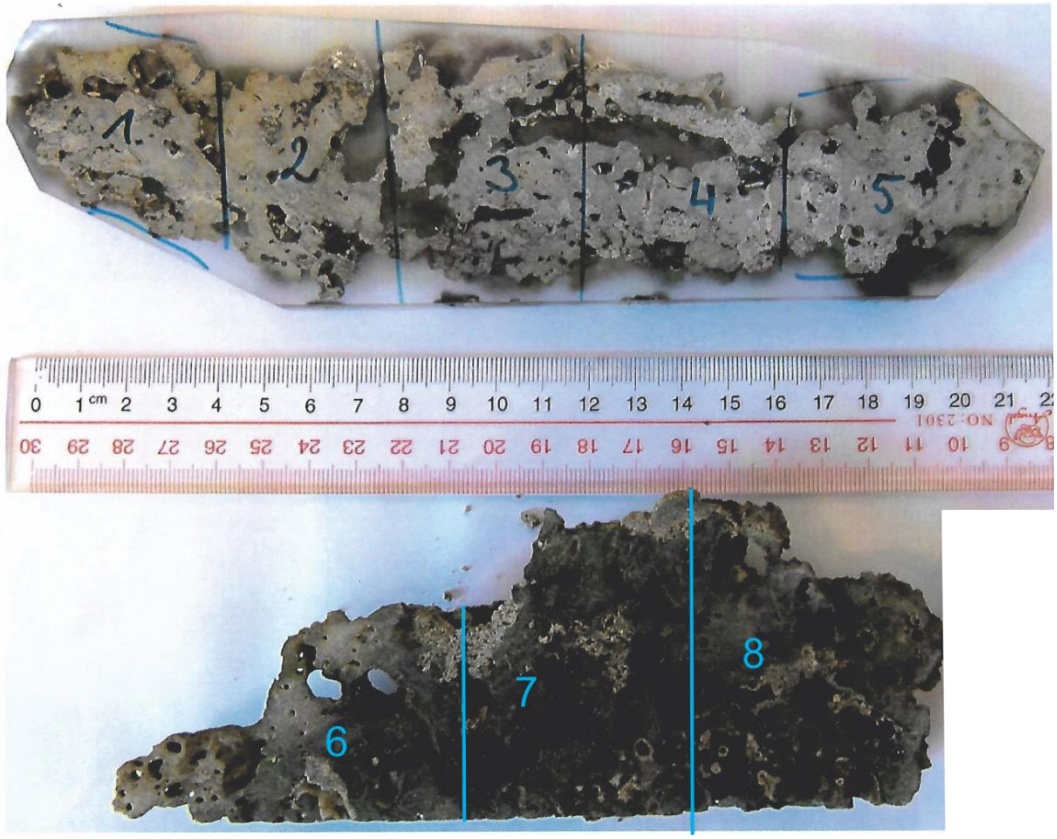

Fig 5.22: Overview of the Hola crusts, with eight thin sections (marked with blue) CS-11-1 to CS-11-8.

The Hola sample (Fig 5.22) area is located off the coast of Vesterålen, amongst all studied sites, it is the shallowest sampling site with the water depth 218 m. The sediment grains in the crust are angular to sub-rounded and mostly in the same size range, which makes it well sorted. The precipitated carbonate cementing the sediments consists of small needle like crystals, whilst the cavities are infilled with larger needle like crystals.

The foraminiferal assembly is almost entirely made up by benthic species, very few to none planktonic species were observed. Even though the specimens are barren of planktonic species, there are several benthic foraminifera present; ranging from 100 µm to over 500 µm in size. *Cibicides sp.* is the dominating species in all thin sections. The foraminifera in the crust exhibited different stages of both recrystallization and overgrowth see Fig 5.24, from the pristine smooth appearance of the test to a completely recrystallized test without any preservation of the smooth pristine appearance. The majority of the foraminifera in the

seemed to still behold the pristine characterizations of the test, surrounded by cement (Fig 5.23), needle like crystals were also observed growing in the chambers of several of tests,

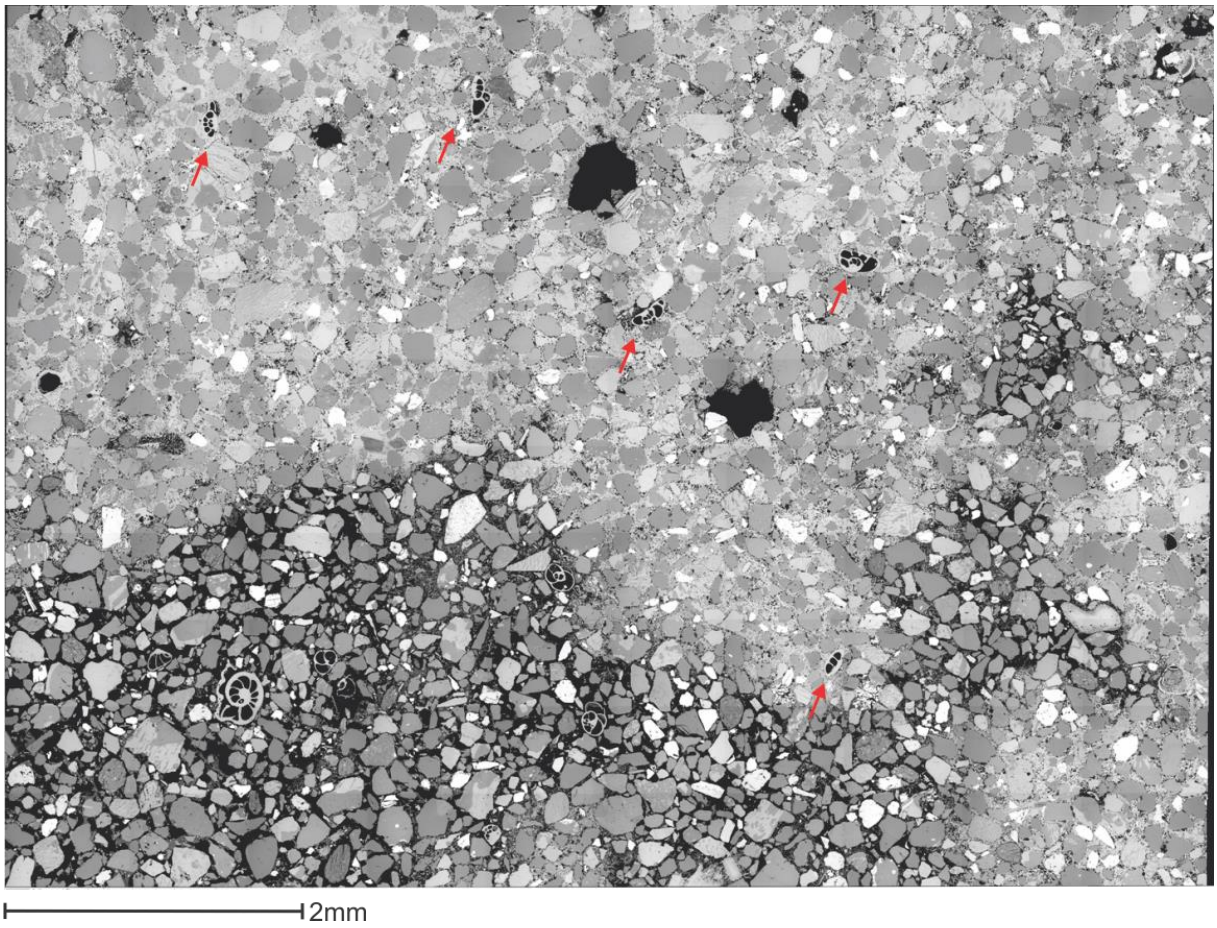

Fig 5.23: Overview of a larger area in one of the Hola crusts. The red arrows indicates benthic species, Cibicides sp.. In the lower part of the image there is an area with a variety of benthic foraminifera where the carbonate cement is less abundant compared to the upper part of the image.

No examples of strongly altered tests as observed in several of the Loppa High sections were found within the Hola crust. The recrystallized tests if found within the Hola crust had a crumbled appearance, with dark rims of small Mg-calcite on surrounding the outer and inner walls. This dark rim of consists of very small crystals of microcrystalline size. The typical foraminifera found within the Hola crust are represented in Fig 5.24. EDS-analysis revealed that several of pristine smooth tests often had a small Mg-enrichment on some of the inner chamber walls.

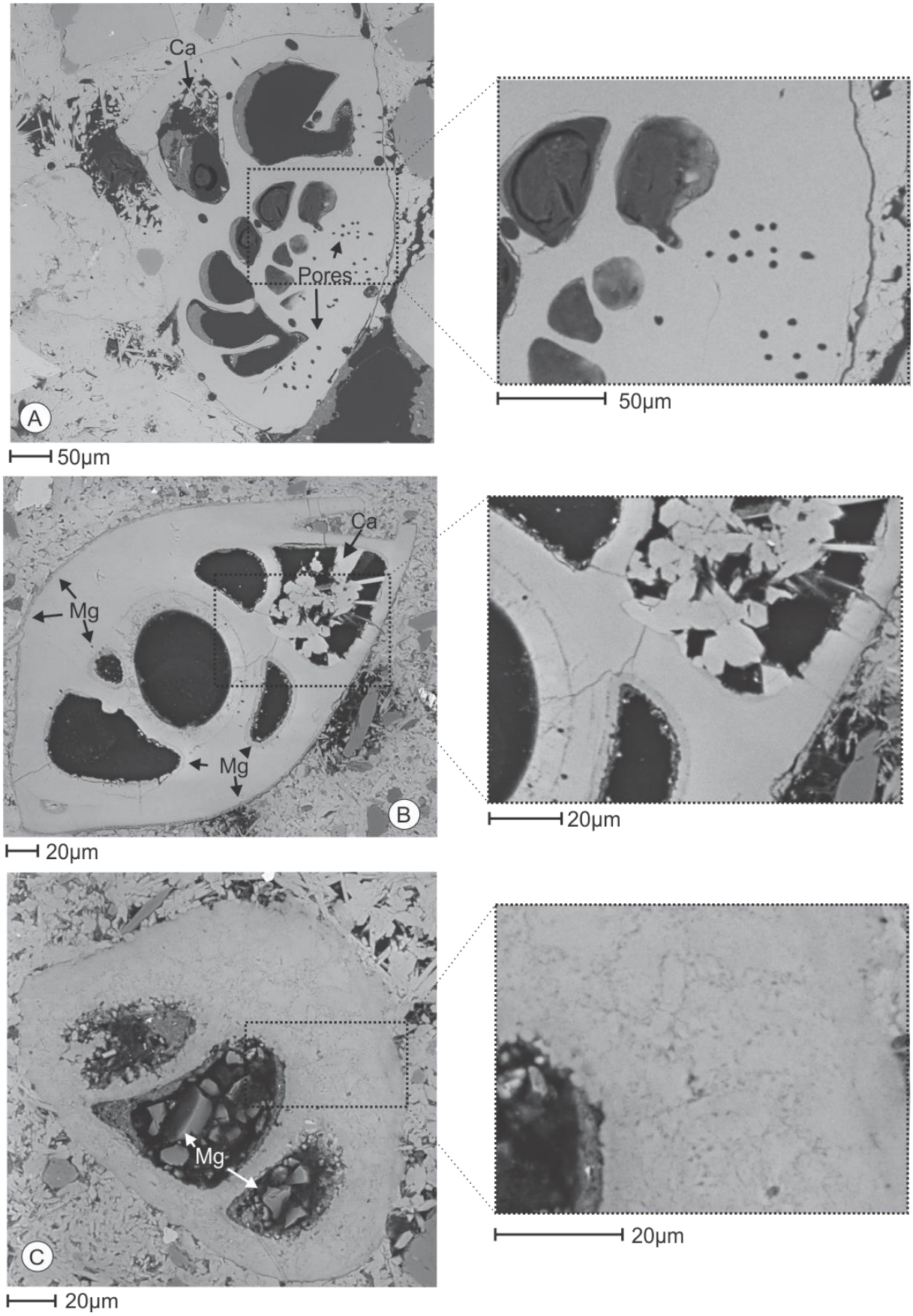

Fig 5.24: Overview of different stages of recrystallization and overgrowth of the benthic species found in the Hola crust A.) A benthic species where the test has a smooth appearance and original pores are still intact. B.) Miliolida sp. with thin Mg-calcite-overgrowths on the inner chamber walls and on the outer test wall. One of the chambers have a small infill of bigger

radiating aragonite, which are brighter on the BSE image compared to the test and Mg-calcite overgrowths. C.) A benthic foraminifera, probably a Miliolida sp. where the test is recrystallized and rhombohedral Mg-calcite crystals are present in the chambers. Compared to the tests in A.) and B.) this appears darker on the BSE image.

5.4 Summary and comparison

Following is a short summary and comparison of the two study areas based on the observations. In general the MDAC crusts are comprised of two different materials; mud to gravel-size detrital glacial sediments lithified with carbonate cement. The dominating carbonate cement was aragonite, whilst Mg-calcite occurred on the tests of foraminifera as overgrowths, whilst calcite represented the foraminifera tests.

The crust from Hola had a uniform authigenic carbonate content and appearance compared to the crusts from Loppa High. The benthic assemblage is mainly represented of Cibicides sp.. No circular/needle-shaped siliceous microfossils occurred in the Hola crusts. The occurrence of planktonic species were scarce.

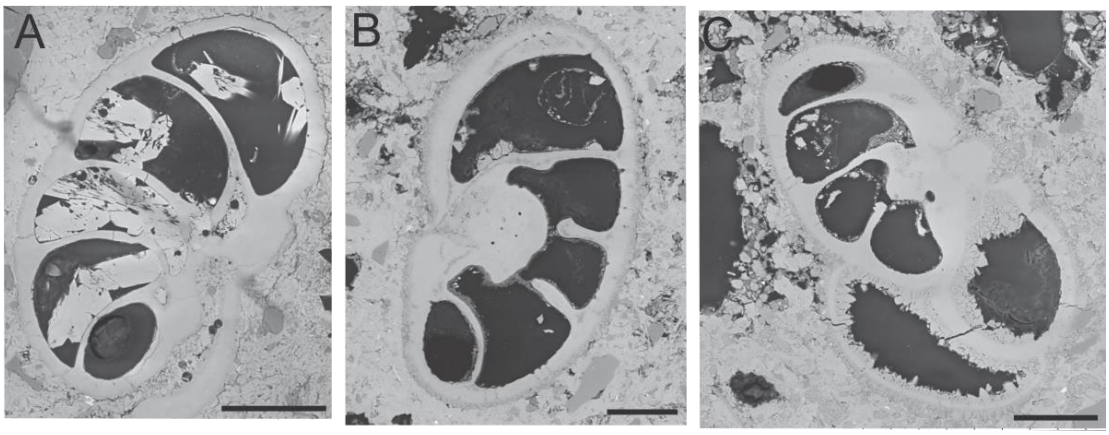

Fig 5.25: An overview image of a benthic species showing the typical alteration states of the foraminiferal tests (black scale bar: 60 µm). A.) A pristine test with aragonite infill of chambers. B.) Thin coating of Mg-calcite on outer test wall. C.) Mg-calcite overgrowths on both inner and outer test wall.

The different alteration states of foraminifera tests were mainly the same in both study areas, where the typical states are indicated in Fig 5.25.

6 Discussion

In this chapter the combined observations of BSE-images and EDS-analysis will be summarized and interpreted. The main purpose of the petrographic investigation of the methane-derived authigenic (MDAC) crusts was to document the nature of the biogenic debris capsuled in the crusts. Assessment was made if the precipitated authigenic carbonates used the tests of the foraminifera as nucleation templates by addressing the following questions:

- Is there any difference in the secondary carbonate overgrowth on biogenic debris/ are there overgrowths always when authigenic carbonate formation occurs?
- Is there any differences between the foraminifera species in their response to authigenic precipitation; does the precipitation affect preferentially benthic of planktonic species.

The petrographic investigations are further listed.

6.1 Sediments within the MDACs

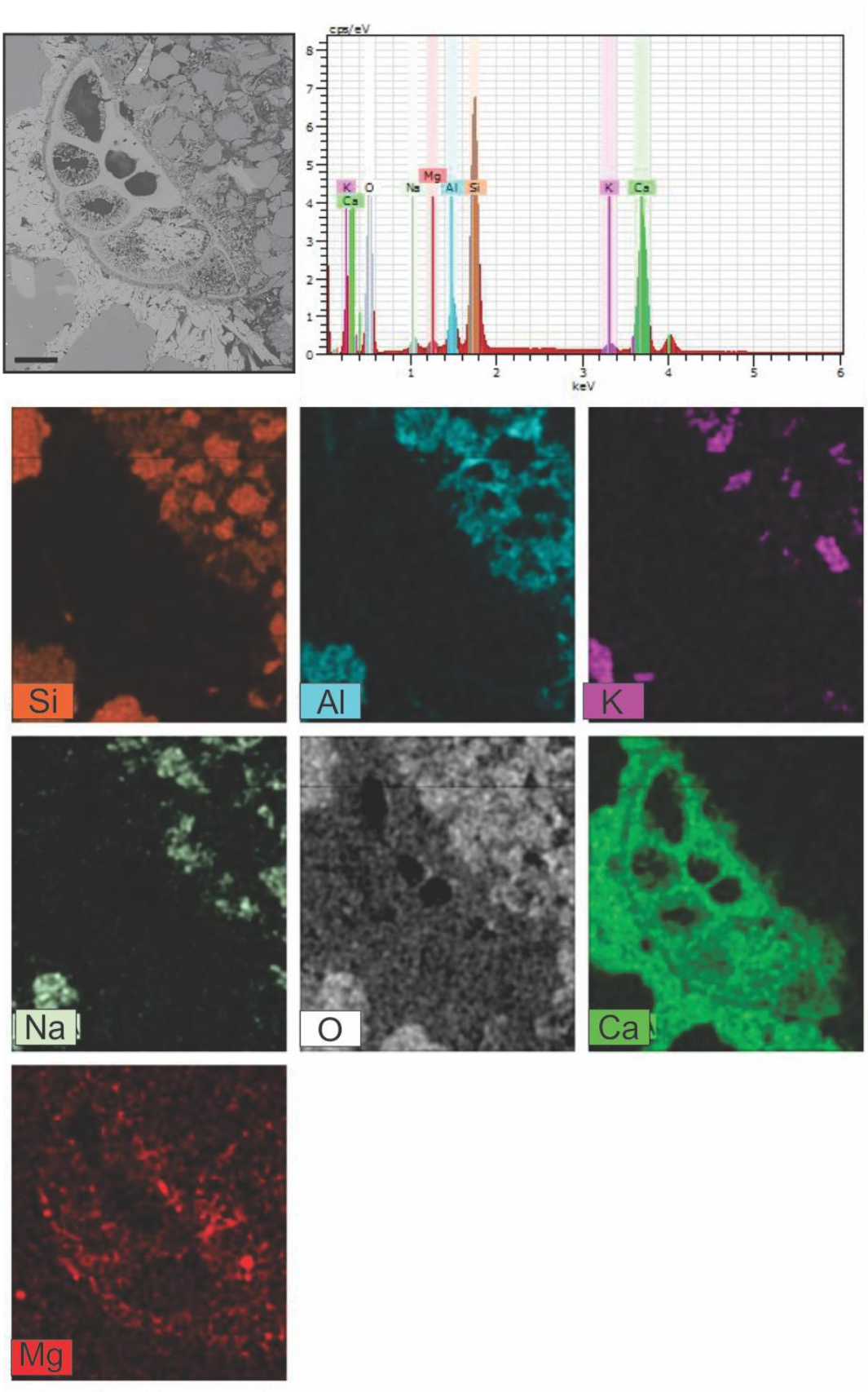

Fig 6.1: BSE-image (black scale-bar: 60 µm, EDS-spectra obtained by scanning the whole area (BSE-image) with its respective elemental maps. Sub-rounded to angular detrital sediment grains (5- 150 µm), a foraminiferal test and aragonitic

carbonate cement (BSE-image). The Si map indicates that many detrital grains contain Si, but the abundance (the brighter the color on the element map, the higher the abundance), is variable amongst different Si-containing grain. Grain with highest Si abundance represent quartz (SiO_2). Whereas the lower Si abundance correlates with high Al and, -either K or Na representing f-feldspar and plagioclase respectively. Ca map tracks the aragonite cement and the calcite test of the foraminifera. Mg occurs within the Mg-calcite overgrowths on the foraminifera test.

Carbonate crusts represent carbonate cemented mud to gravel-size detrital glacial/glaciomarine sediments, the latter being mainly comprised quartz, feldspars and clay (Fig 6.1).

The formation of the MDAC occurs at the SMTZ within the subsurface of the seafloor, where the precipitated carbonate forms a cement lithifying the host sediments. Quartz and feldspars are resistant against weathering, after the grains were derived from the parent rock, glacial processes have transported and deposited the grains on the shelves offshore Norway. Clay minerals rich in Al, K and Na are common constituents of marine sediments, derived from the continent (Nichols, 2009). The depositional regime at the respective study areas is best described by grain size distributions and sorting.

The Hola crusts are constituted by a uniform size range of sand particles; generally, the sand is indicative of a indicating a higher energy environment. This is supported by geomorphological features as big sandwave fields, and elongated coral reefs aligned towards the main current in the Hola area, as described in (Boe *et al.*, 2009; Buhl-Mortensen *et al.*, 2012). Strong currents will prevent the deposition of finer grains of silt and mud size, resulting in a better sorted sediment size distribution (Nichols, 2009). Which supports the observations of sediments observed in the Hola crust.

Detrital particles in the Loppa High crusts are in general less sorted, comprising grains from mud to gravel size, the coarsest and less sorted sediments were found within the crusts from areas PR4 and PR5, indicating a higher energy environment compared to the other study areas PR1 and PR3. The amount of foraminifera decreased with the increased grain-size of sediments.

6.2 Authigenic pyrite

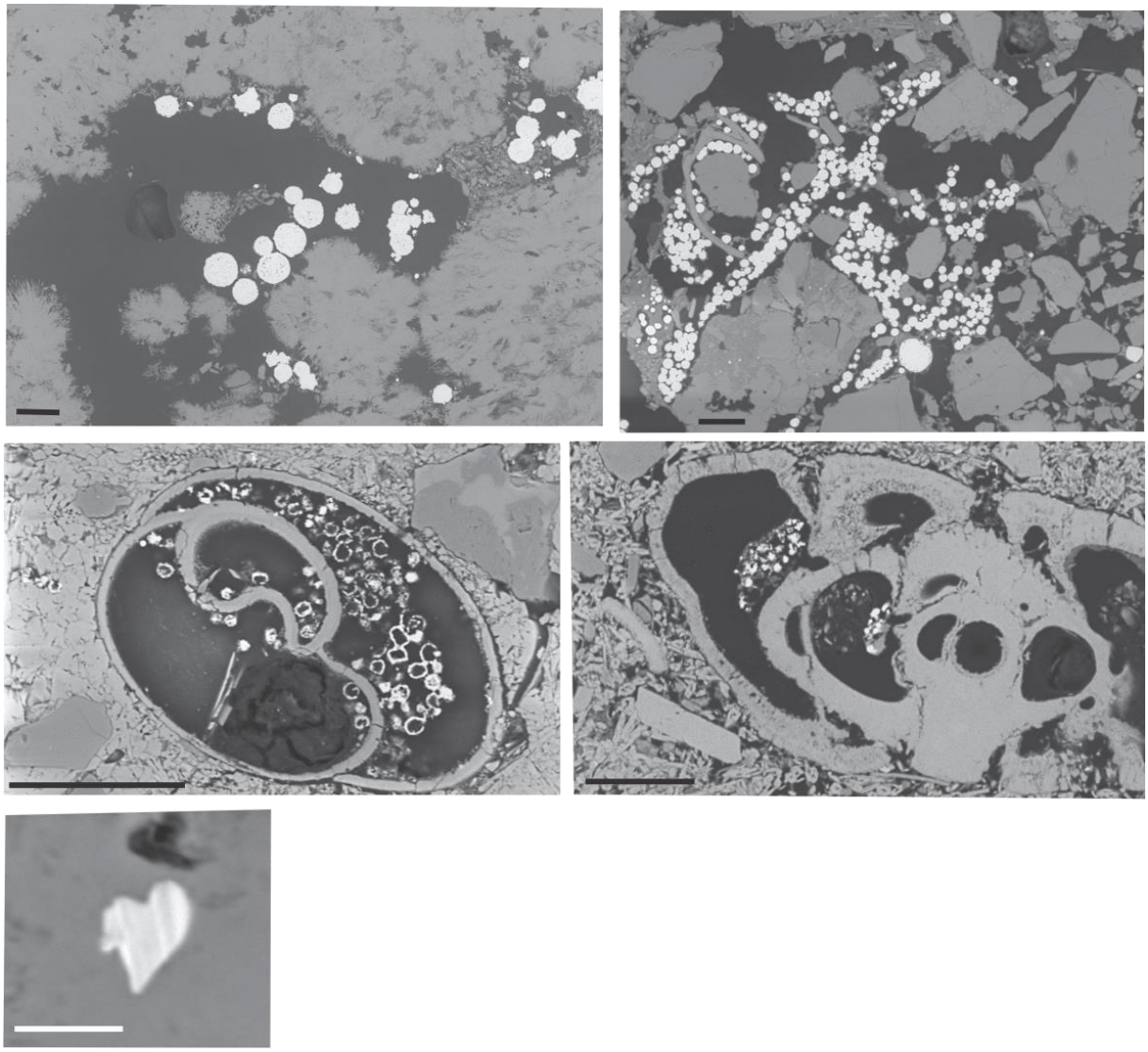

Fig 6.2 Authigenic pyrite occurring in different parts of the crusts, and in different shapes and sizes (black scale-bar: 50 µm, white scale-bar: 5 µm).

Pyrite occurs in different shapes and sizes, but generally in the size range of 2-to10 µm, commonly associated with the biogenic components as well as concentrated in the pore spaces between the grains together with the carbonate cement (Fig 6.2). Framboidal pyrite was often occured within the tests of the foraminifera; in the BSE-image pyrite appeared as the brightest phase due to the high content of Fe. Formation of authigenic pyrite is induced by the coupled process of anaerobic oxidation of methane and sulfate reduction that generates hydrogen sulfide, which in turn forms pyrite through reaction with dissolved Fe (Ritger *et al.*, 1987).

6.3 Biogenic components

The biogenic components in carbonate crust comprise shells and remnants of different organisms. The main identified biogenic components ant their content are further discussed below.

6.3.1 Siliceous spicules

In all of the Loppa High MDAC crusts there were abundant siliceous circular/needle-shaped structures present. They were very abundant and the size range varied widely. These structures are interpreted to be spicules (skeletal elements) of siliceous sponges. Sponges are aquatic, sessile multicellular organisms, which are divided into three classes; Hexactinellida (siliceous sponges), Demospongiae (siliceous/sponging sponges) and Calcarea (calcareous sponges) (Müller *et al.*, 2009). The siliceous spicules, Hexactinellida and Demospongia are composed of amorphous opal (noncrystalline silica) (SiO_2*nH_2O) (Müller *et al.*, 2009; Müller *et al.*, 2008). The siliceous spicules of Demospongiae and Hexactinellida are found in a high diversity of shapes and sizes, with lengths varying from micrometers to centimeters, usually divided into microscleres and megaslceres (Uriz *et al.*, 2003). The spicules observed embedded in the carbonate cement in the crust did not exhibit any recrystallization or overgrowths.

No spicules occurred in the Hola crust, in agreement with the results of the MAREANO mapping of benthic habitats on the seafloor off the coast of Vesterålen. The sponge communities occur at banks and plains with water depths between 200-300 m, on muddy substrates (Buhl-Mortensen *et al.*, 2012).

6.3.2 Bivalve shells

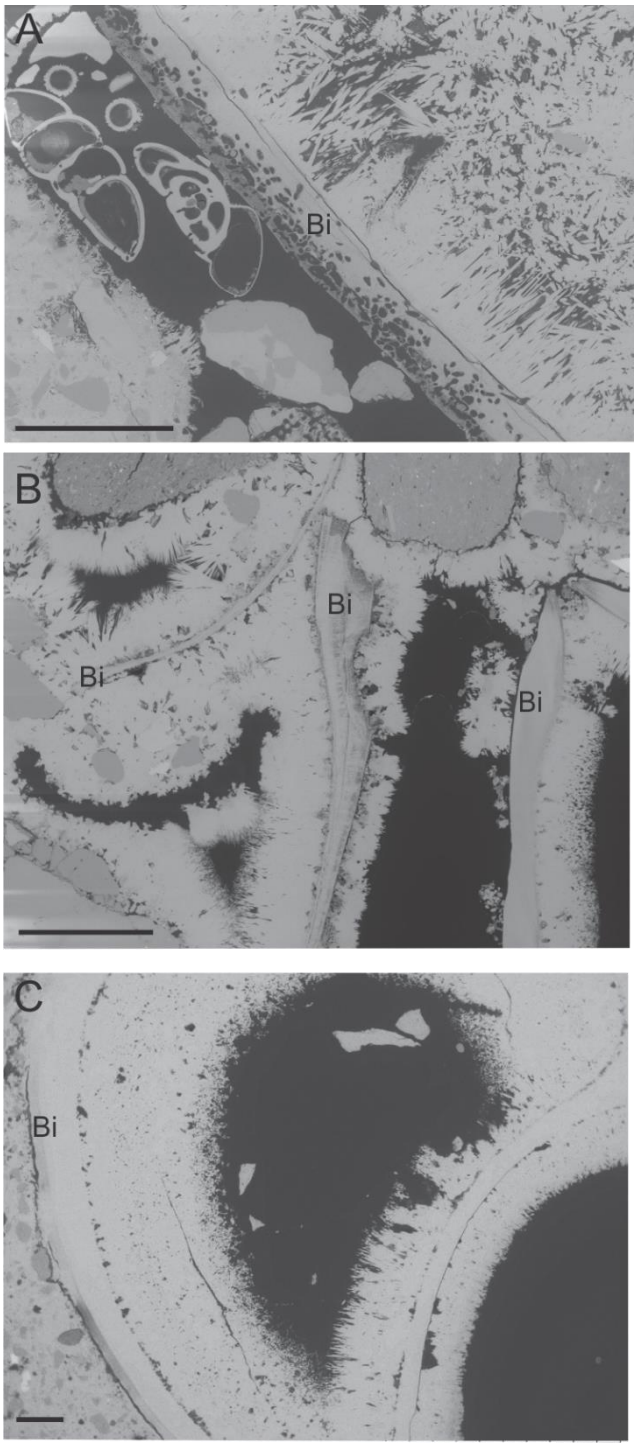

Fig 6.3: Overview of bivalves observed in different crusts (Bi-bivalve, black scale-bar: 200 µm). A.) Part of a bivalve with aragonite crystals radiating out on one side, on the left side there is a cavity with two tests belonging to Cibicides. B.) Shell fragments of bivalves in the carbonate cement. C.) Aragonite crystals radiating out in pore space within the bivalve.

Shell fragments of bivalves were one of the main contributors to the biogenic content, observed in all of the crusts including the crusts from PR4 and PR5 where the other organisms rarely occur in crust. The fragments of bivalve shells were often observed with big crystals radiating out from the walls (Fig 6.3). If that was a result of the pore space provided by the bivalves, or if the carbonate cement nucleated on the shell is not closely investigated. The authigenic carbonate phase forming needle-like crystals associated with bivalves is aragonite as indicated but BSE-images (aragonite is brighter in BSE-images compared to bivalve calcite) and by EDS-analysis. Therefore, the aragonite crystals radiating out from the walls of the bivalves are proposed to be results of the provided pore spaces.

6.4 Foraminifera

The aim of this study was to investigate if the precipitation of authigenic carbonate cement nucleated on the tests of foraminifera, and to assess if the different species responded differently to authigenic carbonate precipitation.

The foraminiferal assemblage in the studied crust is dominated by benthic foraminifera species in the size range from 100 µm to 250 µm. In the weakly cemented sediments, the foraminiferal assemblage were composed of both planktonic and benthic species, similar to the species in the crusts.

As the tests of the foraminifera occur randomly crosscut in the thin sections, identifying the different species was difficult; the main classifications is therefore set by planktonic species and benthic species. However, for some specimens it was possible to identify the Genus.

In the samples, the foraminiferal tests have different state of alteration: some of them are very well preserved whereas other show alteration due to the precipitation of methane-derived authigenic carbonate on their tests after burial. The main characteristics are listed below:

- Pristine tests embedded in the cement.
- Overgrowth of Mg-calcite crystals on test walls.
- Recrystallization or “neomorphism” of the test.
- Carbonate cement infill of the chambers either as aragonite crystals or as microcrystalline cement.

6.4.1 Planktonic foraminifera

The amount of planktonic foraminifera occurring in the crusts were low, and the main planktonic assemblage occurs within the weakly cemented areas and in cavities. The planktonic foraminifera tests are deposited by “falling” down the water column and onto the seafloor, if the currents are too strong the tests will be carried away and deposited at lower energy environments. Which is proposed to be the main reason for the low amount of planktonic foraminifera occurring in the crust specimens.

Even though the amount of tests of planktonic foraminifera was low compared to tests of benthic foraminifera, the preservation states are similar. The planktonic tests were observed with all the main preservations states as earlier listed.

6.4.2 Benthic foraminifera

Benthic foraminifera were the main contributors to the foraminiferal assemblages, they were observed in all of the crusts except the crust PR1210036. The coarse grained crust represent depositional environment too harsh for the foraminifera, or most likely it could be a result of the thin sections not covering the entire crust.

Based on all the observations there were no indications of some species working as better nucleation templates for the carbonate precipitation compared to others. Likewise, there is no indication that some specific species are more resistant to alteration than others as all of the different species were observed occurring in different alteration/preservation states. The majority of the foraminifera have tests composed by calcite, but species belonging to *Miliolids* secrete tests of high Mg-calcite (Sen Gupta, 2003), the *Miliolida sp.* in the studied MDAC crusts did not differ from the rest of the benthic species.

The most common species are further discussed below.

6.4.3 Cibicides sp.

One of the most dominant species is interpret to belong to the genus *Cibicides*. The alteration state varied from pristine to recrystallized, but most often occurred with a rather pristine test, with minor Mg-calcite coating on some of the inner chambers, and cement infilling in the chambers. Overview of different and characteristic alteration states are seen in Fig 6.4

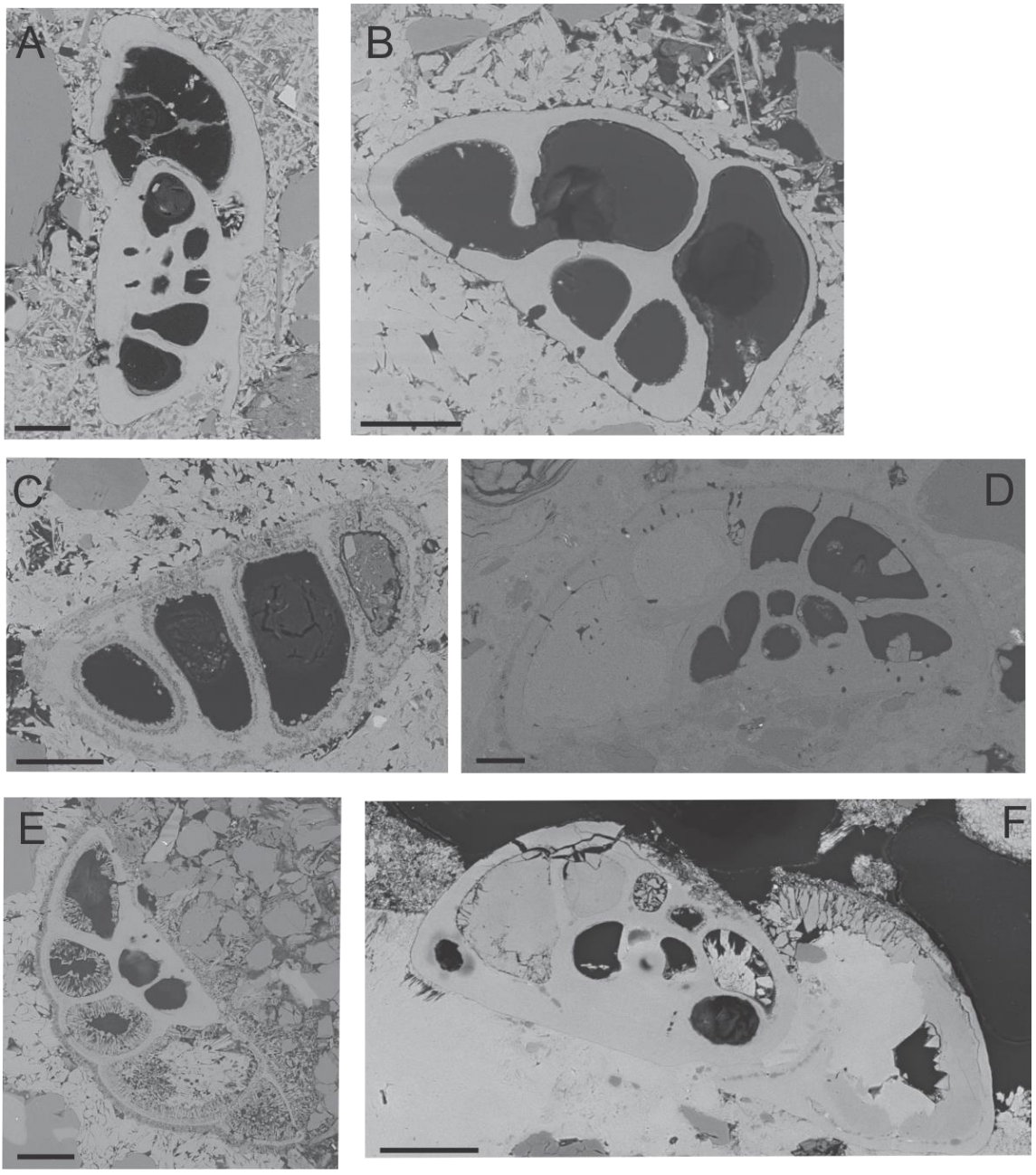

Fig 6.4: Overview of different preservation states observed within the species Cibicides sp.; examples from both the study areas Loppa High and Hola. A) and B) represent the pristine tests, with no overgrowth or recrystallization. C) The test has been altered by recrystallization, but no overgrowth. D) No recrystallization on the test, original pores are still visible but a small coating of Mg-calcite crystals covers the outer test wall, seen as a BSE darker rim. E) Test with both recrystallization and overgrowth, the crystals on the inner chamber walls are equal in size and bigger than the crystals on the outer test wall. F) Test partially recrystallized and some Mg-calcite overgrowth. Most of the overgrowth of Mg-calcite crystals are only seen as a BSE darker coating. Carbonate cement within the chambers. Some BSE darker areas internally in the calcite test represent an Mg-calcite enrichment within some of the lamellar walls. (Black scale-bar 60µm).

6.4.4 Cassidulina sp.

Cassidulina sp. is amongst the dominant species observed within the crusts. Similar alteration states of the tests compared to the species of *Cibicides sp.*, which are shown in Fig 6.5. Some of the most representative examples of recrystallized test with overgrowths on the outer chamber walls occurred in species of the Loppa High crusts.

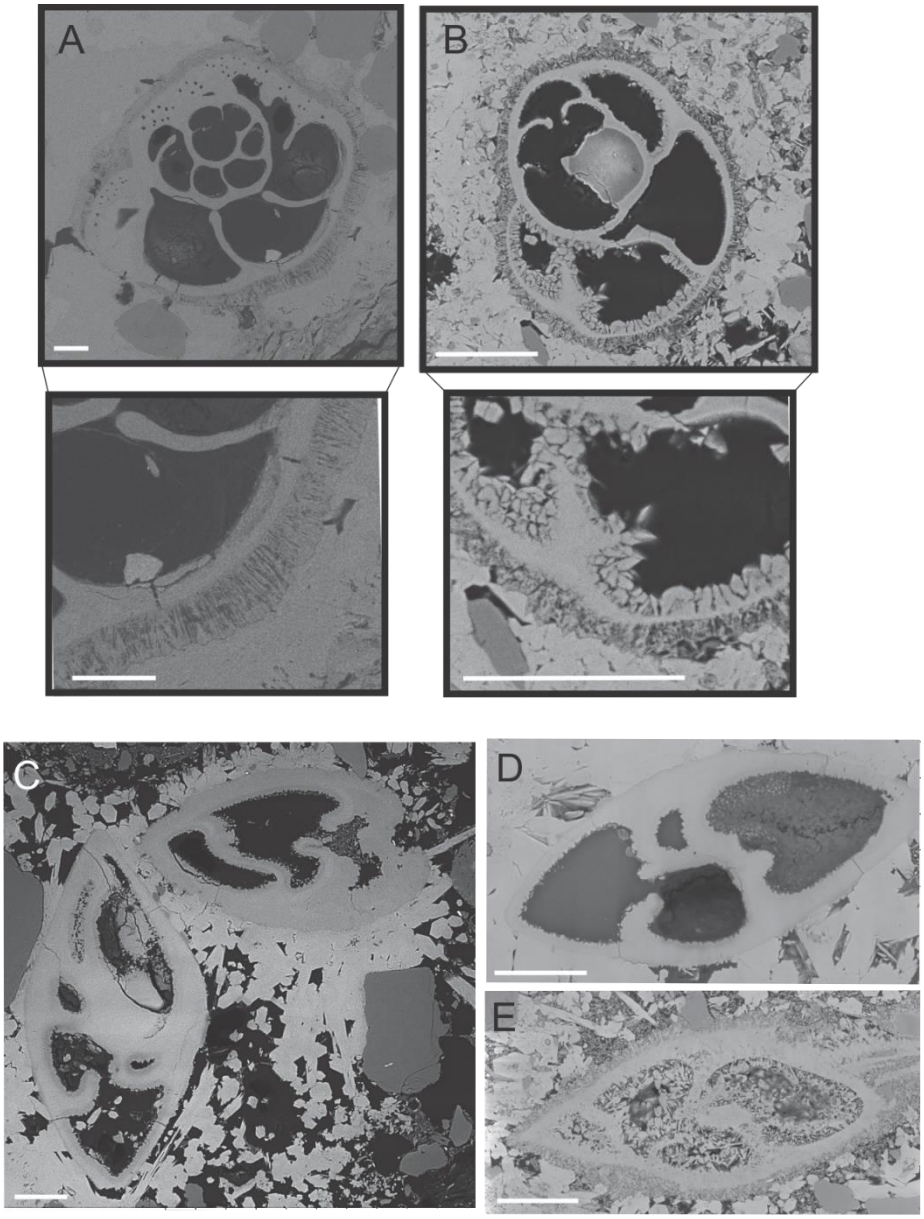

Fig 6.5: Different examples of the species Cassidulina sp. from both the study areas. A.) The test has a smooth appearance with primary pores intact, but with Mg-calcite crystals on the outer test wall. Surrounding aragonite cement has a smooth appearance but no clear nucleation on the test. B.)A test with overgrowth on the outer walls, and on the inner walls. Surrounding cement with a more fibrous appearance. C.) Overgrowth only seen as BSE darker coatings, no recrystallization of the test. D.) Overgrowth only on inner chambers. E.) Completely recrystallized test, with overgrowth of big crystals on all the inner walls, and smaller crystals on the outer test. Fibrous aragonite cement surrounding the specimen. (White scale-bar 50µm).

6.4.5 Buliminella sp.

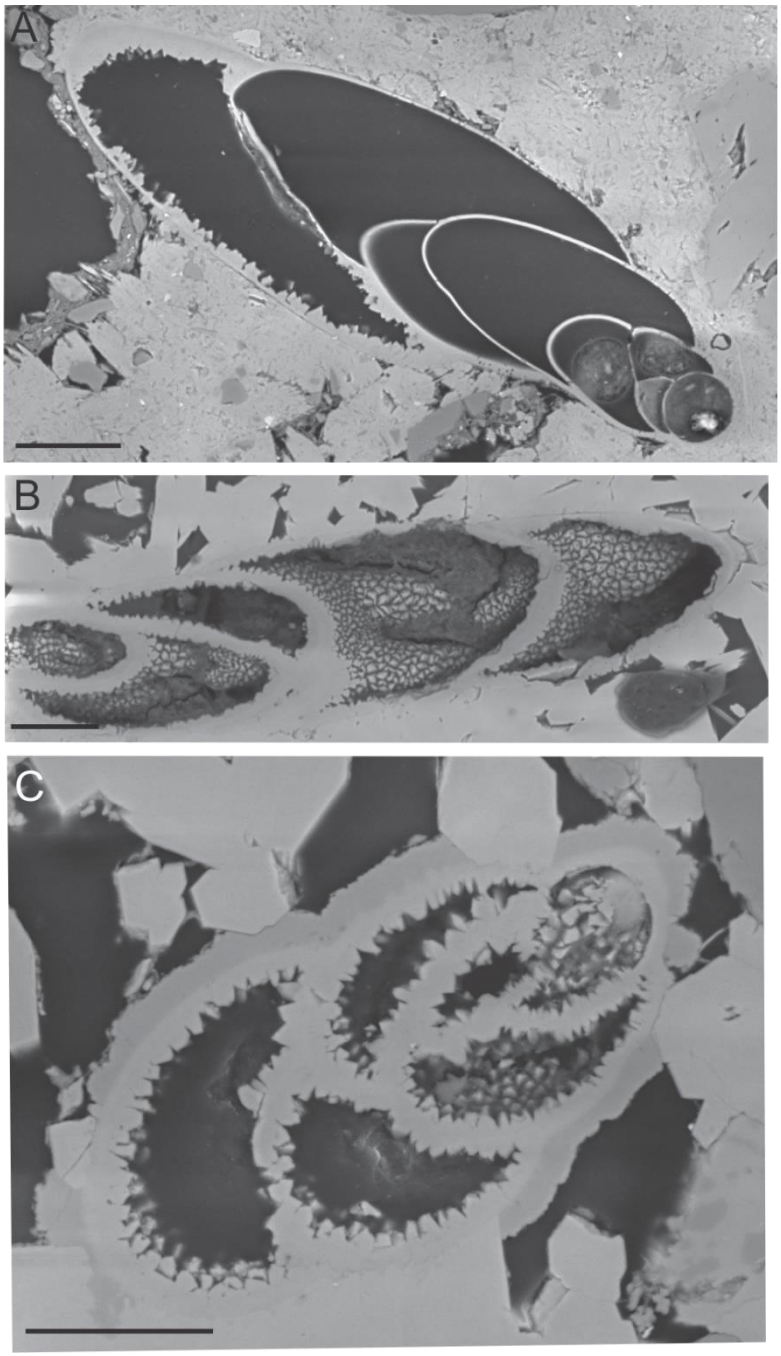

Fig 6.6: Overview of the most common states found within Buliminella sp.. A.)Overgrowth only found on the inner chamber walls of the oldest chambers. B.) Overgrowth of rhombohedral crystals seen on all the inner chamber walls. C.) Same as B.) but also a dark coating of Mg on the outer test wall. (Black scale-bar: 30μm.

Species interpret to belong to the genus *Buliminella* were observed in the crusts from both Loppa High and Hola. The majority of the specimens observed had rhombohedral Mg-calcite crystals growing the inner chamber walls (Fig 6.6).

6.4.6 Agglutinated foraminifera

Agglutinated benthic foraminifera are rare in the benthic foraminiferal assemblage, but some species were observed. EDS-analysis revealed that the agglutinated species selected siliceous grains, commonly quartz, to build the tests. The cement among the grains in the test was aragonite, some examples are given in Fig 6.7. Clearly, the agglutinated tests composed of quartz grains did not serve as a template for the precipitated authigenic carbonates, as there were no signs of overgrowth or recrystallization, but they often exhibited aragonite cement within the chambers.

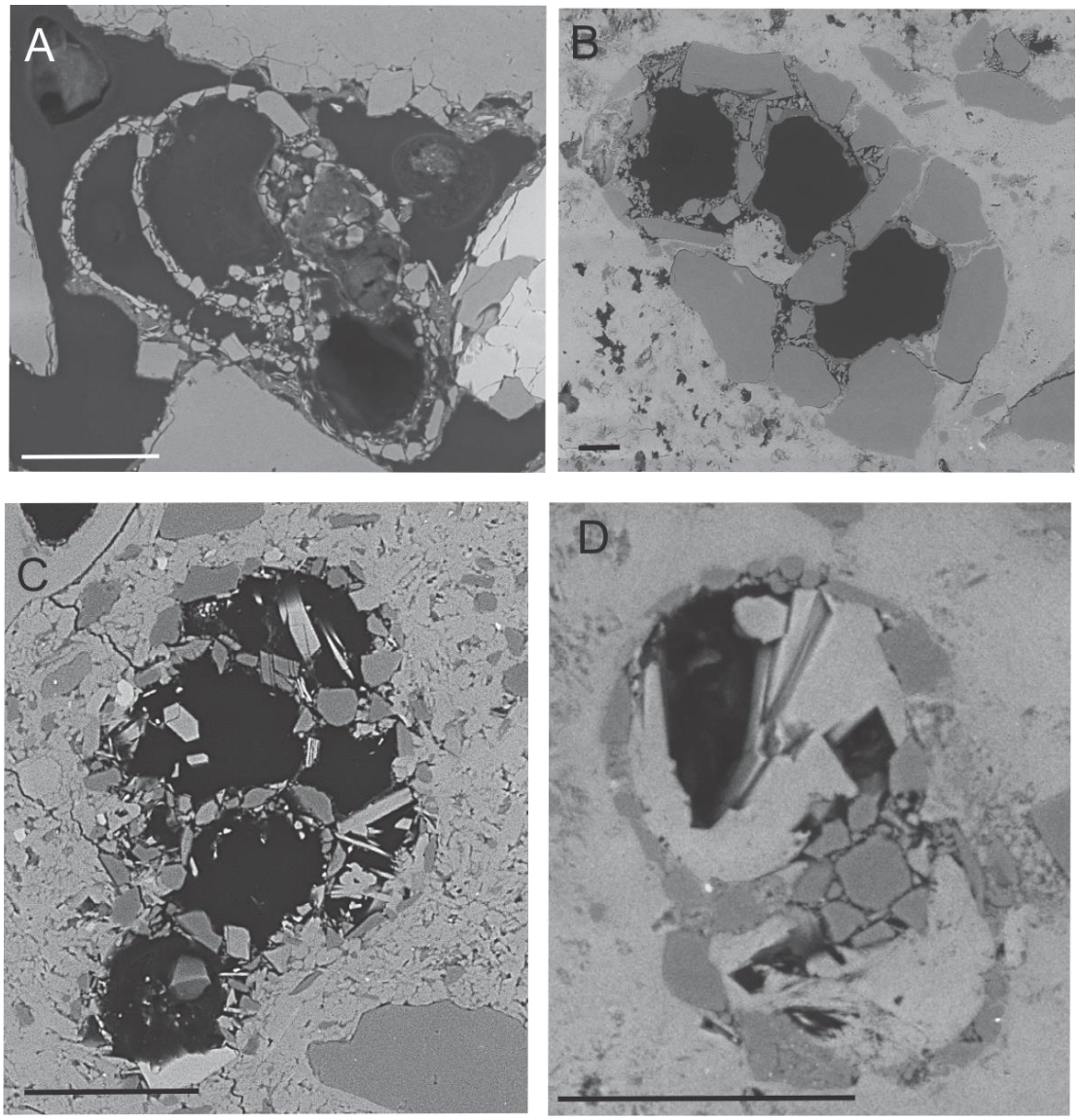

Fig 6.7: An overview of some of the agglutinated benthic foraminifera (black or white scale-bar: 50 µm). A) A benthic test occurring in poorly cemented area of the crust. B) A rather big specimen, which seems to prefer elongated grains of quartz to build the test. C) Agglutinated test with quartz grains of similar size and roundness, aragonite crystals within the chambers. D) Agglutinated test with chamber infill of aragonite cement.

6.5 Cement mineralogy

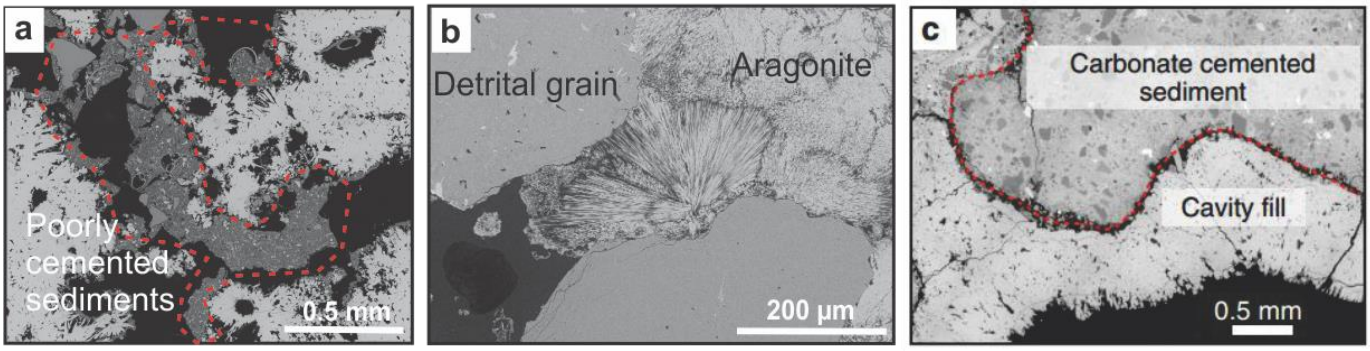

Fig 6.8: A) Overview of detrital sediments with biogenic components in poorly cemented areas within cavities. B) Fibrous aragonite between pore spaces of detrital grains. C) From (Cremiere et al., 2016a), with early-stage cements marked in carbonate cemented sediment, and clean radial fibrous aragonite cavity fill.

The presented observations indicate that aragonite is the dominating phase authigenic carbonate cement (Fig 6.8),based on the EBS-image intensity, and the EDS-analysis (contains minor Sr). Minor Mg-calcite is also present, commonly occurring as overgrowths on the tests of the foraminifera. These carbonate mineralogy observations coincides with the XRD results of Cremiere *et al.* (2016a), shown in Table 2.

Table 2: Supplementary table, from (Cremiere et al., 2016a)

Sample	Area	Carbonate minerals	Detrital minerals
P1210001	PR1	Aragonite	Quartz, plagioclase, illite/muscovite, chlorite
P1210002	PR1	Aragonite	Quartz, plagioclase, illite/muscovite, chlorite
P1210010	PR3	Aragonite, high-Mg calcite (14% mol $MgCO_3$)	Quartz, plagioclase, chlorite
P1210011	PR3	Aragonite	Quartz, plagioclase, illite/muscovite, chlorite
P1210017	PR4	Aragonite, high-Mg calcite (15% mol $MgCO_3$)	Quartz, plagioclase, illite/muscovite, amphibolite, chlorite
P1210032	PR5	Aragonite	Quartz, plagioclase, illite/muscovite, amphibolite, chlorite
P1210036	PR5	Aragonite, Calcite	Quartz, plagioclase, illite/muscovite, amphibolite, chlorite
Hola	Hola	Aragonite	Quartz, plagioclase, illite/muscovite

The main carbonate phases observed within MDACs are authigenic aragonite and Mg-calcite (Aloisi *et al.*, 2000; Cremiere *et al.*, 2016b; Peckmann & Thiel, 2004). According to Burton (1993), the mineralogy of carbonates in diagenetic environments is controlled by several environmental parameters; sulfate concentration, alkalinity, Ca^{2+}/Mg^{2+} ratios and carbonate saturation state. Precipitation of aragonite occurs with high sulfate concentrations under conditions of high methane flux, when the thought SMTZ are shallower in the seafloor subsurface. Whereas Mg-calcite precipitates at lower sulfate concentration and methane flux, deeper in the subsurface (Aloisi *et al.*, 2000; Luff, R. *et al.*, 2005). The dominated aragonite phase could be a result of carbonate precipitation occurring in a more open system conditions, within subsurface sediments containing sulfate, and Mg-calcite precipitation happens with a more diffusive methane seepage flux deeper within the subsurface sediments (Cremiere *et al.*, 2016b).

6.6 Carbonate mineralogy of precipitated authigenic carbonates and foraminiferal tests

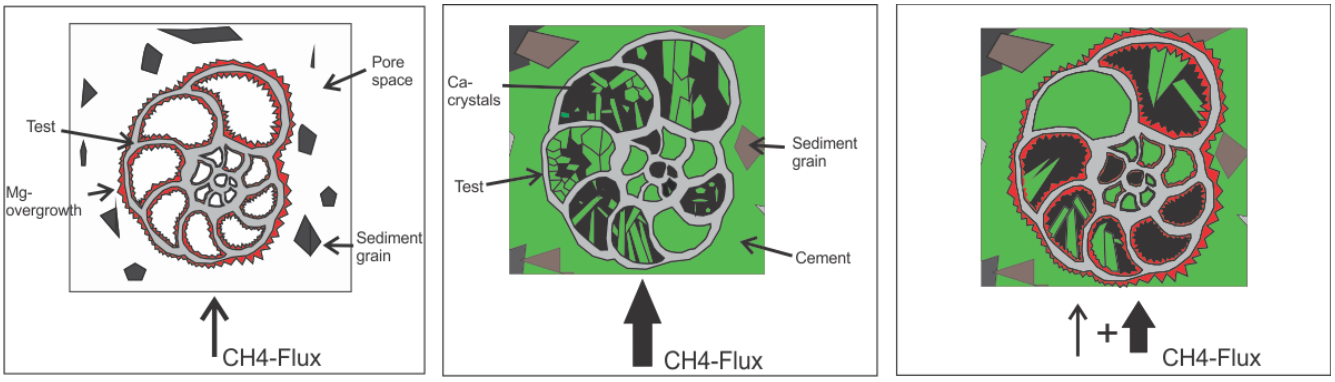

Fig 6.9: Schematic diagram of authigenic carbonate precipitation associated with foraminiferal tests. During conditions of low methane flux precipitation of Mg-calcite phase is right, and it occurs on the inner and/or outer walls of the test. A higher flux favors the aragonite phase, which does not nucleate on the foraminiferal test due to a different crystal structure. When Mg-calcite and aragonite are observed together in the foraminifera tests it is therefore interpreted to reflect changes in the intensity of the methane flux. Thick arrow represents high methane flux, thin arrow represents a lower flux.

Aragonite and calcite are polymorphs, meaning that they have the same chemical formula, but the crystal structure is not the same. Whereas calcite and Mg-calcite share the same crystalline structure (Burton, 1993; Flugel, 2004). Therefore, the calcite tests of foraminifera could serve as nucleation centers for the authigenic Mg-calcite, but this is not true for the authigenic aragonites. Which matches the results of the observations, where the occurrences of Mg-calcite that overgrows could be results of a low methane flux, and a SMTZ located lower in the sediment column. Followed by a change in the flux to a higher intensity supporting in a rapid precipitation of aragonite carbonate cement embedding and lithifying the sediments and biogenic content (Fig 6.9).

During the Last Glacial Maximum the Scandinavian Ice Sheet covered the Norwegian shelf and the entire Barents Sea, the pressure effects on the seafloor due to ice- sheet loading resulted in thickening of the GHSZ. Furthermore, the ice-sheet caused also the reactivation of the fault systems enhancing the migration of methane from deeper sources which in turn supported the formation of gas hydrates. The retreat of the SIS from the shelf margin began at 19 ka (Ottesen *et al.*, 2005; Winsborrow *et al.*, 2010), where the unloading of ice led to thinning of the GHSZ and gas hydrate dissociation. So the precipitation of Mg-calcite could represent the early stages of methane flux due to gas hydrate dissociation. And the aragonite phase could be interpreted to have precipitated with further changes in glacial unloading, isostatic rebound with seafloor rising and inflow of warmer bottom water, which led to a higher methane flux and a shallower SMTZ supporting the rapid aragonite precipitation (Cremiere *et al.*, 2016a)

6.7 Nucleation centers or not

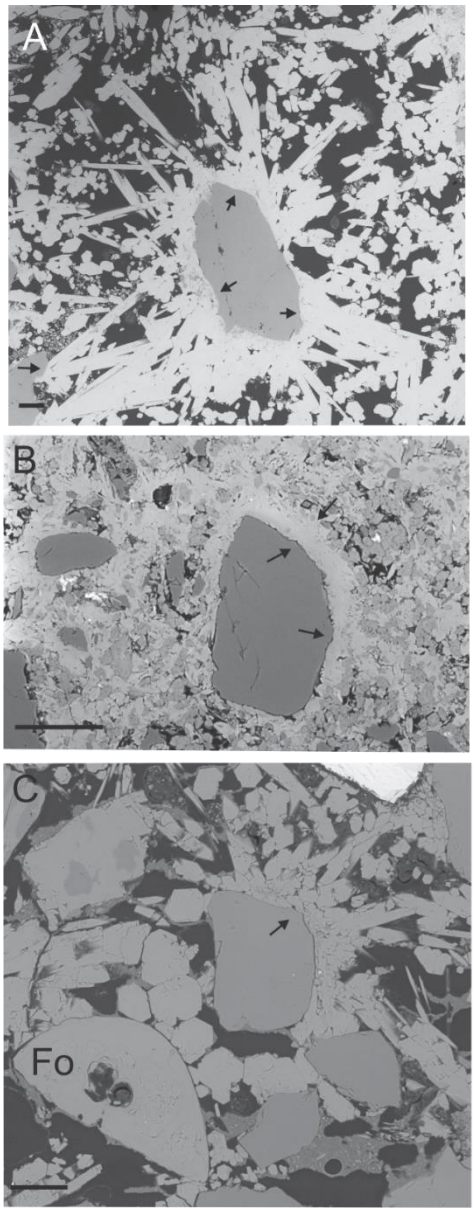

Fig 6.10: (Black scale-bar 50 µm). Different detrital quartz grains embedded aragonite cement, indicated by black arrows.

Based on the observations of the biogenic components within the MDAC crusts, it seems fair to say that the Mg-calcite overgrowths occur on the calcite tests of foraminifera. Interestingly, however, the overgrowth of Mg-calcite crystals was not observed on the bivalves. The Mg-calcite masking the primary test is interpreted to be most effective under low flux of methane, whereas the tests act passively during aragonite precipitation during higher intensity of methane flux. It is discussed if diagenetic processes equally alters tests of benthic and planktonic foraminifera by the means of dissolution, recrystallization and overgrowth. Where it has been suggested that benthic foraminifera are considered less receptive to these processes due to the more heavily calcified test compared to planktonic tests (Edgar *et al.*, 2013; Sexton, Philip F & Wilson, 2009). However the observations in this thesis clearly shows diagenetic alteration on the tests of benthic foraminifera, which is also reported in other studies, e.g. (Consolaro *et al.*, 2015; Edgar *et al.*, 2013; Sexton, Philip F & Wilson, 2009). Whether tests of planktonic foraminifera are less resistant of diagenetic alterations in relation to the cold seep environments is not concluded in this thesis, as there is not enough planktonic test observations to make a statistically founded conclusion. But it is interpreted that there is no significant differences in the alteration states in the occurring tests of both planktonic and benthic foraminifera as well as in the different species. The most common preservation states observed are tests with Mg-calcite either as small overgrowths seen as a darker BSE coating, or as bigger crystals on the inner chamber walls of the test and/or on the outer walls, and recrystallization of the calcite tests itself. The aragonite cement occurs as embedding the foraminifer test and/or forming relatively large crystals within chambers. Aragonite precipitation does not seem to be controlled by any specific biogenic template or other components in the crusts as nucleation centers rather utilizing the available pore spaces during precipitation, e.g. Fig 6.10.

6.8 For further studies using tests of foraminifera related to methane seeps and MDAC

Geochemical analysis of the calcite foraminifer test has increased in paleoenvironmental studies. Assuming that the isotopic composition of foraminifera is a function of the temperature and the isotopic composition of the ambient water (Poole & Vorren, 1993), the different isotopic compositions of oxygen and carbon of foraminifera tests can be used to reconstruct different paleoenvironmental parameters such as ice-volume, sea-level, carbon cycle, paleocirculation patterns etc. and how these records have varied trough time (Katz *et al.*, 2010). Diagenetic alterations of the tests could obscure the primary isotopic values, so it is crucial that the calcite tests that are used for paleoenvironmental impretations are well preserved (Drury *et al.*, 2014). Because the average chemical composition of the test can be affected by secondary recrystallization, overgrowth and authigenic carbonates within chambers and/or on the test, with secondary precipitation processes occurring at different temperature and geochemical conditions than the water mass in which the foraminifera live (Sexton, P. F. *et al.*, 2006).

The foraminifera tests occurring in the studied MDAC crusts exhibit several different alteration states often with secondary alterations induced by authigenic carbonates. If used in geochemical studies it is important to bear this in mind. Secondary Mg-calcite overgrowths on inner chamber walls as well as aragonite chamber infill would be important to “clean off”, if possible, prior to these studies, for most reliable results.

7 Summary and conclusions

Methane-derived authigenic carbonate (MDAC) crusts from four seepage sites at the Loppa High in the southwestern Barents Sea, and one seepage site at Hola, off Vesterålen in the Norwegian Sea, have been investigated, with the main focus of understanding if and how the tests of benthic and planktonic foraminifera occurring in the crusts could serve as nucleation centers for the precipitated carbonates, and if so – were there any differences between species?

- The MDAC crusts represent carbonate cemented detrital sediments, mainly comprised of quartz, feldspars and clay.
- Biogenic components in the crusts mainly comprise shells of bivalves, tests of foraminifera and siliceous spicules, except for the Hola crusts.
- Aragonite is the dominating phase of authigenic carbonate cement, but minor Mg-calcite is also present, commonly occurring as overgrowths on the tests of foraminifera. No Mg-calcite overgrowths were observed on the shells of bivalves or on the siliceous spicules.
- Authigenic pyrite are common in MDAC crusts, as they are induced by the coupled process of AOM and sulfate reduction generating hydrogen sulfide which forms pyrite through reaction with dissolved Fe.
- Different alteration states of foraminifera tests were observed: pristine tests embedded in the carbonate cement, tests with overgrowth of Mg-calcite crystals, tests completely recrystallized, and tests where the carbonate fill the chambers.
- There were no indications of variations of alteration states between neither the planktonic- or benthic tests of foraminifera, or between species.
- Precipitation of Mg-calcite nucleate on the tests of foraminifera, which is interpret to occur during low fluxes of methane at SMTZ deeper within the sediments.
- No indications of aragonite nucleating on the tests, as aragonite and calcite has two different crystal structures, but aragonite cement often occurs infill the foraminiferal chambers.
- For geochemical studies it is important to understand the effects of authigenic carbonates on foraminifera test, as the primary geochemical record “stored in the tests” can be masked with the presence of secondary overgrowth and recrystallization.

8 References

Aarseth, I. (1997). Western Norwegian fjord sediments: age, volume, stratigraphy, and role as temporary depository during glacial cycles. *Marine Geology, 143*(1-4), 39-53. doi:Doi 10.1016/S0025-3227(97)00089-3

Aloisi, G., Bouloubassi, I., Heijs, S. K., Pancost, R. D., Pierre, C., Damsté, J. S. S., . . . Rouchy, J. (2002). CH 4-consuming microorganisms and the formation of carbonate crusts at cold seeps. *Earth and Planetary Science Letters, 203*(1), 195-203.

Aloisi, G., Pierre, C., Rouchy, J. M., Foucher, J. P., Woodside, J., & Party, M. S. (2000). Methane-related authigenic carbonates of eastern Mediterranean Sea mud volcanoes and their possible relation to gas hydrate destabilisation. *Earth and Planetary Science Letters, 184*(1), 321-338. doi:Doi 10.1016/S0012-821x(00)00322-8

Aloisi, G., Wallmann, K., Bollwerk, S. M., Derkachev, A., Bohrmann, G., & Suess, E. (2004). The effect of dissolved barium on biogeochemical processes at cold seeps. *Geochimica Et Cosmochimica Acta, 68*(8), 1735-1748.

Andreassen, K., Laberg, J. S., & Vorren, T. O. (2008). Seafloor geomorphology of the SW Barents Sea and its glaci-dynamic implications. *Geomorphology, 97*(1), 157-177.

Armstrong, H., & Brasier, M. D. (2005). *Microfossils* (2nd ed.). Malden, Mass.: Blackwell Pub.

Barbieri, R., & Panieri, G. (2004). How are benthic foraminiferal faunas influenced by cold seeps? Evidence from the Miocene of Italy. *Palaeogeography, Palaeoclimatology, Palaeoecology, 204*(3), 257-275.

Bayon, G., Henderson, G., & Bohn, M. (2009). U–Th stratigraphy of a cold seep carbonate crust. *Chemical Geology, 260*(1), 47-56.

Boe, R., Bellec, V. K., Dolan, M. F. J., Buhl-Mortensen, P., Buhl-Mortensen, L., Slagstad, D., & Rise, L. (2009). Giant sandwaves in the Hola glacial trough off Vesteralen, North Norway. *Marine Geology, 267*(1-2), 36-54. doi:10.1016/j.margeo.2009.09.008

Borowski, W. S., Paull, C. K., & Ussler, W. (1996). Marine pore-water sulfate profiles indicate in situ methane flux from underlying gas hydrate. *Geology, 24*(7), 655-658.

Bruker. (2010). QUANTAX 70

EDS System for

Hitachi Tabletop Microscope TM3000.

Bugge, T., Mangerud, G., Elvebakk, G., Mørk, A., Nilsson, I., Fanavoll, S., & Vigran, J. (1995). The Upper Palaeozoic succession on the Finnmark Platform, Barents Sea. *Norsk Geologisk Tidsskrift, 75*(1), 3-30.

Buhl-Mortensen, L., & Buhl-Mortensen, P. (2007). Mareanotokt i Barentshavet, mars-april & oktober 2007.

Buhl-Mortensen, L., Bøe, R., Dolan, M. F., Buhl-Mortensen, P., Thorsnes, T., Elvenes, S., & Hodnesdal, H. (2012). Banks, troughs and canyons on the continental margin off Lofoten, Vesterålen, and Troms, Norway. *Seafloor Geomorphology as Benthic Habitat: GeoHab Atlas of Seafloor Geomorphic Features and Benthic Habitats. Elsevier Insights, London. http://dx. doi. org/10.1016/B978-0-12-385140-6.00051-7*.

Bunz, S., & Mienert, J. (2004). Acoustic imaging of gas hydrate and free gas at the Storegga Slide. *Journal of Geophysical Research-Solid Earth, 109*(B4).

Burton, E. A. (1993). Controls on marine carbonate cement mineralogy: review and reassessment. *Chemical Geology, 105*(1-3), 163-179.

Campbell, K. A. (2006). Hydrocarbon seep and hydrothermal vent paleoenvironments and paleontology: Past developments and future research directions. *Palaeogeography Palaeoclimatology Palaeoecology, 232*(2-4), 362-407. doi:10.1016/j.palaeo.2005.06.018

Chand, S., & Minshull, T. A. (2003). Seismic constraints on the effects of gas hydrate on sediment physical properties and fluid flow: a review. *Geofluids, 3*(4), 275-289.

References

Chand, S., Thorsnes, T., Rise, L., Brunstad, H., Stoddart, D., Boe, R., . . . Svolsbru, T. (2012). Multiple episodes of fluid flow in the SW Barents Sea (Loppa High) evidenced by gas flares, pockmarks and gas hydrate accumulation. *Earth and Planetary Science Letters, 331*, 305-314. doi:10.1016/j.epsl.2012.03.021

Consolaro, C., Rasmussen, T., Panieri, G., Mienert, J., Bünz, S., & Sztybor, K. (2015). Carbon isotope (δ 13 C) excursions suggest times of major methane release during the last 14 kyr in Fram Strait, the deep-water gateway to the Arctic. *Climate of the Past, 11*(4), 669-685.

Cremiere, A., Lepland, A., Chand, S., Sahy, D., Condon, D. J., Noble, S. R., . . . Brunstad, H. (2016a). Timescales of methane seepage on the Norwegian margin following collapse of the Scandinavian Ice Sheet. *Nat Commun, 7*, 11509. doi:10.1038/ncomms11509

Cremiere, A., Lepland, A., Chand, S., Sahy, D., Kirsimae, K., Bau, M., . . . Brunstad, H. (2016b). Fluid source and methane-related diagenetic processes recorded in cold seep carbonates from the Alvheim channel, central North Sea. *Chemical Geology, 432*, 16-33. doi:10.1016/j.chemgeo.2016.03.019

Crémière, A., Lepland, A., Chand, S., Sahy, D., Kirsimäe, K., Bau, M., . . . Thorsnes, T. (2016). Fluid source and methane-related diagenetic processes recorded in cold seep carbonates from the Alvheim channel, central North Sea. *Chemical Geology, 432*, 16-33.

Devol, A. H., & Ahmed, S. I. (1981). Are High-Rates of Sulfate Reduction Associated with Anaerobic Oxidation of Methane. *Nature, 291*(5814), 407-408.

Devol, A. H., Anderson, J. J., Kuivila, K., & Murray, J. W. (1984). A Model for Coupled Sulfate Reduction and Methane Oxidation in the Sediments of Saanich Inlet. *Geochimica Et Cosmochimica Acta, 48*(5), 993-1004.

Dore, A. G. (1995). Barents Sea Geology, Petroleum Resources and Commercial Potential. *Arctic, 48*(3), 207-221.

Drury, A. J., Lee, G. P., Pennock, G. M., & John, C. M. (2014). *Data report: late Miocene to early Pliocene coccolithophore and foraminiferal preservation at Site U1338 from scanning electron microscopy.* Paper presented at the Proceedings of the Integrated Ocean Drilling Program.

Edgar, K. M., Pälike, H., & Wilson, P. A. (2013). Testing the impact of diagenesis on the δ18O and δ13C of benthic foraminiferal calcite from a sediment burial depth transect in the equatorial Pacific. *Paleoceanography, 28*(3), 468-480.

Ersdal, G. (2001). *An overview of ocean currents with emphasis on currents on the Norwegian continental shelf*. Retrieved from

Faleide, J. I., Solheim, A., Fiedler, A., Hjelstuen, B. O., Andersen, E. S., & Vanneste, K. (1996). Late Cenozoic evolution of the western Barents Sea-Svalbard continental margin. *Global and Planetary Change, 12*(1-4), 53-74. doi:Doi 10.1016/0921-8181(95)00012-7

Faleide, J. I., Tsikalas, F., Breivik, A. J., Mjelde, R., Ritzmann, O., Engen, O., . . . Eldholm, O. (2008). Structure and evolution of the continental margin off Norway and Barents Sea. *Episodes, 31*(1), 82-91.

Feng, D., & Roberts, H. H. (2011). Geochemical characteristics of the barite deposits at cold seeps from the northern Gulf of Mexico continental slope. *Earth and Planetary Science Letters, 309*(1), 89-99.

Flugel, E. (2004). *Microfacies of carbonate rocks: analysis, interpretation and application*: Springer.

Færseth, R. B. (2012). Structural development of the continental shelf offshore Lofoten–Vesterålen, northern Norway. *Norwegian Journal of Geology/Norsk Geologisk Forening, 92*(1).

Gabrielsen, R. H., Faerseth, R. B., & Jensen, L. N. (1990). *Structural elements of the Norwegian continental shelf*. [Oslo]: Oljedirektoratet.

Gjevik, B. (1996). Models of drift and dispersion in tidal flows. *Waves and Nonlinear Processes in Hydrodynamics, 34*, 343-354.

Gjevik, B. (2000). Summary and assessment of the NDP metocean project. Project report to the Norwegian Deepwater Project.

Gudlaugsson, S. T., Faleide, J. I., Johansen, S. E., & Breivik, A. J. (1998). Late Palaeozoic structural development of the South-western Barents Sea. *Marine and Petroleum Geology, 15*(1), 73-102. doi:Doi 10.1016/S0264-8172(97)00048-2

Hald, M., Saettem, J., & Nesse, E. (1990). Middle and Late Weichselian Stratigraphy in Shallow Drillings from the Southwestern Barents Sea - Foraminiferal, Amino-Acid and Radiocarbon Evidence. *Norsk Geologisk Tidsskrift, 70*(4), 241-257.

Haq, B. U., Hardenbol, J., & Vail, P. R. (1987). Chronology of Fluctuating Sea Levels since the Triassic. *Science, 235*(4793), 1156-1167. doi:DOI 10.1126/science.235.4793.1156

Harris, P. T., & Baker, E. K. (Cartographer). (2012). Seafloor geomorphology as benthic habitat : GeoHAB atlas of seafloor geomorphic features and benthic habitats [xlv, 900 p]

Henriksen, E., Bjornseth, H. M., Hals, T. K., Heide, T., Kiryukhina, T., Klovjan, O. S., . . . Stoupakova, A. (2011). Uplift and erosion of the greater Barents Sea: impact on prospectivity and petroleum systems. *Arctic Petroleum Geology, 35*. doi:10.1144/M35.17

Hitachi. (2013). Let's Familiarize Ourselves with the SEM.

Hovland, M. (2008). *Deep-water coral reefs : unique biodiversity hot-spots*. Dordrecht: Springer.

Hustoft, S., Bünz, S., Mienert, J., & Chand, S. (2009). Gas hydrate reservoir and active methane-venting province in sediments on< 20 Ma young oceanic crust in the Fram Strait, offshore NW-Svalbard. *Earth and Planetary Science Letters, 284*(1), 12-24.

Judd, A. G., & Hovland, M. (2007). *Seabed fluid flow : the impact of geology, biology and the marine environment*. Cambridge ; New York: Cambridge University Press.

Judd, A. G., Hovland, M., Dimitrov, L. I., Garcia-Gil, S., & Jukes, V. (2002). The geological methane budget at Continental Margins and its influence on climate change. *Geofluids, 2*(2), 109-126.

Katz, M. E., Cramer, B. S., Franzese, A., Hönisch, B., Miller, K. G., Rosenthal, Y., & Wright, J. D. (2010). Traditional and emerging geochemical proxies in foraminifera. *The Journal of Foraminiferal Research, 40*(2), 165-192.

Kvenvolden, K. A. (1988). Methane hydrate—a major reservoir of carbon in the shallow geosphere? *Chemical Geology, 71*(1-3), 41-51.

Kvenvolden, K. A. (1993). Gas Hydrates - Geological Perspective and Global Change. *Reviews of Geophysics, 31*(2), 173-187. doi:Doi 10.1029/93rg00268

Kvenvolden, K. A. (1998). A primer on the geological occurrence of gas hydrate. *Geological Society, London, Special Publications, 137*(1), 9-30.

Laberg, J. S., Andreassen, K., & Vorren, T. O. (2012). Late Cenozoic erosion of the high-latitude southwestern Barents Sea shelf revisited. *Geological Society of America Bulletin, 124*(1-2), 77-88.

Landvik, J. Y., Bondevik, S., Elverhøi, A., Fjeldskaar, W., Mangerud, J., Salvigsen, O., . . . Vorren, T. O. (1998). The last glacial maximum of Svalbard and the Barents Sea area: ice sheet extent and configuration. *Quaternary Science Reviews, 17*(1), 43-75.

Larsen, E., Andreassen, K., Nilssen, L., & Raundalen, S. (2003). The prospectivity of the Barents Sea: ice ages, erosion and tilting of traps. *NGU Report, 102*.

Luff, R., Greinert, J., Wallmann, K., Klaucke, I., & Suess, E. (2005). Simulation of long-term feedbacks from authigenic carbonate crust formation at cold vent sites. *Chemical Geology, 216*(1-2), 157-174. doi:10.1016/j.chemgeo.2004.11.002

Luff, R., Wallmann, K., & Aloisi, G. (2004). Numerical modeling of carbonate crust formation at cold vent sites: significance for fluid and methane budgets and chemosynthetic biological communities. *Earth and Planetary Science Letters, 221*(1), 337-353.

Makogon, Y. F. (2010). Natural gas hydrates–A promising source of energy. *Journal of Natural Gas Science and Engineering, 2*(1), 49-59.

Milkov, A. V. (2004). Global estimates of hydrate-bound gas in marine sediments: how much is really out there? *Earth-Science Reviews, 66*(3-4), 183-197. doi:10.1016/j.earscirev.2003.11.002

Milkov, A. V., Vogt, P. R., Crane, K., Lein, A. Y., Sassen, R., & Cherkashev, G. A. (2004). Geological, geochemical, and microbial processes at the hydrate-bearing Hakon Mosby mud volcano: a review. *Chemical Geology, 205*(3-4), 347-366.

Milliman, J., Müller, G., & Förstner, F. (2012). *Recent sedimentary carbonates: Part 1 marine carbonates*: Springer Science & Business Media.

Murray, J. W. (2006). *Ecology and applications of benthic foraminifera*. Cambridge ; New York: Cambridge University Press.

Müller, W. E., Wang, X., Cui, F.-Z., Jochum, K. P., Tremel, W., Bill, J., . . . Wiens, M. (2009). Sponge spicules as blueprints for the biofabrication of inorganic–organic composites and biomaterials. *Applied microbiology and biotechnology, 83*(3), 397-413.

Müller, W. E., Wang, X., Kropf, K., Boreiko, A., Schloßmacher, U., Brandt, D., . . . Wiens, M. (2008). Silicatein expression in the hexactinellid Crateromorpha meyeri: the lead marker gene restricted to siliceous sponges. *Cell and tissue research, 333*(2), 339-351.

Nichols, G. (2009). *Sedimentology and stratigraphy*: John Wiley & Sons.

Niemann, H., Losekann, T., de Beer, D., Elvert, M., Nadalig, T., Knittel, K., . . . Boetius, A. (2006). Novel microbial communities of the Haakon Mosby mud volcano and their role as a methane sink. *Nature, 443*(7113), 854-858. doi:10.1038/nature05227

Niewöhner, C., Hensen, C., Kasten, S., Zabel, M., & Schulz, H. (1998). Deep sulfate reduction completely mediated by anaerobic methane oxidation in sediments of the upwelling area off Namibia. *Geochimica Et Cosmochimica Acta, 62*(3), 455-464.

Nøttvedt, A., Berglund, L., Rasmussen, E., & Steel, R. (1988). Some aspects of Tertiary tectonics and sedimentation along the western Barents Shelf. *Geological Society, London, Special Publications, 39*(1), 421-425.

Ottesen, D., Dowdeswell, J. A., & Rise, L. (2005). Submarine landforms and the reconstruction of fast-flowing ice streams within a large Quaternary ice sheet: The 2500-km-long Norwegian-Svalbard margin (57 degrees-80 degrees N). *Geological Society of America Bulletin, 117*(7-8), 1033-1050. doi:10.1130/B25577.1

Ottesen, D., Stokes, C. R., Rise, L., & Olsen, L. (2008). Ice-sheet dynamics and ice streaming along the coastal parts of northern Norway. *Quaternary Science Reviews, 27*(9), 922-940.

Panieri, G., Camerlenghi, A., Cacho, I., Cervera, C. S., Canals, M., Lafuerza, S., & Herrera, G. (2012). Tracing seafloor methane emissions with benthic foraminifera: Results from the Ana submarine landslide (Eivissa Channel, Western Mediterranean Sea). *Marine Geology, 291*, 97-112.

Panieri, G., Camerlenghi, A., Conti, S., Pini, G. A., & Cacho, I. (2009). Methane seepages recorded in benthic foraminifera from Miocene seep carbonates, Northern Apennines (Italy). *Palaeogeography, Palaeoclimatology, Palaeoecology, 284*(3), 271-282.

Panieri, G., & Sen Gupta, B. K. (2008). Benthic Foraminifera of the Blake Ridge hydrate mound, Western North Atlantic Ocean. *Marine Micropaleontology, 66*(2), 91-102.

Park, A., Dewers, T., & Ortoleva, P. (1990). Cellular and Oscillatory Self-Induced Methane Migration. *Earth-Science Reviews, 29*(1-4), 249-265.

Paull, C. K., Ussler, W., & Dillon, W. (1991). Is the extent of glaciation limited by marine gas-hydrates? *Geophysical Research Letters, 18*(3), 432-434.

Peckmann, J., & Thiel, V. (2004). Carbon cycling at ancient methane–seeps. *Chemical Geology, 205*(3), 443-467.

Peckmann, J., Walliser, O. H., Riegel, W., & Reitner, J. (1999). Signatures of hydrocarbon venting Middle Devonian carbonate mound (Hollard Mound) at the Hamar Laghdad (Antiatlas, Morocco). *Facies, 40*, 281-296. doi:Doi 10.1007/Bf02537477

Poole, D. A., & Vorren, T. O. (1993). Miocene to Quaternary paleoenvironments and uplift history on the mid Norwegian shelf. *Marine Geology, 115*(3-4), 173-205.

Ravelo, A. C., & Hillaire-Marcel, C. (2007). Chapter Eighteen the use of oxygen and carbon isotopes of foraminifera in Paleoceanography. *Developments in Marine Geology, 1*, 735-764.

Reeburgh, W. S. (1980). Anaerobic Methane Oxidation - Rate Depth Distributions in Skan Bay Sediments. *Earth and Planetary Science Letters, 47*(3), 345-352.

Reemst, P., Cloetingh, S., & Fanavoll, S. (1994). Tectonostratigraphic modelling of Cenozoic uplift and erosion in the south-western Barents Sea. *Marine and Petroleum Geology, 11*(4), 478-490.

Rise, L., Bellec, V. K., Chand, S., & Bøe, R. (2014). Pockmarks in the southwestern Barents Sea and Finn mark fjords. *NORWEGIAN JOURNAL OF GEOLOGY, 94*(4), 263-282.

Rise, L., Bøe, R., Riis, F., Bellec, V. K., Laberg, J. S., Eidvin, T., . . . Thorsnes, T. (2013). The Lofoten-Vesterålen continental margin, North Norway: canyons and mass-movement activity. *Marine and Petroleum Geology, 45*, 134-149.

Rise, L., Ottesen, D., Berg, K., & Lundin, E. (2005). Large-scale development of the mid-Norwegian margin during the last 3 million years. *Marine and Petroleum Geology, 22*(1), 33-44.

Ritger, S., Carson, B., & Suess, E. (1987). Methane-Derived Authigenic Carbonates Formed by Subduction Induced Pore-Water Expulsion Along the Oregon Washington Margin. *Geological Society of America Bulletin, 98*(2), 147-156.

Rokoengen, K., Rise, L., Bugge, T., & Sættem, J. (1988). Bedrock geology of the mid Norwegian continental shelf. *Map in scale, 1*(1.000), 000.

Schoell, M. (1988). Multiple origins of methane in the earth. *Chemical Geology, 71*(1), 1-10.

Sen Gupta, B. K. (2003). *Modern Foraminifera*. Dordrecht: Springer Netherlands.

Sexton, P. F., & Wilson, P. A. (2009). Preservation of benthic foraminifera and reliability of deep-sea temperature records: Importance of sedimentation rates, lithology, and the need to examine test wall structure. *Paleoceanography, 24*(2).

Sexton, P. F., Wilson, P. A., & Pearson, P. N. (2006). Microstructural and geochemical perspectives on planktic foraminiferal preservation:“Glassy” versus “Frosty”. *Geochemistry, Geophysics, Geosystems, 7*(12).

Sibuet, M., & Olu, K. (1998). Biogeography, biodiversity and fluid dependence of deep-sea cold-seep communities at active and passive margins. *Deep Sea Research Part II: Topical Studies in Oceanography, 45*(1), 517-567.

Siedlecka, A., & Roberts, D. (1996). Berggrunnskart; Finnmark fylke. *Norges Geologiske Undersøkelse*.

Siegert, M. J., Dowdeswell, J. A., Hald, M., & Svendsen, J.-I. (2001). Modelling the Eurasian Ice Sheet through a full (Weichselian) glacial cycle. *Global and Planetary Change, 31*(1), 367-385.

Sigmond, E. M. (1992). *Berggrunn, Norge med havområder*: Norges geologiske undersøkelse.

Sigmond, E. M., Gjelle, S., Marker, M., Rindstad, B. I., & Herrevold, T. (2002). *Geological map, land and sea areas of northern Europe*: Geological Survey of Norway. Special publication 10 Norges geologiske undersokelse Commission for the Geological Map of the World.

Sloan, E. D. (1990). *Clathrate hydrates of natural gases*. New York: M. Dekker.

Sloan, E. D. (1998). Gas hydrates: Review of physical/chemical properties. *Energy & Fuels, 12*(2), 191-196. doi:DOI 10.1021/ef970164+

Sund, T. (1984). Tectonic Development and Hydrocarbon Potential Offshore Troms, Northern Norway. *Aapg Bulletin-American Association of Petroleum Geologists, 68*(9), 1206-1206.

Svendsen, J. I., Alexanderson, H., Astakhov, V. I., Demidov, I., Dowdeswell, J. A., Funder, S., . . . Houmark-Nielsen, M. (2004). Late Quaternary ice sheet history of northern Eurasia. *Quaternary Science Reviews, 23*(11), 1229-1271.

Sættem, J., Rise, L., & Westgaard, D. A. (1991). Composition and properties of glacigenic sediments in the southwestern Barents Sea. *Marine Georesources & Geotechnology, 10*(3-4), 229-255.

Torres, M. E., Martin, R. A., Klinkhammer, G. P., & Nesbitt, E. A. (2010). Post depositional alteration of foraminiferal shells in cold seep settings: New insights from flow-through time-resolved analyses of biogenic and inorganic seep carbonates. *Earth and Planetary Science Letters, 299*(1-2), 10-22. doi:10.1016/j.epsl.2010.07.048

Torres, M. E., Mix, A. C., Kinports, K., Haley, B., Klinkhammer, G. P., McManus, J., & de Angelis, M. A. (2003). Is methane venting at the seafloor recorded by delta C-13 of benthic foraminifera shells? *Paleoceanography, 18*(3). doi:Artn 1062

10.1029/2002pa000824

Uriz, M. J., Turon, X., Becerro, M. A., & Agell, G. (2003). Siliceous spicules and skeleton frameworks in sponges: origin, diversity, ultrastructural patterns, and biological functions. *Microscopy research and technique, 62*(4), 279-299.

Vincent, E., & Berger, W. (1981). Planktonic foraminifera and their use in paleoceanography. *The sea, 7*, 1025-1119.

Vorren, T. O., Hald, M., & Lebesbye, E. (1988). Late cenozoic environments in the Barents Sea. *Paleoceanography, 3*(5), 601-612.

Vorren, T. O., Lebesbye, E., Andreassen, K., & Larsen, K. B. (1989). Glacigenic Sediments on a Passive Continental-Margin as Exemplified by the Barents Sea. *Marine Geology, 85*(2-4), 251-272. doi:Doi 10.1016/0025-3227(89)90156-4

Wheeler, A. J., & Stadnitskaia, A. (2011). *Developments in Sedimentology* (Vol. 63). Amsterdam: The Netherlands: Elsevier.

Whiticar, M. J. (1999). Carbon and hydrogen isotope systematics of bacterial formation and oxidation of methane. *Chemical Geology, 161*(1), 291-314.

Winsborrow, M. C., Andreassen, K., Corner, G. D., & Laberg, J. S. (2010). Deglaciation of a marine-based ice sheet: Late Weichselian palaeo-ice dynamics and retreat in the southern Barents Sea reconstructed from onshore and offshore glacial geomorphology. *Quaternary Science Reviews, 29*(3), 424-442.

Wood, R., Edrich S., & Hutchison, I. (1989). Influence of North Atlantic tectonics on the large scale uplift of the Stappen High and Loppa High , western Barents Shelf. In A. J. Tankard & H. R. Balkwill (Eds.), *Extensional tectonics and stratigraphy of the North Atlantic margins* (pp. 641 s., fold. pl.). Tulsa, Okla.: Published jointly by American Association of Petroleum Geologists and Canadian Geological Foundation.

Worsley, D. (2008). The post-Caledonian development of Svalbard and the western Barents Sea. *Polar Research, 27*(3), 298-317.

9 Appendix

A: Scanned images of studied thin sections

B: EBS-images from PR1

- B.1: PR1210001
- B.2: PR1210002

C: EBS-images from PR3

- C.1: PR1210010
- C.2: PR1210011

D: EBS-images from PR4

- D.1: PR1210017

F: EBS-images from Hola

- F.1: HOLA

A: Scanned thin sections

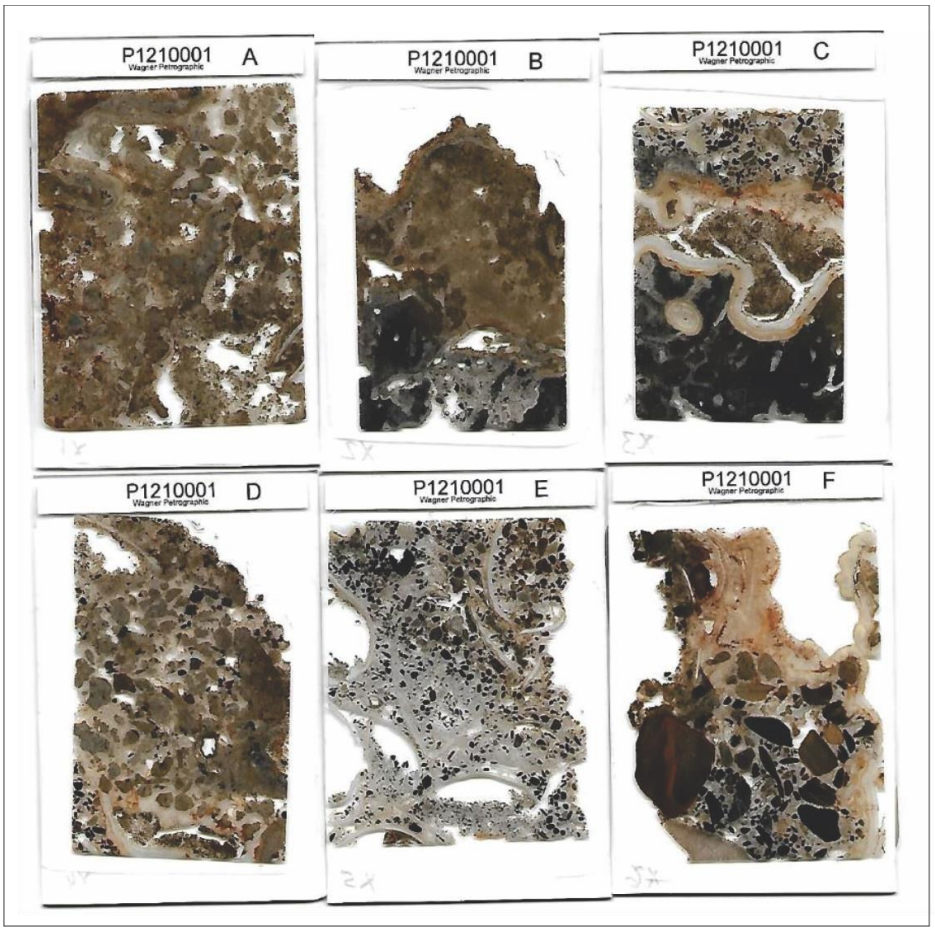

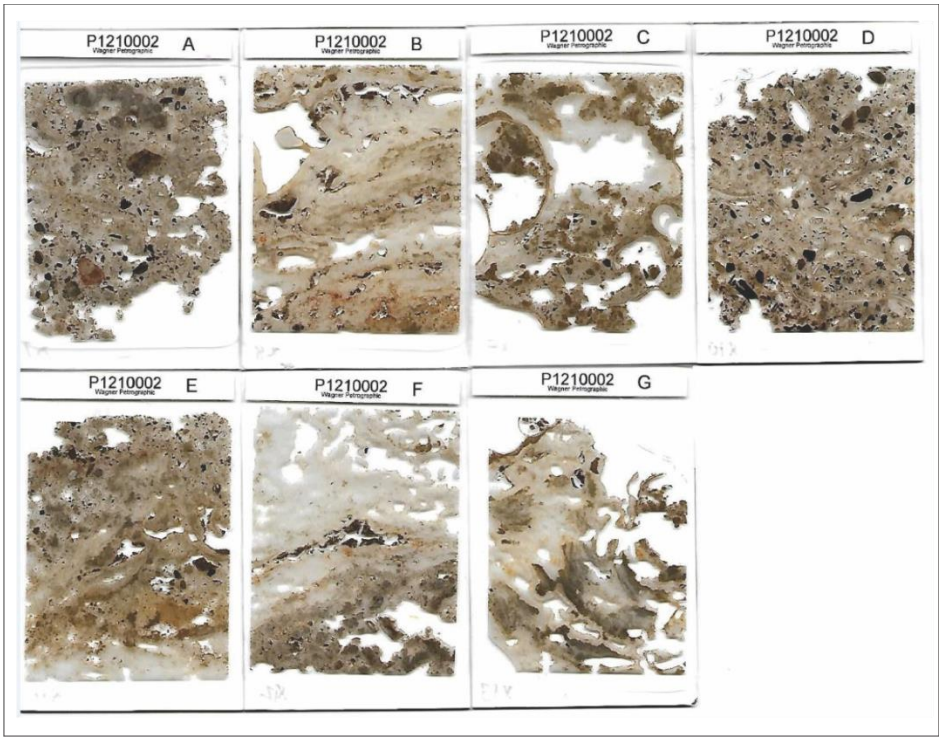

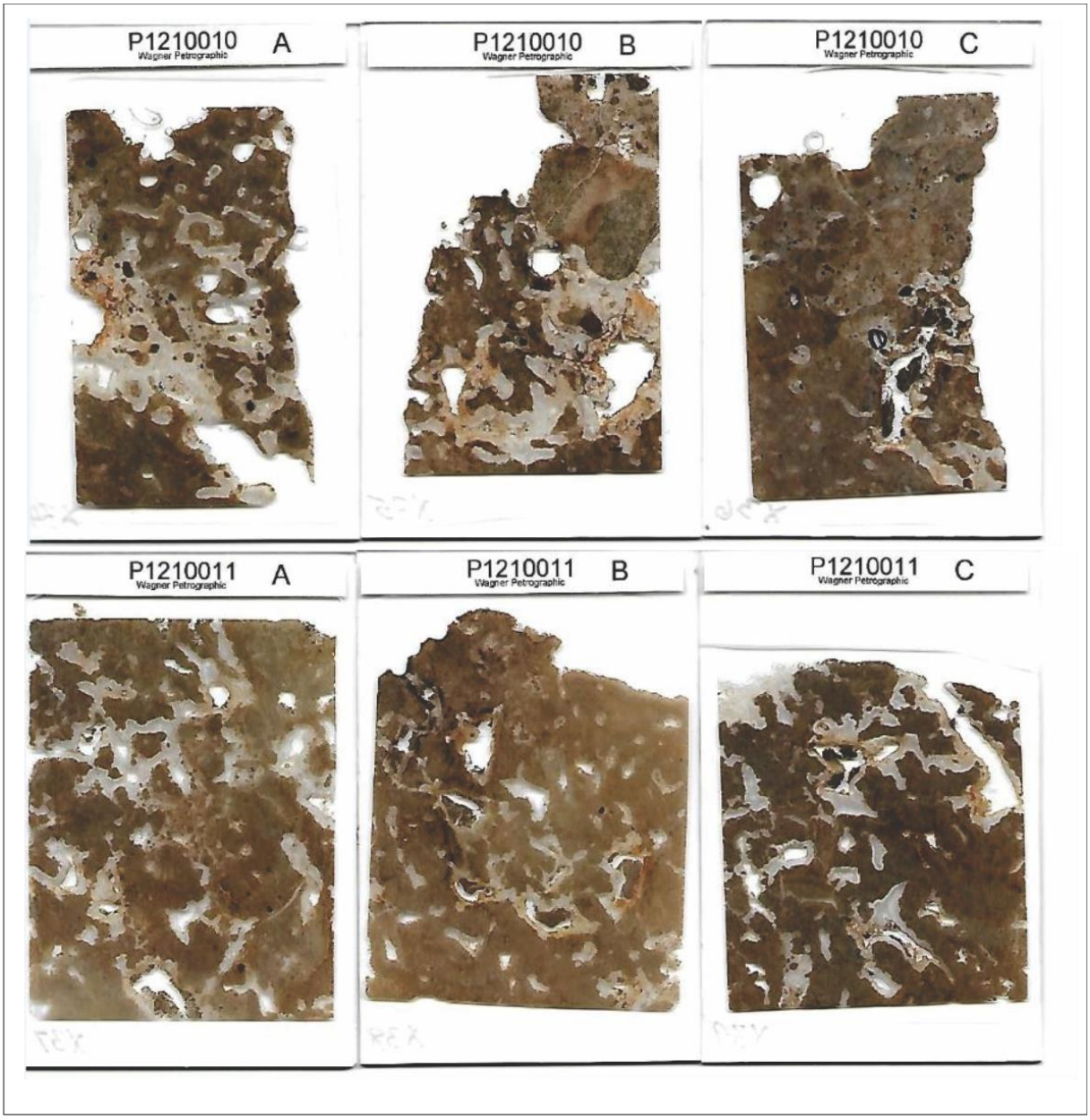
P1210010 A
Wagner Petrographic
P1210010 B
Wagner Petrographic
P1210010 C
Wagner Petrographic
P1210011 A
Wagner Petrographic
P1210011 B
Wagner Petrographic
P1210011 C
Wagner Petrographic

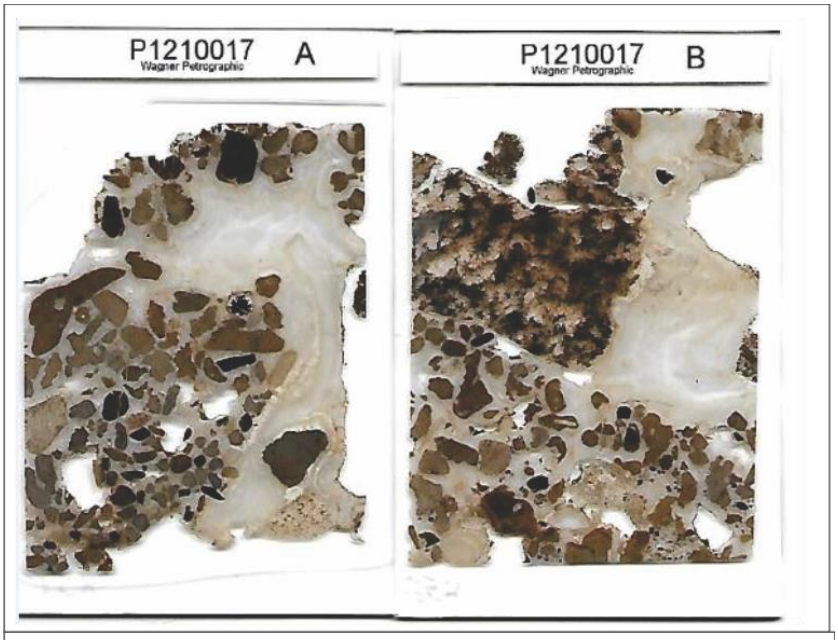
P1210017 A
Wagner Petrographic
P1210017 B
Wagner Petrographic

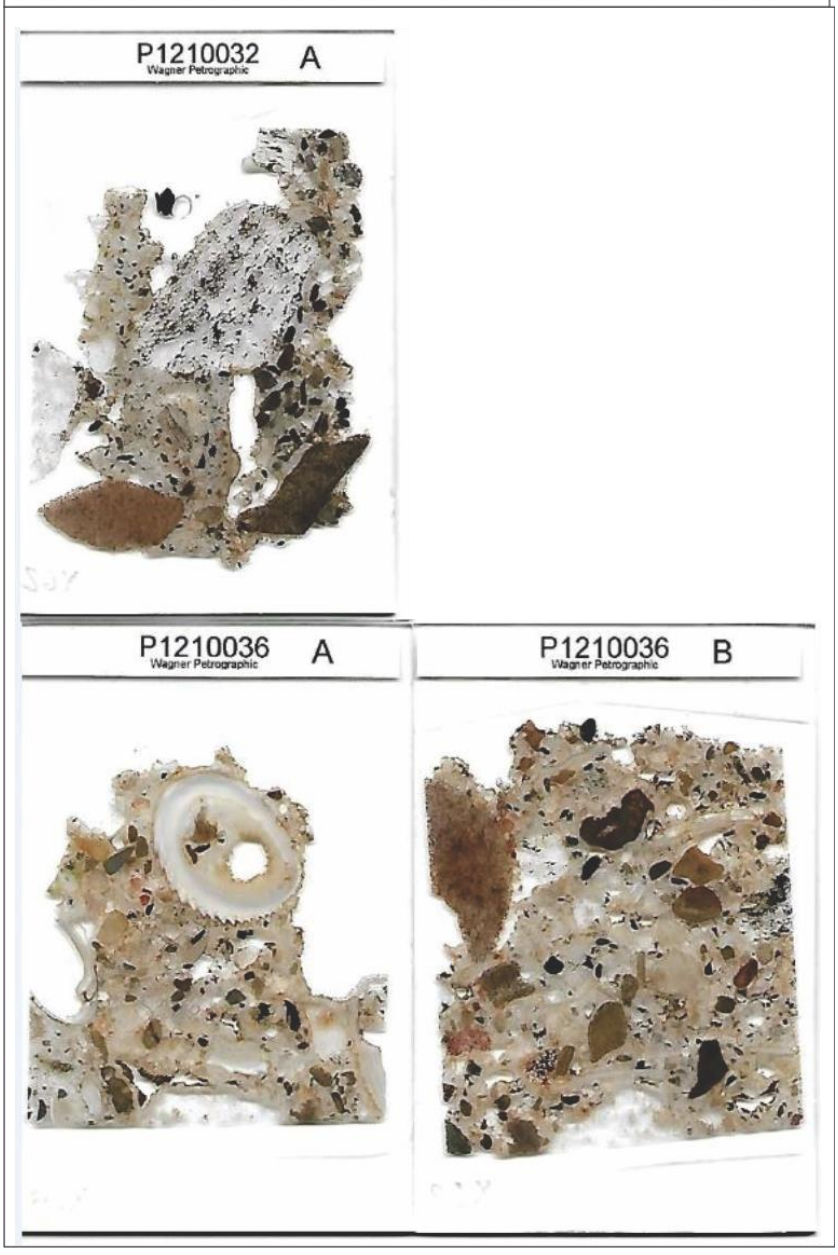
P1210032 A
Wagner Petrographic
P1210036 A
Wagner Petrographic
P1210036 B
Wagner Petrographic

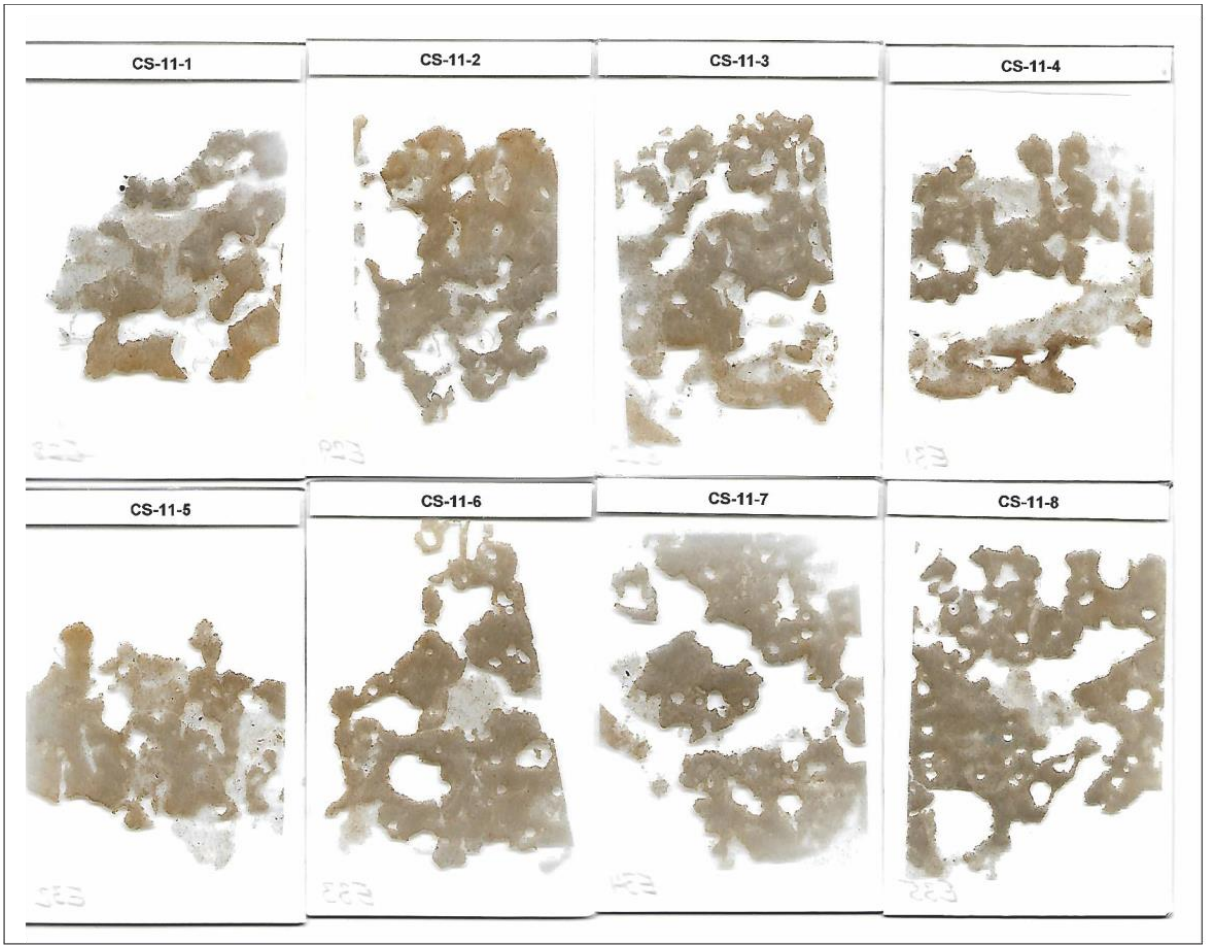
CS-11-1
CS-11-2
CS-11-3
CS-11-4
CS-11-5
CS-11-6
CS-11-7
CS-11-8

B.1 P1210001

B.1.1 Poorly cemented detrital sediments and biogenic debris (mainly foraminifera which exhibits pristine tests), different benthic species in B), E) and F). Planktonic species in C), D) and E).

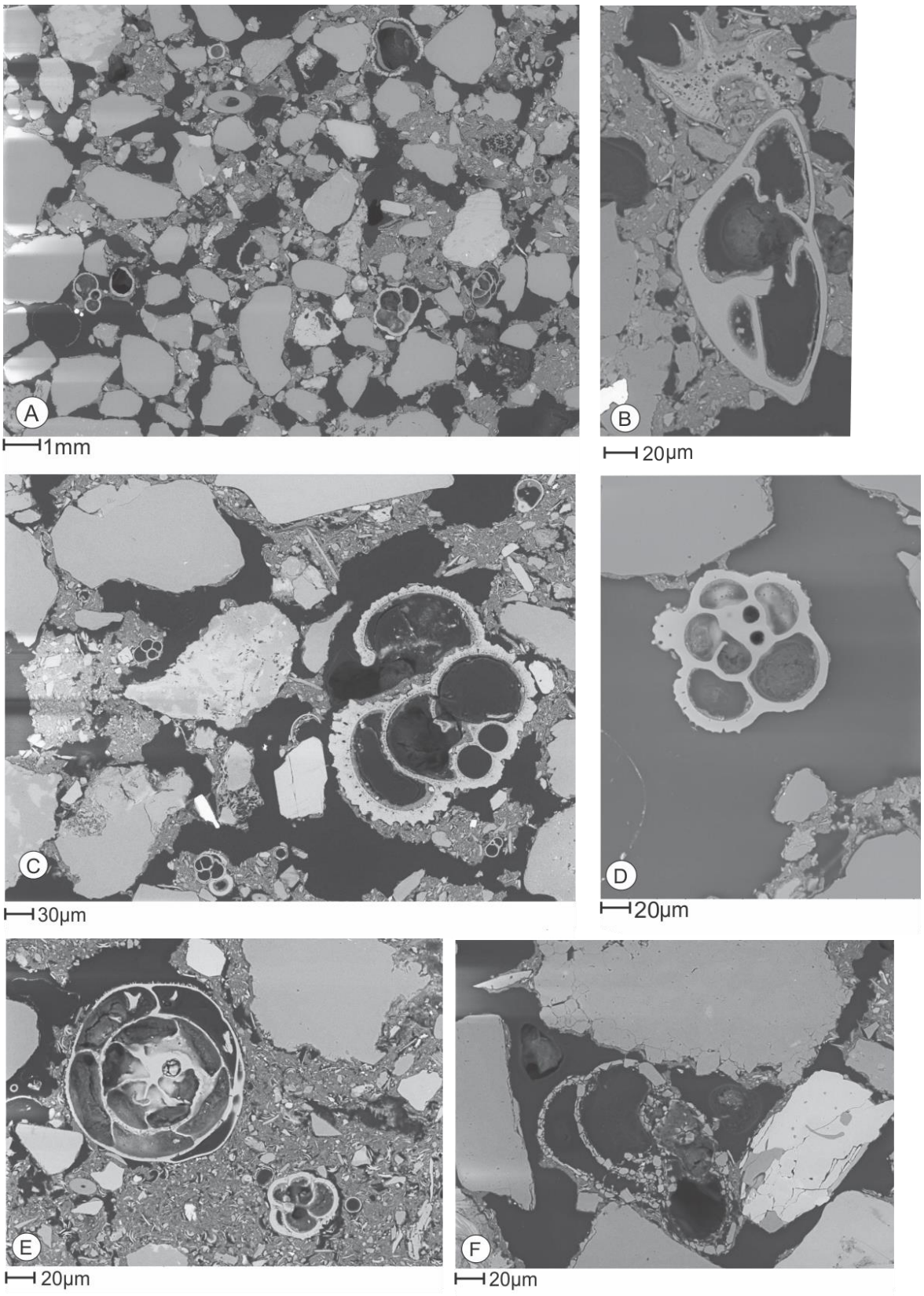

B.1.2 Planktonic species, some with MG-calcite overgrowths (dark coating on tests on images) occurring in the aragonite cement. A), B), D), E), F), and G) exhibits thick tests with Mg-calcite on outer and inner walls. C) Thinner test but minor overgrowths visible on inner and outer test.

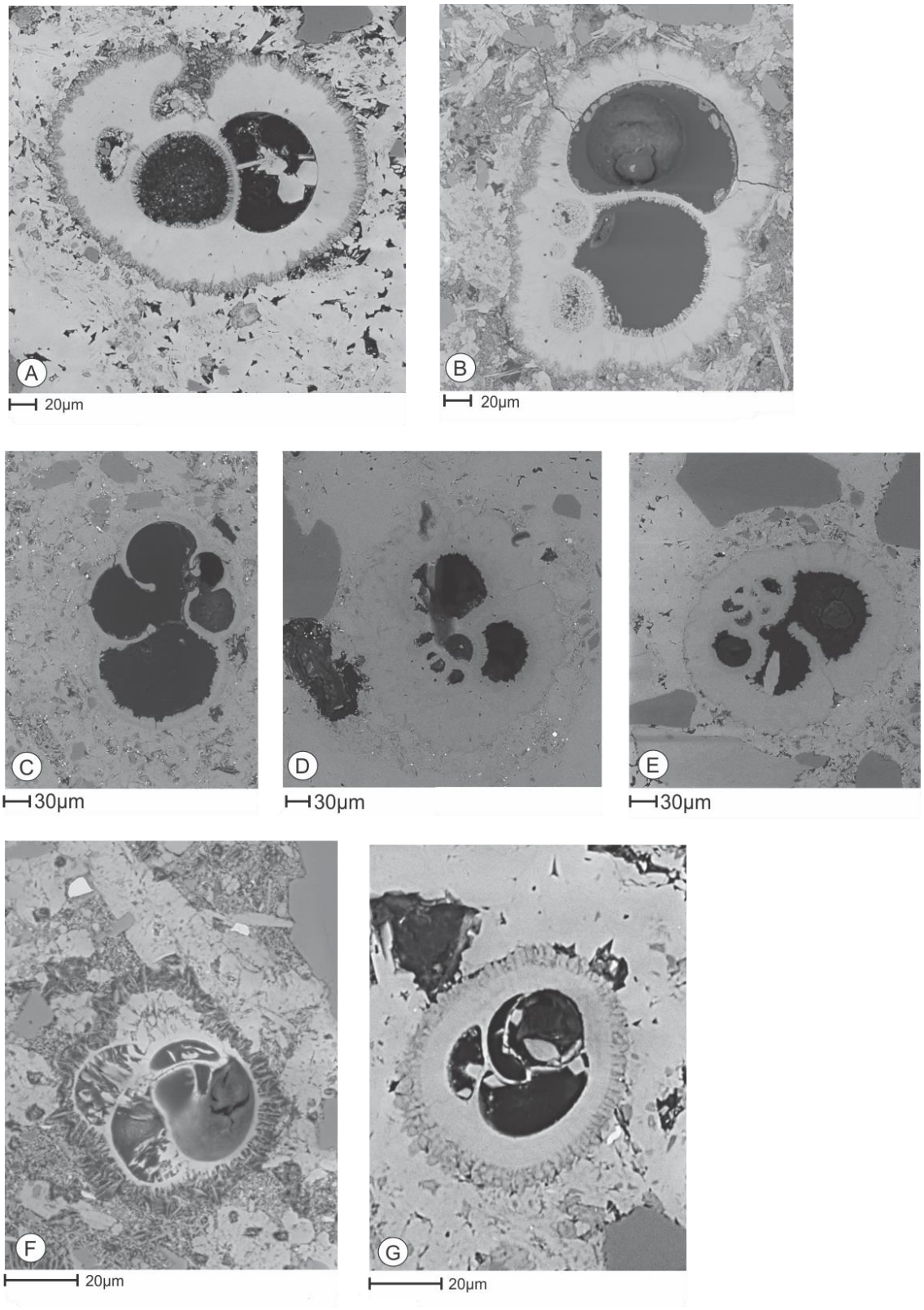

B.1.3 Pristine tests of benthic foraminifera embedded in aragonite cement, and in C) there is aragonite cement filling in chambers.

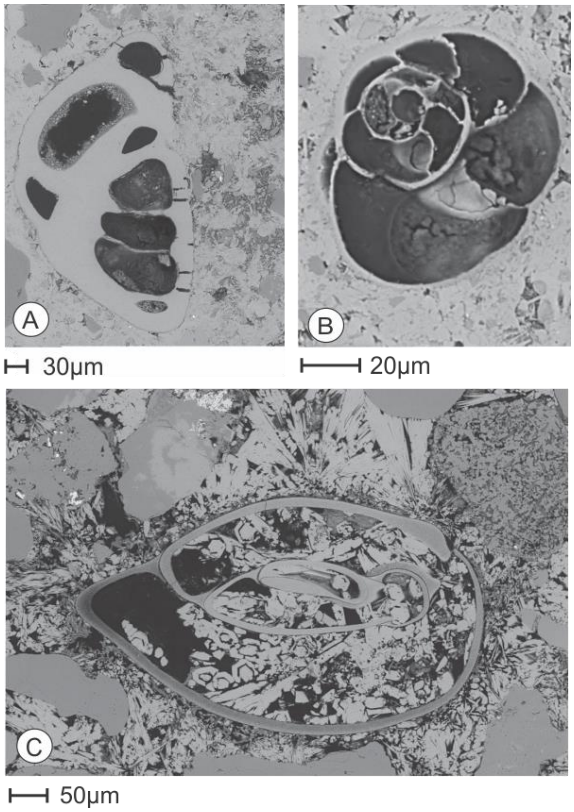

B.1.4 Benthic foraminifera tests with Mg-calcite overgrowths embedded in aragonite cement. Overgrowths occurs either as crystals ((A), B), C)), or as darker BSE coatings ((D),E)), either on inner chamber walls or outer, and/or on both.

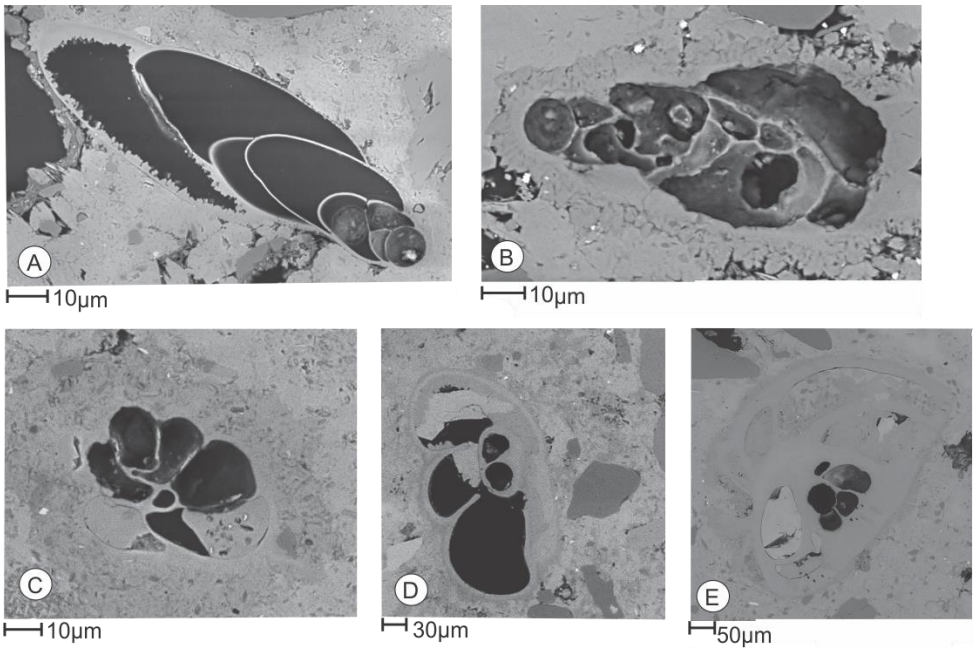

B.1.5 Recrystallized tests of benthic foraminifera, with Mg-calcite overgrowths embedded in aragonite cement. The overgrowths are on outer test wall of all the specimens, but C) lack inner test wall Mg-calcite overgrowths. D) exhibits aragonite cement infilling of chambers.

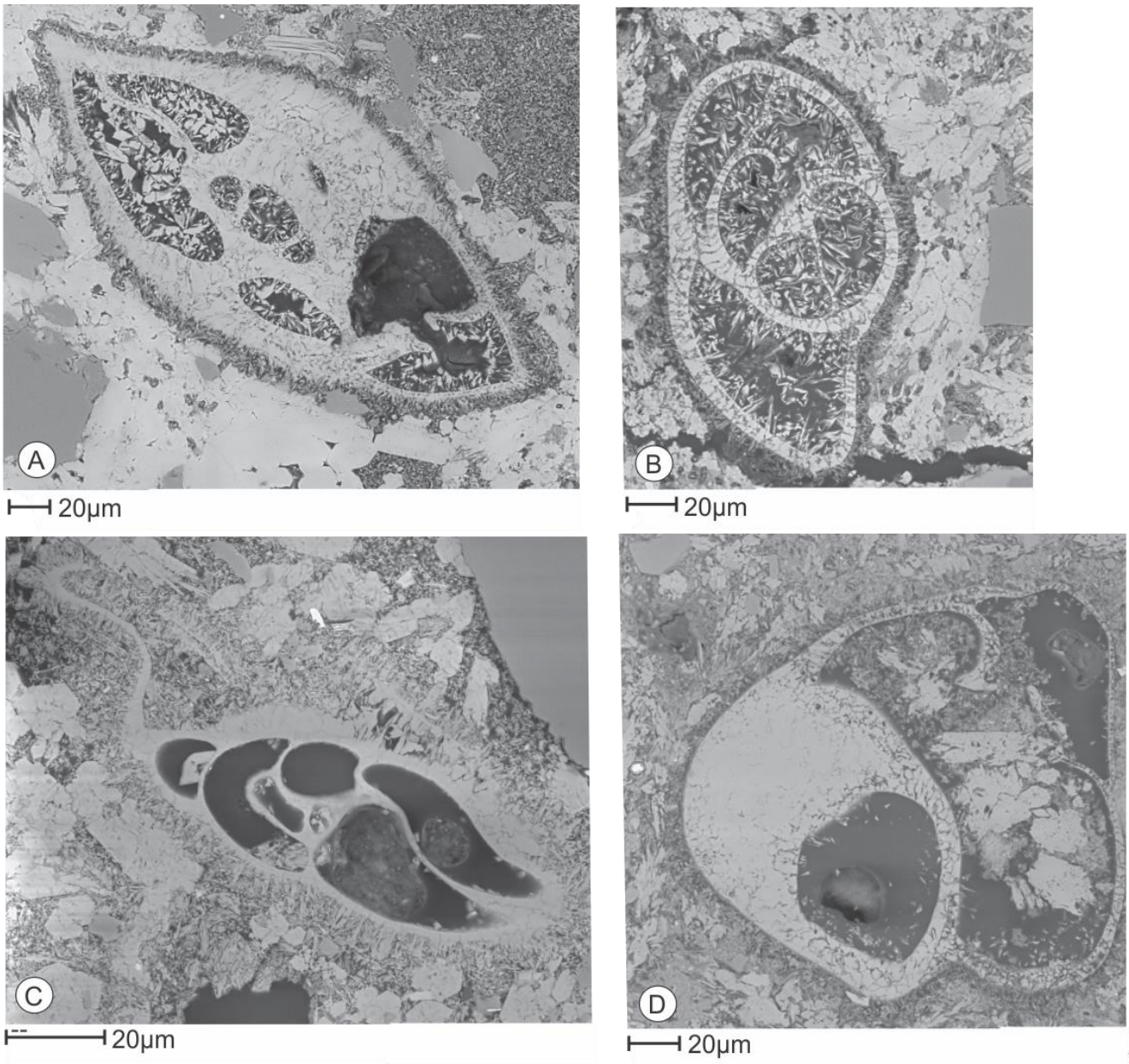

B.2 P1210002

B.2.1 Weakly cemented detrital sediments and biogenic components. A) unidentified microfossils. B) benthic and planktonic tests of foraminfiera. C) Planktonic foraminifera with pristine ornamentation. D) Accumulation of siliceous spicules. E) Radiating aragonite crystals in aragonite cement.

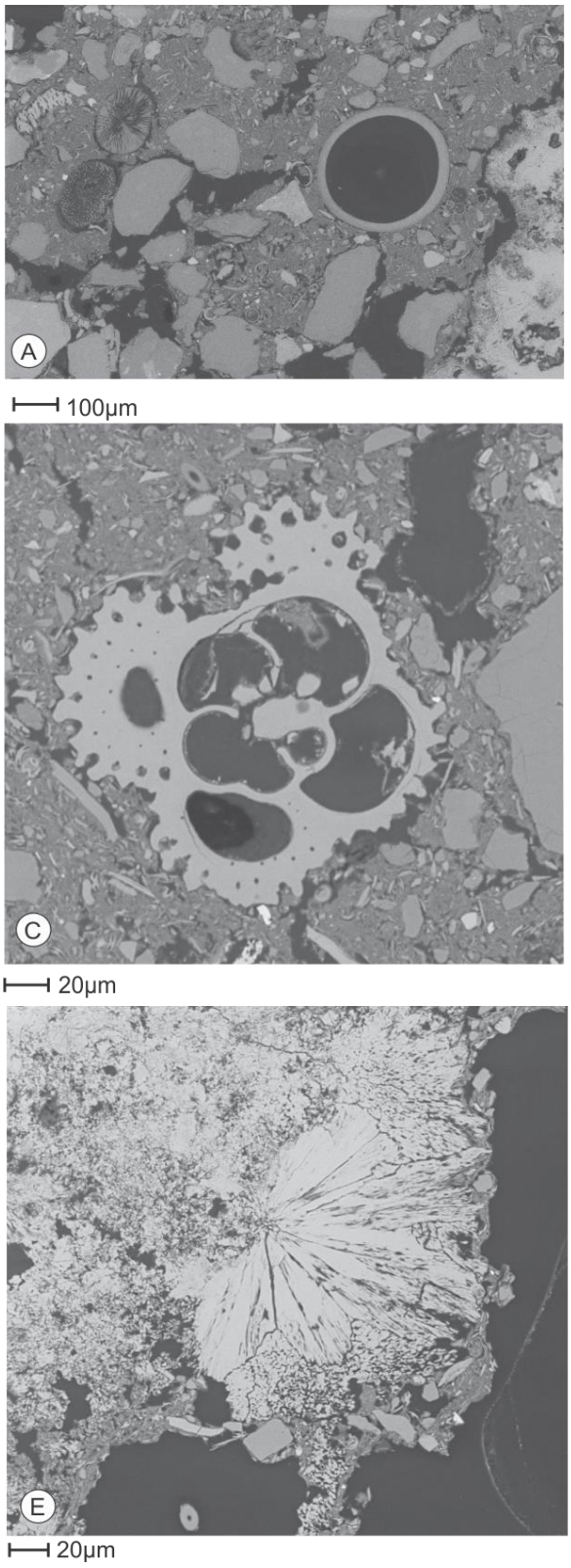

B.2.2 Relatively pristine tests without obvious Mg-calcite overgrowths of benthic foraminifera embedded in aragonite cement, no chamber infill.

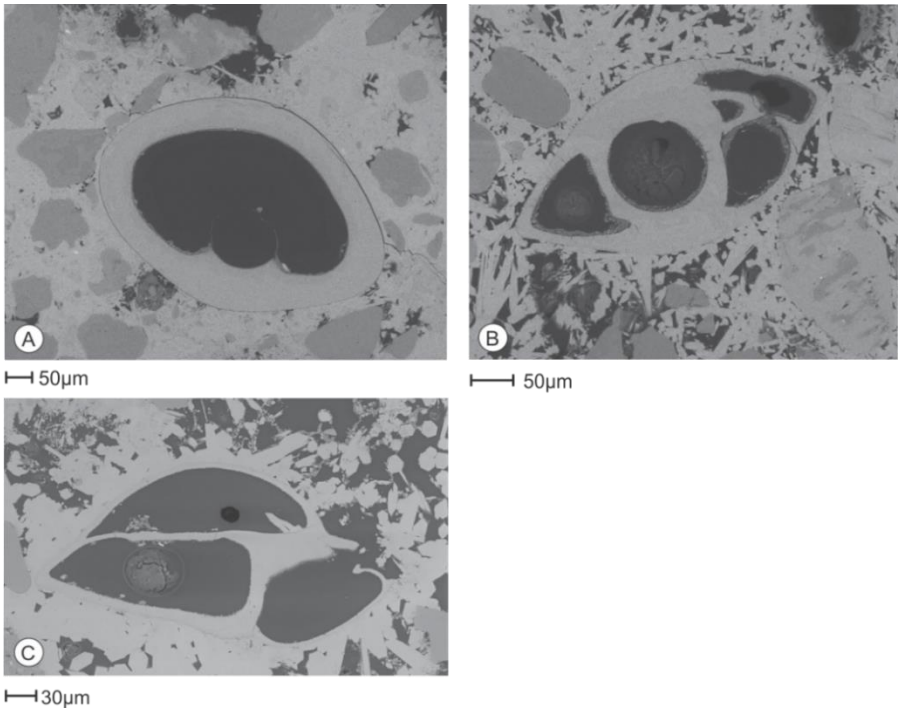

B.2.3 Pristine tests with aragonite cement occurring both outside and inside (chamber infill) of tests.

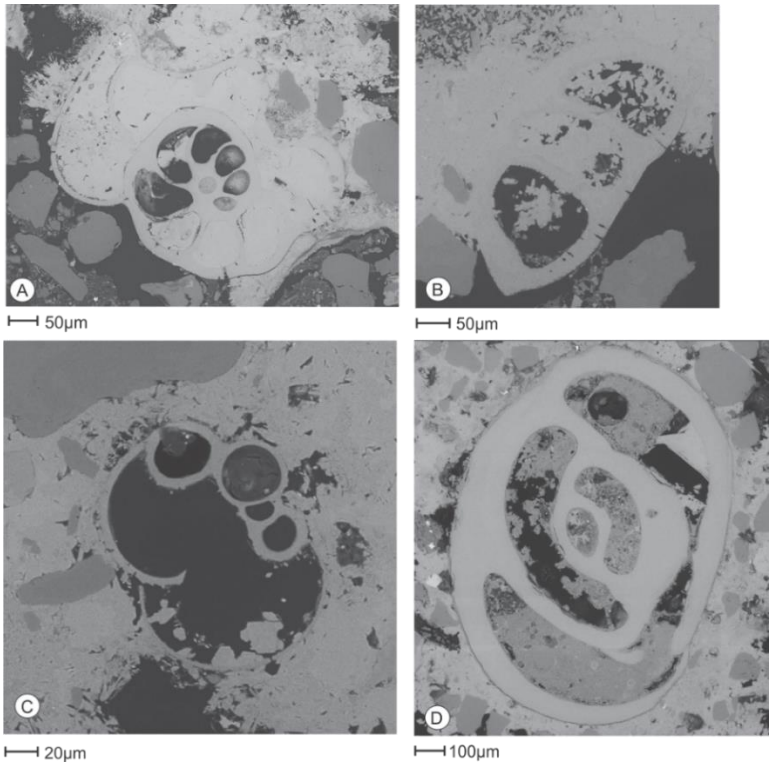

B.2.4 Tests of benthic foraminifera with Mg-calcite overgrowths embedded in aragonite cement A), B), D) and E) Mg-calcite overgrowths seen as dark coatings on outer wall. C) Bigger Mg-calcite crystals on outer and inner walls, aragonite cement as chamber infill. F) A benthic test with Mg-calcite crystals mainly on outer wall and aragonite cement chamber infill. Siliceous spicule occurring in the right corner.

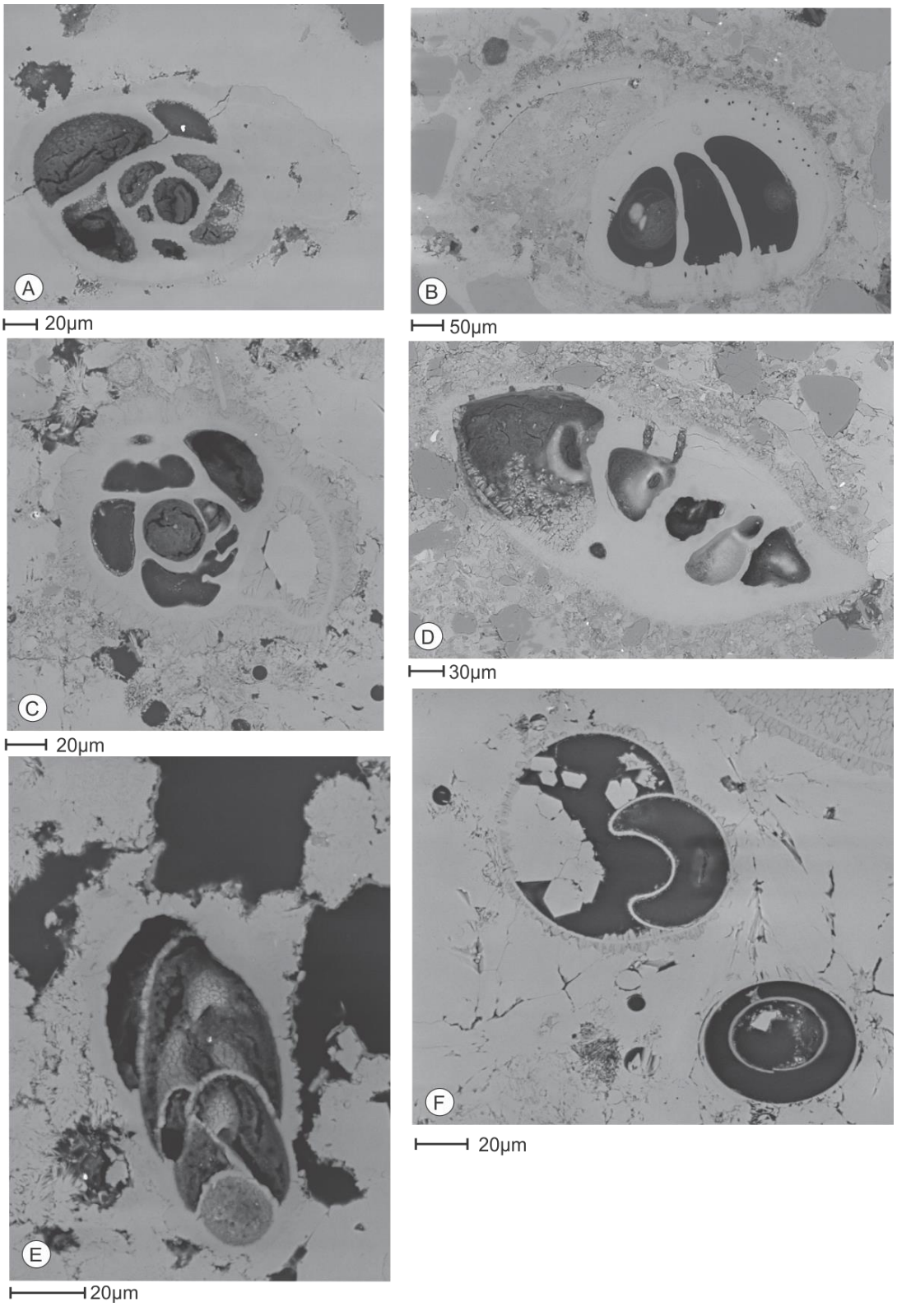

A) Partly recrystallized test with Mg-calcite on outer and inner walls, and aragonite cement as infill of chamber. B), C) and D) Benthic test with Mg-calcite overgrowths seen as dark coatings. E) and F) Mg-calcite crystals clearly visible on inner chamber walls.

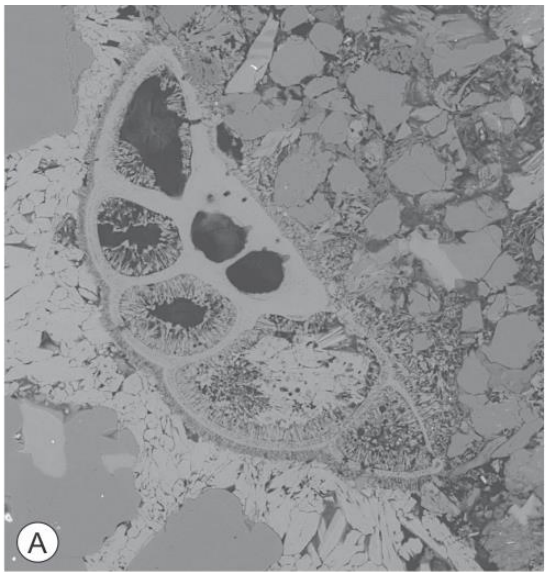

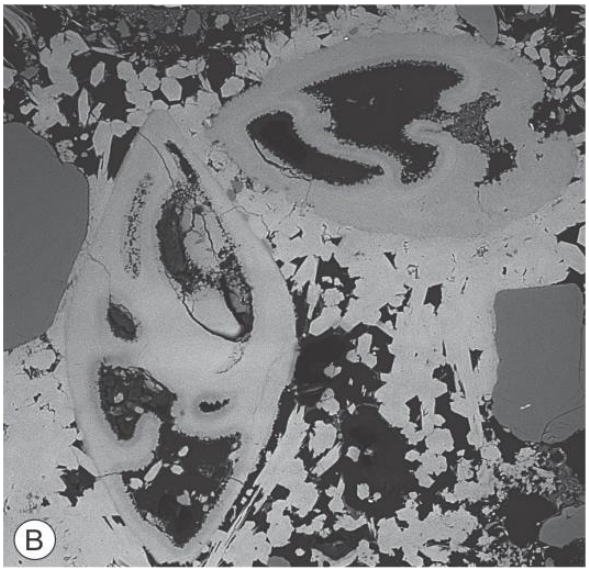

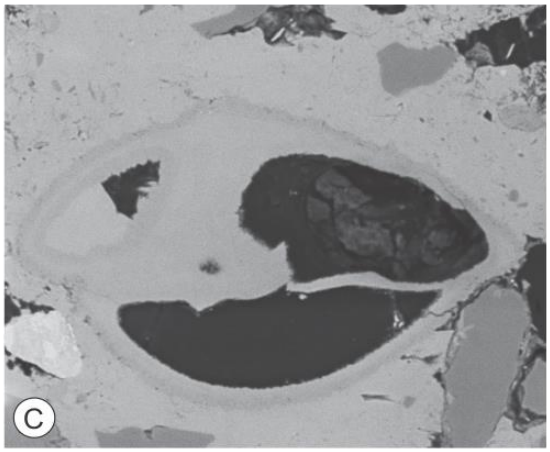

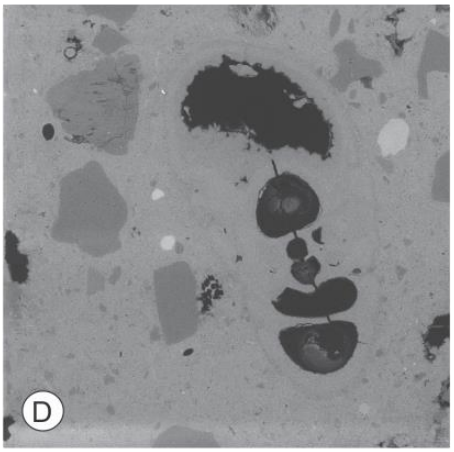

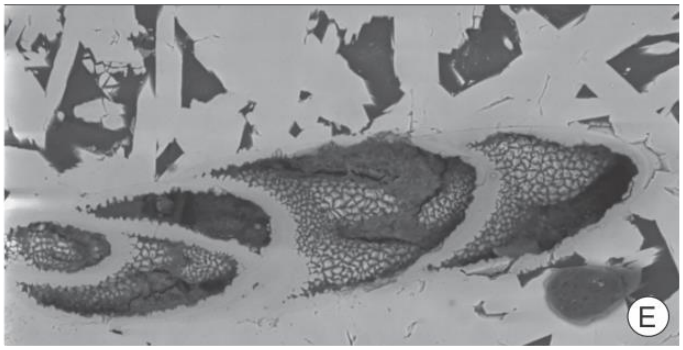

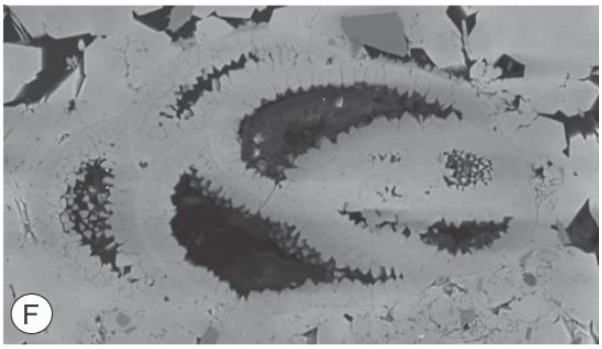

B.2.5 Siliceous spicules in different size ranges and surrounding radial aragonite cement

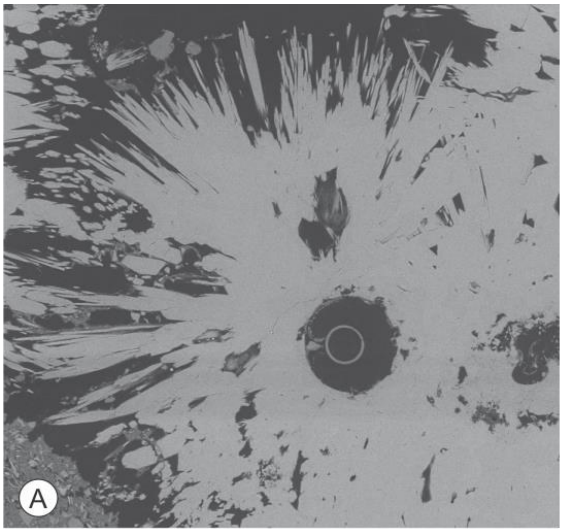

50µm

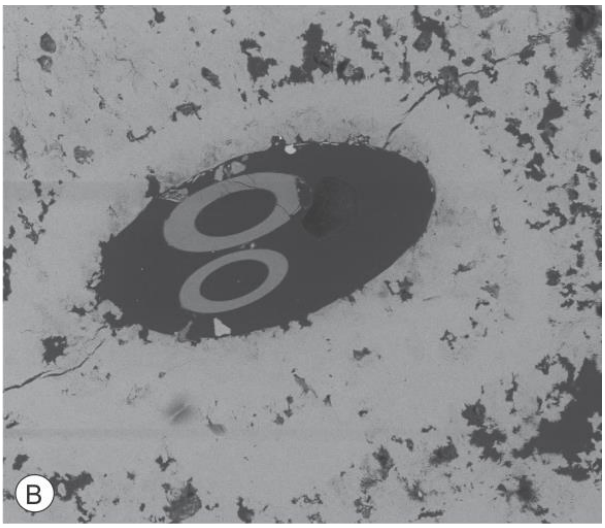

50µm

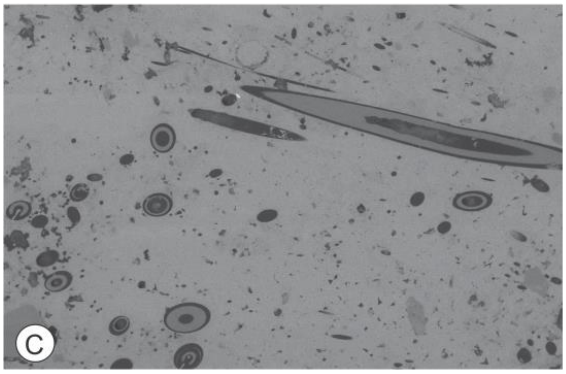

100µm

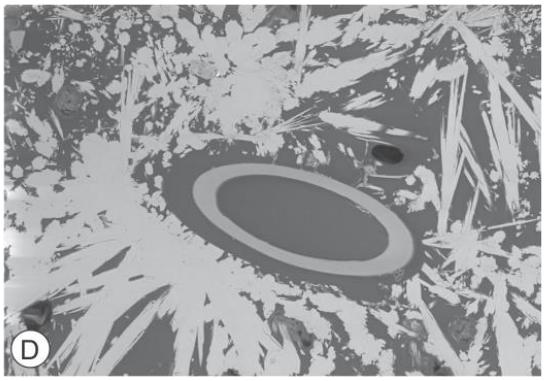

30µm

C: PR3

C.1: P1210010

C.1.1: Recrystallized (A) and non-recrystallized (B-G) tests with Mg-calcite overgrowth.

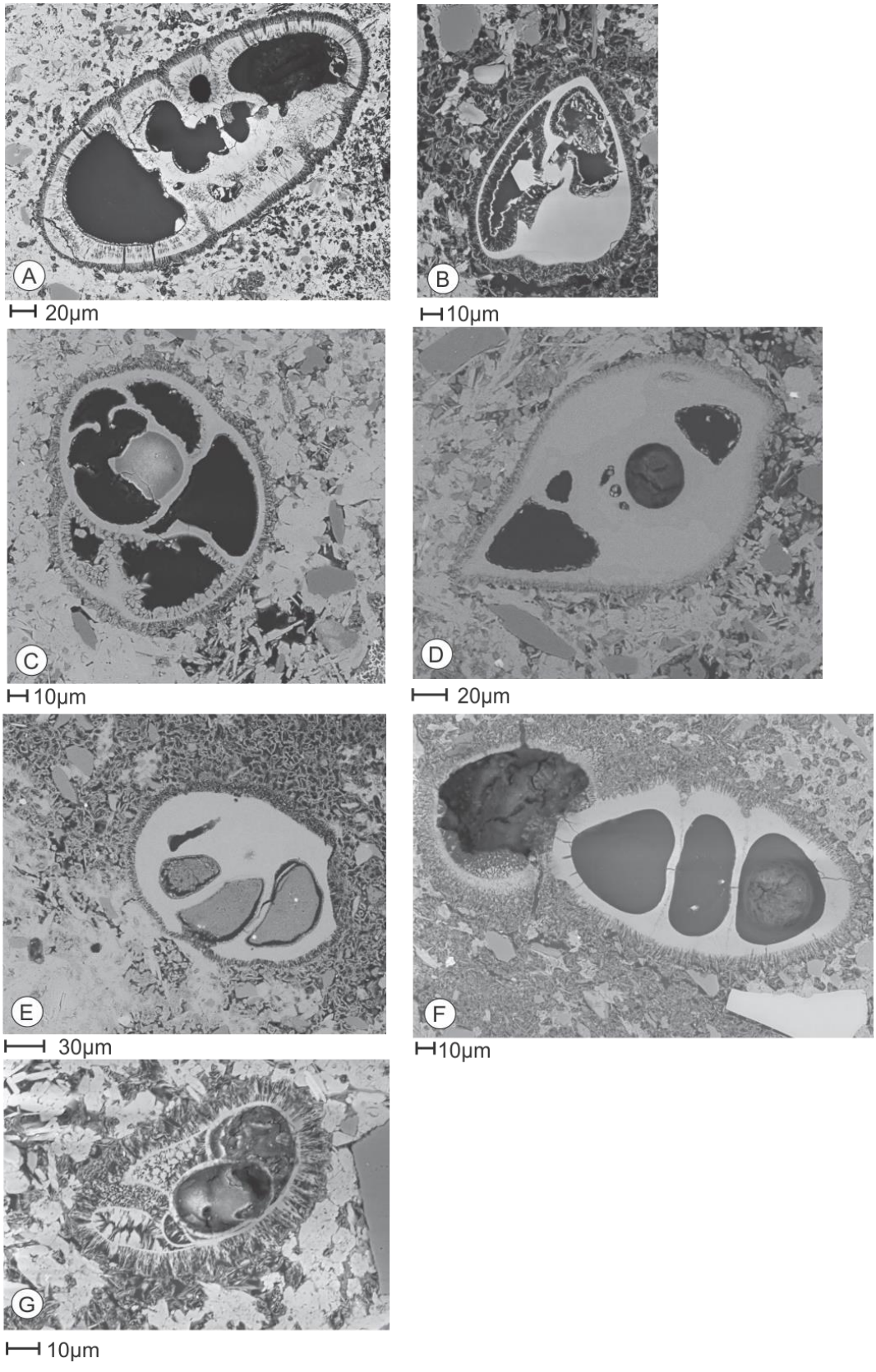

C.1.2 Tests of benthic foraminifera with no Mg-calcite overgrowths embedded in carbonate cement

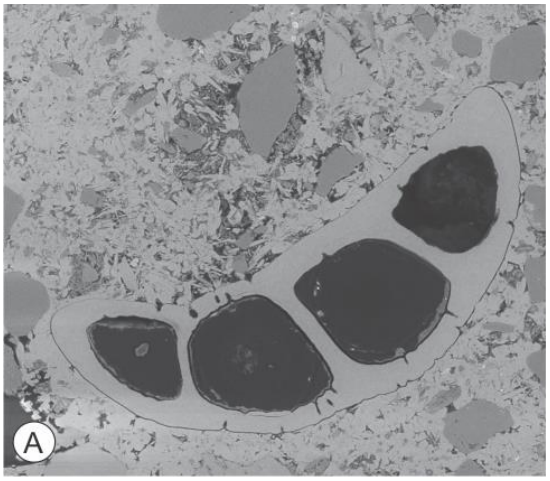

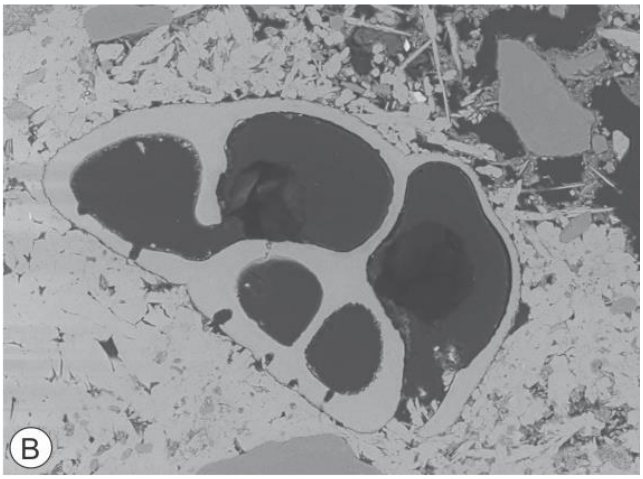

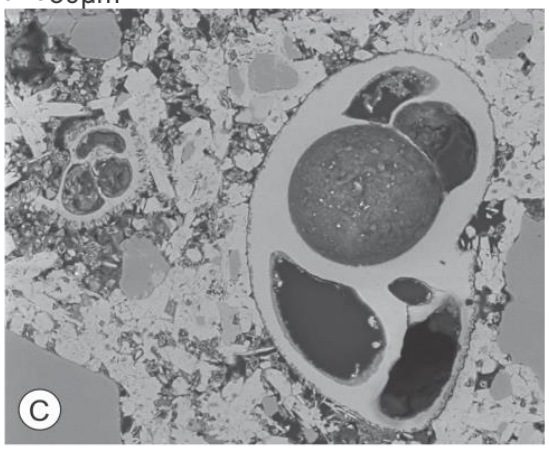

C.1.3 Tests of planktonic species with Mg-calcite overgrowth embedded in aragonite cement

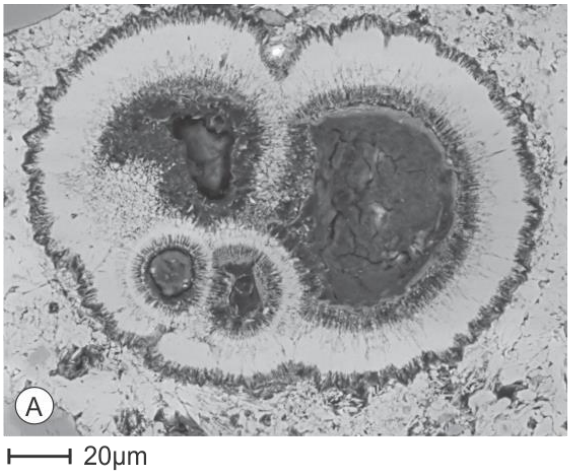

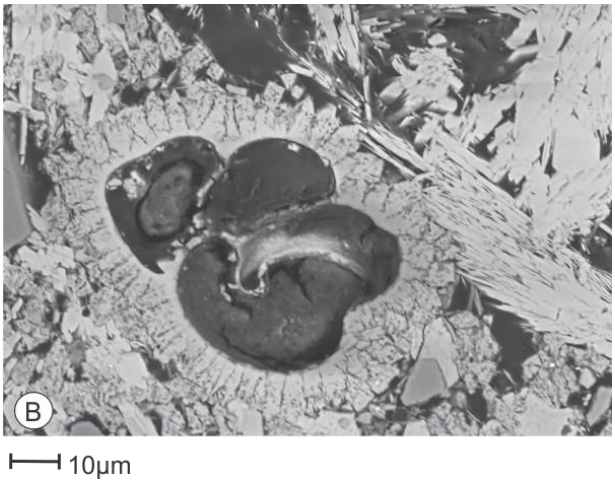

C.2: P1210011

C.2.1: Tests of benthic foraminifera with Mg-calcite overgrowth on outer wall embedded in aragonite cement

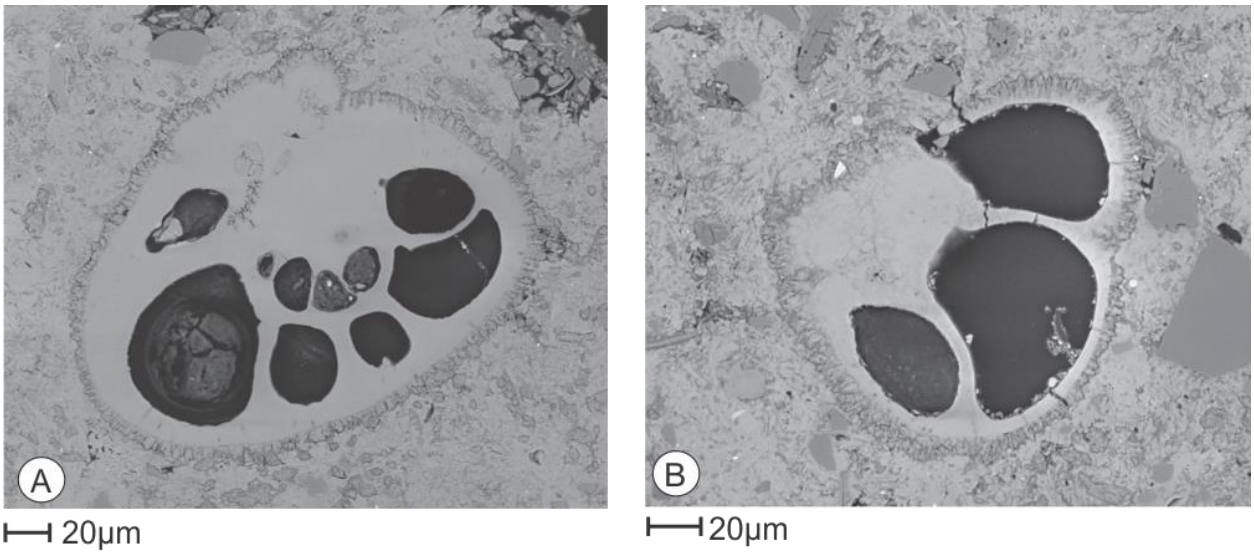

C.2.2: Tests of benthic foraminifera with inner and outer Mg-calcite overgrowths, embedded in aragonite cement

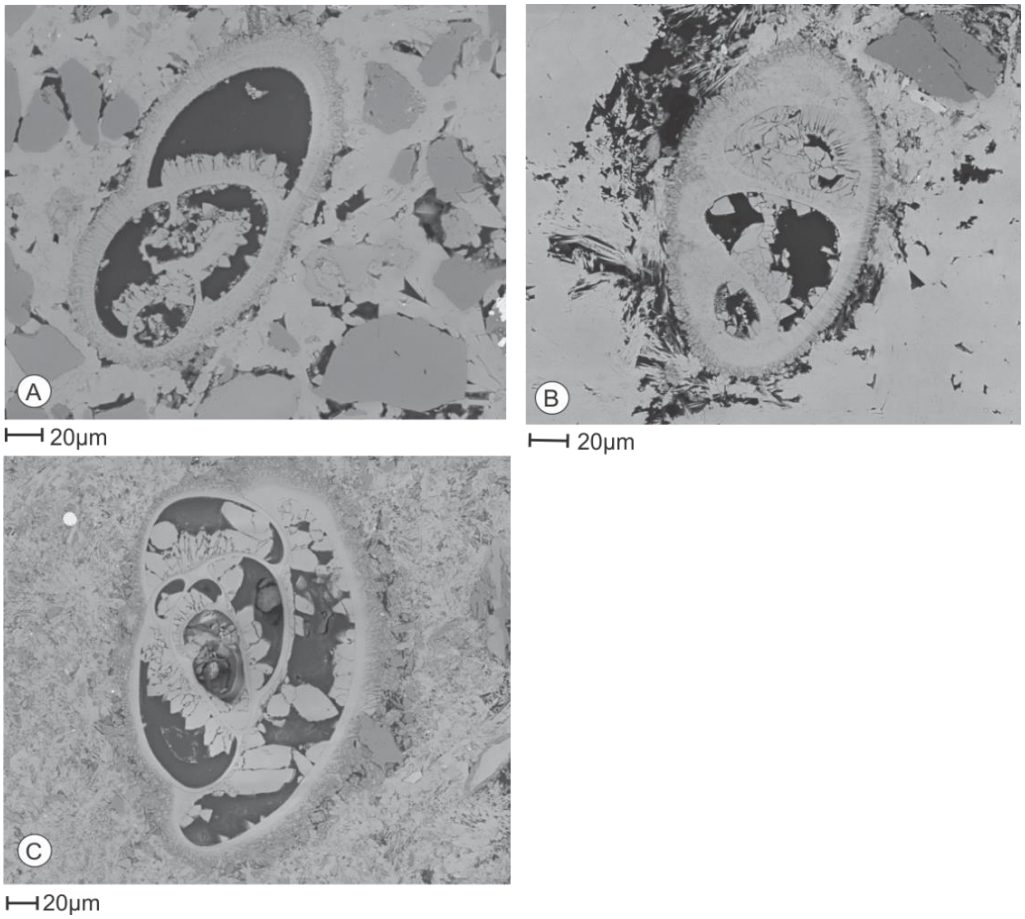

D.1: PR4 – P1210017

D.1.2: Benthic foraminifera exhibiting different preservation states in the crust. A), B), D), and E) exhibits Mg-calcite overgrowths on outer test. C) Precipitation in chamber induced by aperture. All embedded in aragonite cement. Black arrows indicates pyrite.

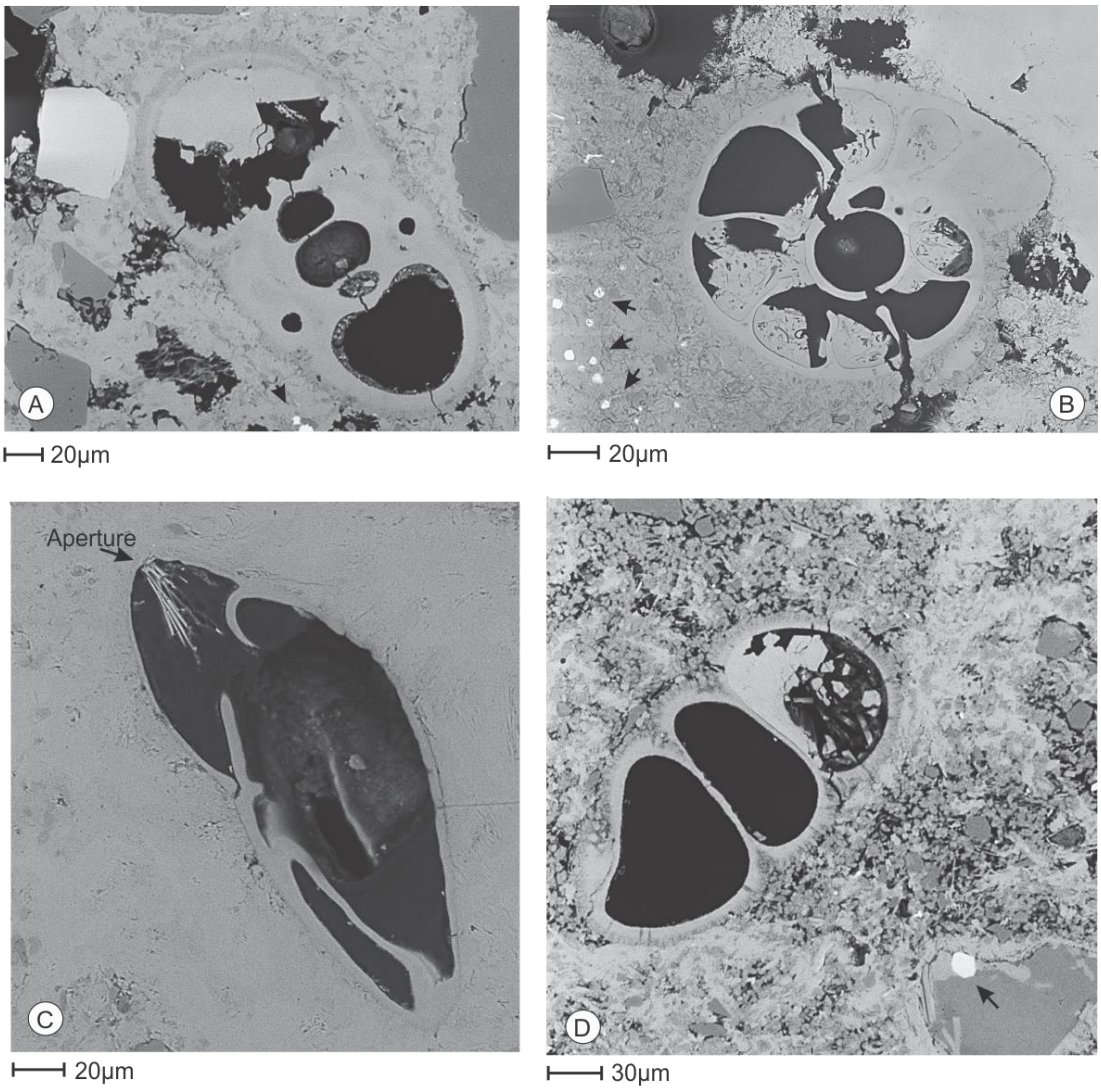

F.1: Hola

F.1.1: Weakly cemented detrital sediments and biogenic debris. A) Coral and foraminifer tests are indicated. B) Foraminifera and shell of bivalve. C) Foraminifera and detrital grains and aragonite crystals. D) Coral in aragonite cement.

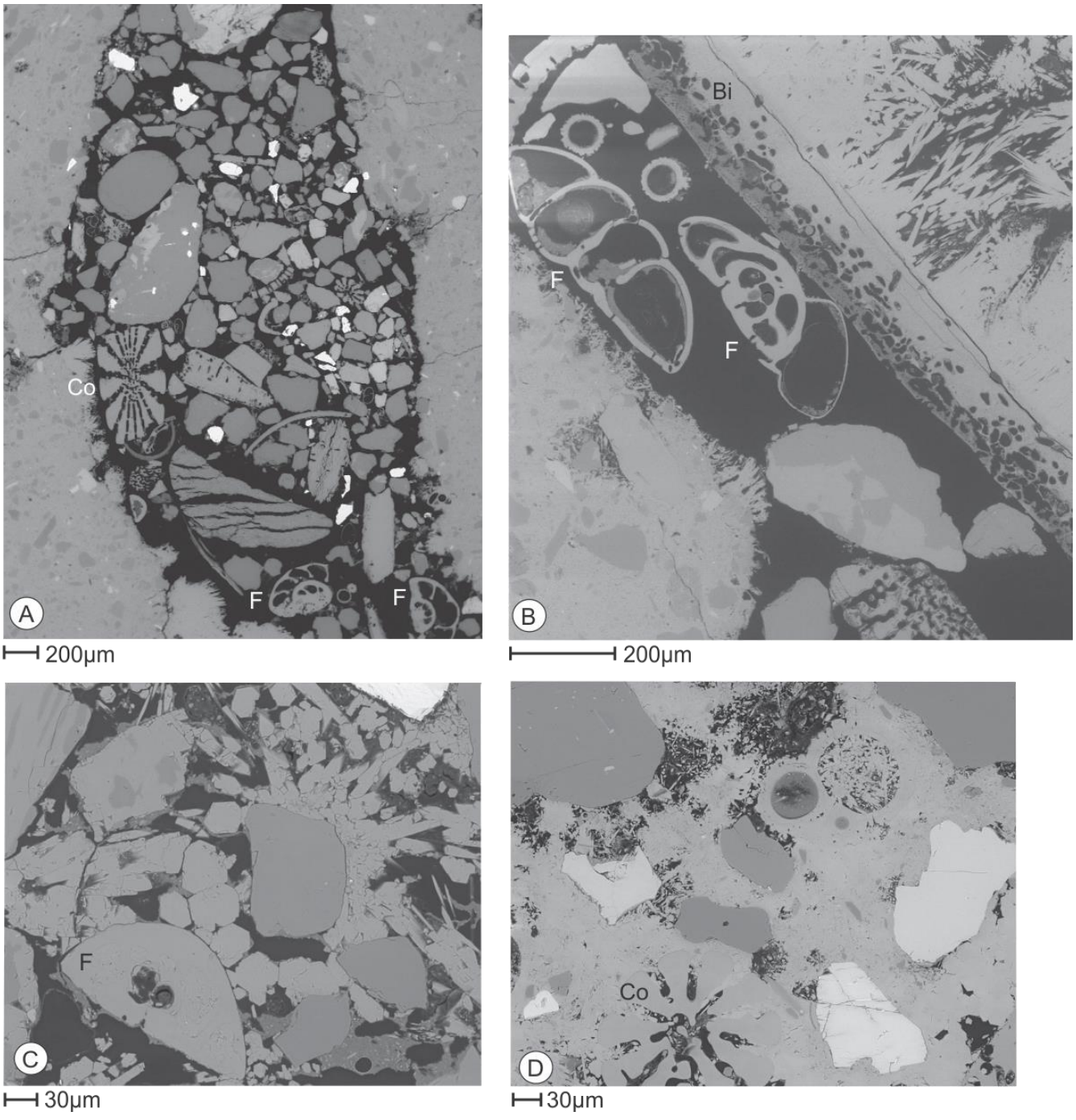

F.1.2: Pristine tests embedded in aragonite cement, and with various degree of aragonite infill of chambers.

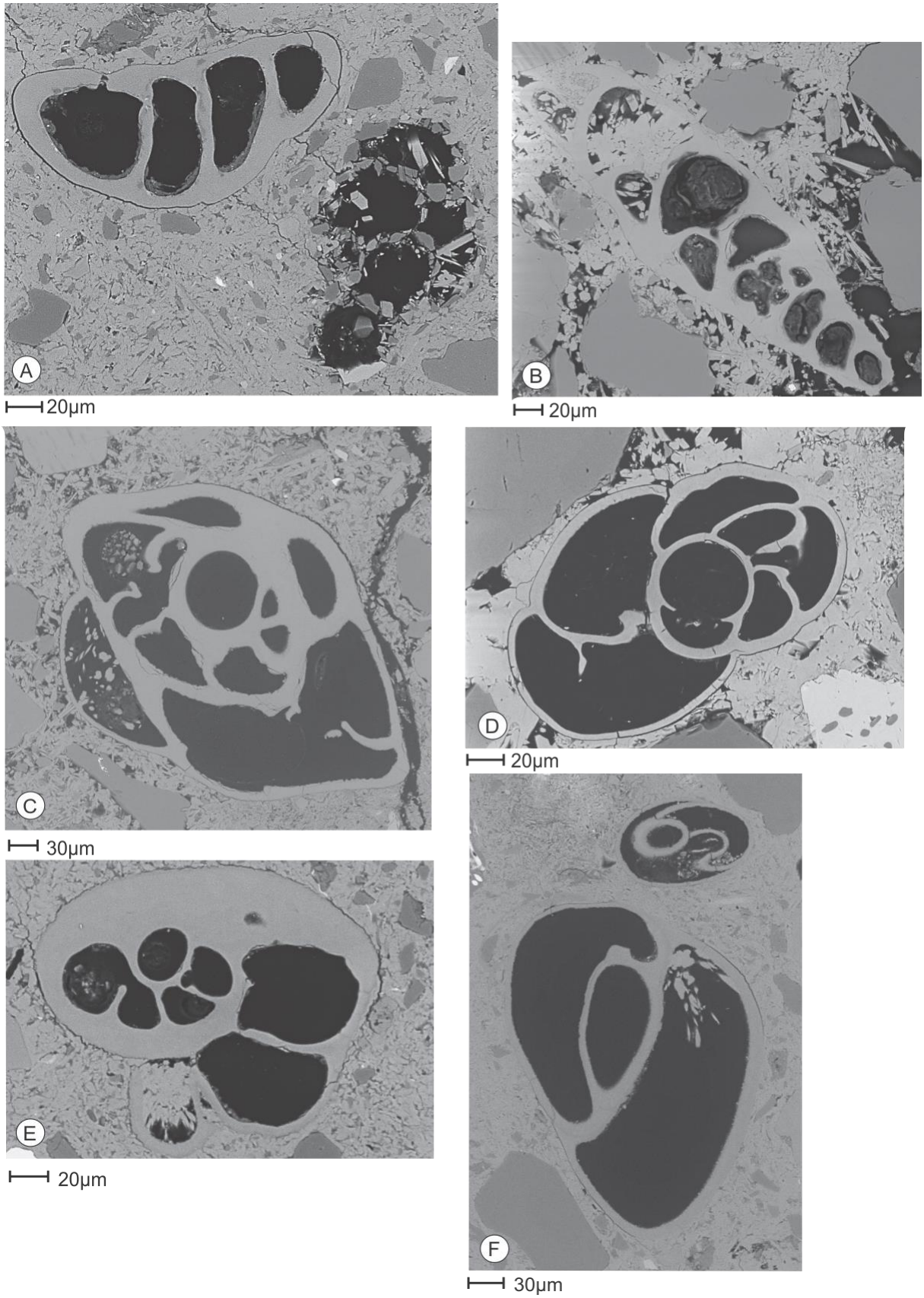

F.1.3: Tests of benthic foraminifera with Mg-calcite overgrowths seen as dark BSE coatings, embedded in aragonite cement.